SYNTHESIS OF TWO-PHOTON DYE LIBRARIES FOR PANCREATIC IMAGING AND UNIQUE POLYPHOSPHATE PROBE DEVELOPMENT

BIKRAM KESHARI AGRAWALLA

NATIONAL UNIVERSITY OF SINGAPORE

2015

SYNTHESIS OF TWO-PHOTON DYE LIBRARIES FOR PANCREATIC IMAGING AND UNIQUE POLYPHOSPHATE PROBE DEVELOPMENT

BIKRAM KESHARI AGRAWALLA
(M.S. Pharm. National Institute of Pharmaceutical Education and Research, Kolkata, India)

A THESIS SUBMITTED
FOR THE DEGREE OF DOCTOR OF PHILOSOPHY
DEPARTMENT OF CHEMISTRY
NATIONAL UNIVERSITY
OF SINGAPORE

2015

Thesis Declaration

I hereby declare that this thesis is my original work and it has been written by me in its entirety, under the supervision of Professor Young-Tae Chang, (in the Chemical Bio-imaging Lab, S9-03-03), Chemistry Department, National University of Singapore and the biological experiments were performed at Laboratory of Bio-imaging Probe development, Lab #02-02 Helios, Singapore Bio-imaging Consortium, (Biomedical Sciences Institutes, Singapore 138667) between 04/01/2011 and 31/12/2014.

I have duly acknowledged all the sources of information which have been used in the thesis.

This thesis has also not been submitted for any degree in any university previously.

The content of the thesis has been partially published in:

- In Situ Investigation of Mammalian Inorganic Polyphosphate Localization Using Novel Selective Fluorescent Probes JC-D7 and JC-D8, Angelova, P. R.; **Agrawalla, B. K.**; Elustondo, P. A.; Gordon, J.; Shiba, T.; Abramov, A. Y.; Chang, Y. T.*; Pavlov, E. V.* *ACS Chem Biol*. **2014**, *9*, 2101-2110. (Co first author)

- Glucagon-Secreting Alpha Cell Selective Two-Photon Fluorescent Probe TP-α: For Live Pancreatic Islet Imaging, **Agrawalla, B. K.**; Chandran, Y.; Phue, W. H.; Lee, S. C.; Jeong, Y. M.; Wan, S. Y.; Kang, N. Y.*; Chang, Y. T.* *J. Am. Chem. Soc*. **2015**, 137, 5355-5362.

- Synthesis and Assessment of Beta Cell Specific Glucosamine Based Two-Photon Probe. **Agrawalla, B. K.**; Chang, Y. T.* Manuscript preparation.

Bikram Keshari Agrawalla		14th January 2015
Name	Signature	Date

Acknowledgements

It gives me immense pleasure to thank Professor Young-Tae Chang for all his faith on me, for the freedom he gave during my Ph.D. work and his valued suggestions and guidance all the way. I must admit that from the very first meeting with him on 4th Jan 2011, he express a glimpse of believing on me which grow over the years. He allowed me to perform the entire range of experiments, starting with combinatorial synthesis, *in vitro* screening (both for analytes and cell lines), handling primary cells, animal works, confocal microscopy and my favorite two-photon imaging all alone. I am extremely thankful to him for this very unique experience and multi-disciplinary research training.

I would like to express my sincere gratitude to Dr. Julian and Dr. Kang for their support, teaching and guidance in my projects. Next my heartfelt thanks to seniors in lab namely Dr. Maiti, Dr. Jeong, Dr. Park, Dr. Srikanta, Dr. Siva and Dr. Yoo for their kindness, emotional support and constant encouragement.

I am expressing my sincere thankfulness to all wonderful people of Chang lab, who not only made this journey so special and memorable but also for being very supportive and helpful Dr. Yun, Dr. Kim Hanjo, Dr. Ha, Kelly, Dr. Kim. Dr. Kim Jimni, Dr. Woo Sirl. Dr. Satoshi Arai, Dr. Jiyeon Ock, Dr. Teoh Chai Lean, Dr. Parag Mukherjee, Dr. Rupankar Paira, Dr. Gopal Yerragorla, Dr. Kale, Dr. Santanu Jana, Dr. Yoo Jae Duk, Dr. Cedrik Massif, Dr. Kim Eung Sam, Dr. Hawyoung Kwon, Dr. Kim Beomsue, Dr. Lee Yongan, Dr. Peng Juanjuan, Dr. Lin Yuan, Dr. Lee Jungyeol, Dr. Uchinomiya Shohei, Dr. Duanting, Dr. Dongdong, Dr. Cheryl, Xu Wang, Jow Zhi Yen, Fronia, Mui Kee, Chee Geng, Tessa, Jun Cheng, Atiqah, Jiaojiao, Jing Yang, Wut Hmone, Hogyu, Wang Lu, Xiaotong, Priscilla and Hui Shan.

I also take this chance to thanks all my seniors, juniors and friends who facilitate my dream come true. I am thankful to Rinku, Rojic, Deepak, Nitin, Anshuman, Saurabh, Satish, Thala, Bijayda, Jayendrada, Ali, Nimaida, Nirmalya, Sabyasachi, Sanjay, Tapan, Tanayda, Mainakda, Pasarida, GKda, Pradiptada, Asimada, Sadanandada, Subhankarda, Srimantada, Hridayda, Vamsi and Sudiptada who made my stay pleasant at NUS.

I am thankful to Tong Yan and Keshmathy for their support at the Two-Photon microscopy facility. My thanks go to Daniel and Najwa at flow-cytometry facility and Yi Hui of Advanced Microscopy Laboratory at BSF-ASTAR. Financial and technical support from the Department of Chemistry of the National University of Singapore (NUS) is deeply acknowledged. I would like to be grateful all the staffs in chemistry administrative office, Lab-supplies for their immense support.

Words are insufficient to express my sincere thanks to Animeshda, Rajuda, Krishnakantada, Rudra, Samira, Yoges, Anand and Diana for being such a wonderful friend, colleague for all these years and supported me like my family member during my PhD.

Eventually, I would like to convey my deepest gratitude towards late grandparents, my parents, my brothers, my sister-in-law, my relatives and Myungwon Choi, my best friend in Singapore. I believe that without their continuous support, constant inspiration and prayers this thesis would not have been done.

Table of Contents

Summary

High throughput screening using fluorescent dye libraries has led the discovery of numerous novel sensors and bio-imaging probes in relatively faster manner. In Chapter 1, we have discussed the benefits of Diversity Oriented Fluorescence Library Approach over traditional designed approach. Next we aim for the development of two-photon fluorescent dye library because of its advantage over the one photon probes for tissue imaging application.

Two-photon (TP) fluorescence imaging has recently gained immense attention due to the deeper tissue penetration capability of near-infrared excitation light, localized excitation and less auto-fluorescence. Therefore in chapter 2, we designed and synthesized TP fluorescent dye libraries (named as **TPG** library and **TPC** library) composed of 80 molecules each. We designed these library based on 2-Acetyl-6-(dimethylamino)-naphthalene (ACEDAN) scaffold. **TPC** library have cyclic ring attached to the 6-amino group which results in more rigid conformation in comparison to **TPG** library.

In chapter 3, these combinatorial fluorescent dye libraries, **TPG** and **TPC** were applied to cell based screening with pancreatic cell lines. One alpha cell specific probe **TP-α** was discovered from the **TPG** library. We found that **TP-α** can selectively stain primary alpha cells of mice pancreatic Langerhans. The two-photon 3D imaging of **TP-α** stained islets revealed the scattered and surface localization of alpha cells in live intact islets. **TP-α** was also found to be useful for flow-cytometry study and alpha cell sorting. The *in vitro* study of **TP-α**, with glucagon along with insulin and various analytes revealed impressive selectivity towards glucagon. This

explains the selectivity of **TP-α** towards glucagon producing alpha cells over the insulin producing beta cells in the pancreatic islets.

After the alpha cell TP imaging of islet, we target to develop TP beta cell imaging probe in Chapter 4. Insulin producing beta cells are well studied due to their involvement in diabetes. Pancreatic Beta cells are known to have higher expression of Glucose transporter-2 (GLUT2) on its cell surface. GLUT2 is a high affinity glucose transporter and have superior affinity towards 2-Amino-2-deoxy-D-glucose (or 2-Glucosamine: GluN) over D-Glucose. We designed and synthesized D-GluN derivatives with various linker sizes and evaluated their cellular uptake in primary beta cells. We found six carbon chain length compounds have better uptake in comparison with other derivatives (C0, C2, C4 and C15-PEG) tested. The GLUT mediated uptake was evaluated by competition assay with D-glucose. C6-GluN compound was used for *ex vivo* pancreatic tissue imaging.

In Chapter 5, we set the goal to discover Polyphosphate sensor through *in-vitro* screening. Inorganic polyphosphate (PolyP), are polymer of phosphate groups and generally presents in mammalian cells and is associated with various metabolic diseases. Here we present the identification of novel fluorescent probes that allow specific labeling of synthetic polyP *in vitro* as well as endogenous polyP in live cells. These probes demonstrate high selectivity for the labeling of polyP. Use of these probes allowed us to demonstrate the real time detection of polyP release from lysosomes in live cells. Furthermore, we have detected the increased levels of polyP in live cells with Parkinson's disease related mutations.

List of Tables

List of Figures

Chapter 1

Chapter 2

Chapter 3

Chapter 4

Chapter 5

List of Charts

List of Schemes

List of Abbreviations

AcOH	Acetic acid
ACEDAN	2-acetyl-6-dimethylamino-naphtalene
BAPTA	(1,2-bis(o-aminophenoxy)ethane-N,N,N',N'-tetraacetic acid)
BCECF	(2',7'-Bis-(2-Carboxyethyl)-5-(and-6)-Carboxyfluorescein)
ACN	Acetonitrile
BSA	Bovine serum albumin
$CDCl_3$	Deuterated chloroform
CD_3OD	Deuterated Methanol
$CHCl_3$	Chloroform
DCM	Dichloromethane
DIEA	N,N-Diisopropylethylamine
DMEM	Dulbecco's modified Eagle's medium
DMF	N, N-Dimethylformamide
DMSO	Dimethyl sulfoxide
DMSO-d_6	Deuterated Dimethyl Sulfoxide
DOS	Diversity oriented synthesis
DOFL	Diversity oriented fluorescence library
DOFLA	Diversity oriented fluorescence library approach
EA	Ethyl acetate
ESI	Electrospray ionization
EtOH	Ethanol
Ex	Excitation
Em	Emission
FACS	Fluorescence-activated cell sorting

FDA	Food and Drug Administration
GluN	2-Amino-2-deoxy-D-glucose
GLUT	Glucose transporter
GY	Glucagon Yellow
h	hour
HATU	2-(1H-7-Azabenzotriazol-1-yl)-1,1,3,3-tetramethyl uranium hexafluorophosphate Methanaminium
HCl	Hydrochloric acid
HEPES	(4-(2-hydroxyethyl)-1-piperazineethanesulfonic acid)
HPLC	High-performance liquid chromatography
HPLC-MS	High-performance liquid chromatography mass Spectrometry
HRMS	High-resolution Mass Spectrometry
HTS	High throughput screening
KOH	Potassium Hydroxide
LSM	Laser Scanning Microscopy
MeI	Methyl iodide
MS	Mass spectrometry
MTT	(3-(4,5-Dimethylthiazol-2-yl)-2,5-Diphenyltetrazolium Bromide)
NADPH	Nicotinamide adenine dinucleotide phosphate
$NaHCO_3$	Sodium bicarbonate
NaI	Sodium iodide
NaOH	Sodium hydroxide

$Na_2S_2O_5$	Sodium metabisulfite
NBDG	2-[(7-nitro-2,1,3-benzoxadiazol-4-yl)amino]- 2-deoxy-D-glucose
NIR	Near infrared
NMP	N-Methylpyrrolidone
NMR	Nuclear magnetic resonance
OP	One photon
PBS	Phosphate buffer saline
QY	Quantum yield
rt	Room temperature
sat.	Saturated
TEA	Triethylamine
THF	Tetrahydrofuran
TP	Two-photon
TPA	Two-photon absorption
TPACS	Two-photon absorption cross section
TPLSM	Two-photon laser scanning microscopy
TPM	Two-photon microscopy
TOS	Target oriented synthesis
UV	Ultraviolet
V	Volume

List of Publications

- Make Caffeine visible: a fluorescent caffeine "traffic light" detector, Xu, W.; Kim, T. H.; Zhai, D.; Er, J. C.; Zhang, L.; Kale, A. A.; **Agrawalla, B. K.**; Cho, Y. K.; Chang, Y. T.* *Sci. Rep.* **2013**, 3, 2255.

- Development of fluorescent sensor for illicit date rape drug-GBL, Zhai, D.; **Agrawalla, B. K.**; Eng, E. S. F.; Lee, S. C.; Xu, W.; Chang, Y. T.* *Chem. Commun.* **2013**, 49, 6170-6172.

- In Situ Investigation of Mammalian Inorganic Polyphosphate Localization Using Novel Selective Fluorescent Probes JC-D7 and JC-D8, Angelova, P. R.; **Agrawalla, B. K.**; Elustondo, P. A.; Gordon, J.; Shiba, T.; Abramov, A. Y.; Chang, Y. T.*; Pavlov, E. V.* *ACS Chem Biol.* **2014**, *9*, 2101-2110. (co first author)

- Glucagon-Secreting Alpha Cell Selective Two-Photon Fluorescent Probe TP-α: For Live Pancreatic Islet Imaging, **Agrawalla, B. K.**; Chandran, Y.; Phue, W. H.; Lee, S. C.; Jeong, Y. M.; Wan, S. Y.; Kang, N. Y.*; Chang, Y. T.* *J. Am. Chem. Soc.* **2015**, 137, 5355-5362.

- Development of Targetable Two-Photon Fluorescent Probes to Image Hypochlorous Acid in Mitochondria and Lysosome in Live Cell and Inflamed Mouse Model, Yuan, L.; Wang, L.; **Agrawalla, B. K.**; Park, S. J.; Zhu, H.; Sivaraman, B.; Peng, J.; Xu, Q. H.; Chang, Y. T.* *J. Am. Chem. Soc.* **2015**, 137, in press.

- A novel and photo-stable probe, CDy6, for long-term real-time visualization of mitosis and proliferating cells. Jeong, Y. M.; Duanting, Z.; Hennig, H.; Samanta, A.; **Agrawalla, B. K.**; Bray, M. A.; Carpenter, A. E.; Chang, Y. T.* *Chem. Biol.* **2015**, 22, 299–307.

- Synthesis and Assessment of Beta Cell Specific Glucosamine Based Two-Photon Probe. **Agrawalla, B. K.**; Chang, Y. T.* Manuscript preparation.

List of patent filed

- “Discovery of Novel α-Cell Selective Probe For Ex-Vivo Two Photon Imaging of Alpha Cells In Intact Pancreatic Islets” Applicant: Bikram Keshari Agrawalla, Young-Tae Chang, National University of Singapore, ILO Ref: 14279N-US/PRV, HBSR Ref: 4459.1115-000

- “Development of β-cell targeting two-photon fluorescent probe based on glucosamine” Under preparation

Chapter 1

1.1 Introduction

Careful observation and logical interpretation has been the founding stone for modern science. Human understanding of microscopic subjects such as: cells, bacteria and other living organism has begun with the invention of Optical Microscope in the mid-16th century.[1] However these microscopic subjects are mostly transparent and required some kind of contrast staining for detailed visualization.[2] For this application several colorimetric dyes has been developed but most of them are unsuitable for the living samples. Whereas the intrinsic fluorescence/color of the chromophoric substances in the living cells (i.e. chlorophyll in plant cell and hemoglobin in red blood cells) was successfully utilized as the contrasting agents under microscope. The use of Ultra-Violet light as excitation source in microscope by Ellinger and Hirt in early 19th century opens a new era of Fluorescence Microscopy.[3] After which fluorescence microscopy has grown enormously with the development of both newer tools for microscope and novel fluorescent dyes. Last year "For the development of super-resolved fluorescence microscopy" the Nobel Prize in Chemistry 2014 was awarded jointly to Eric Betzig, Stefan W. Hell and William E. Moerner.[4] Soon after that, Prof Eric Betzig has reported the invention of rapid lattice light-sheet microscope. With these improvisation now it is possible to perform super-resolution fluorescent imaging of living cells for longer duration of time without toxicity.[5] These developments of fluorescent microscopy certainly create a further demand for more novel fluorescent probes suitable for live cell staining.

1.2 Fluorescence

Fluorescence is the process, in which a substance absorbs light of certain wavelength and emits a longer wavelength light usually after certain interval of time (nano seconds). The absorption of a photon can temporarily promote probe's electron from its ground state to excited state. The difference energy between the excitation and emission wavelength is called Stockes shift, which makes the fluorescence microscopy so useful and sensitive technique.[6] Simply filtering out the excitation light without blocking the emitted fluorescence is possible to see only the fluorescent object. The high sensitivity of this method makes it ideal for studying the distribution of substances in living cells.

1.3 Fluorescent probe

Improvements in fluorescent imaging has been possible because of new optical arrangements, sophisticated light sources, detectors and the most important among them, the novel fluorescent contrast agents. Among the various staining or contrast reagents in use, fluorescent probes represent one of the most widely developing fields.[7] This is because of the wide availability of fluorescent microscopes in laboratories, versatility of probes, easy handling and protein labeling capability. Fluorescent sensors are dyes that can act as "molecular spy" and can give information about, what is going on their molecular vicinity/neighborhood. This information can be seen as change in the fluorescent intensity, based on the change on the probe's environment (i.e. change in ionic concentration, or environmental pH). Fluorescent microscope is the instrument to read these signals and record the localization of probe in the cell. Various properties such

as fluorescent intensity, quantum yield, emission spectrum and lifetime can be used to encode the signal from the fluorescent compound. The most important challenge is to have the right dye at the right place in the cell which can give quantitative/qualitative information regarding the desired change.

Another reason behind the success of fluorescence microscopy is the high sensitivity of fluorescent probes, which can be utilized efficiently at micro-molar concentrations. Because of the bright fluorescent emission of the fluorescent dyes, it has been possible to resolve multiple dyes stained together in the same sample. The most important feature is ability to sense dynamic biological events. Fluorophore has shorter lifetimes (of nano second duration) that are short relative to most biological events. So the fluorescent sensors are suitable to read dynamic physiological changes (i.e. pH, ionic gradient Ca^{2+}) in living cells.

The Green fluorescent protein (GFP) is a well-known biological fluorophore, which was first used as a reporter for gene expression in the 1990s.[8] This work created a new era for fluorescence technique in biology. However, in real samples it is tedious and expensive to express the GFP and the expression label is also low.[9] Other than fluorescent proteins, quantum dots, were developed by Alex Ekimov in the 1980s.[10] The main advantages offered by Quantum dots are multiple color and high photo stability.[11] However the universal use of quantum dots are hindered by their higher cost and toxicity towards the cells.[12] In comparison to fluorescent proteins and quantum dots, fluorescent dyes are more adaptable because of the sensitivity, easy visibility and efficacy.[13] From the first intravital fluorescence imaging by Ellinger and Hirt in 1929 there has been enormous development of fluorescent probes.[2] Up to now, there are number of scaffolds

developed as efficient fluorophore and they cover almost all colors of the emission spectrum, from UV to Visible to NIR (**Figure 1.1**). The scaffolds includes pyrenes, naphthalene derivatives, coumarins, xanthone, fluorescein, NBD, rhodol, BODIPY, dapoxyl, styryl, Rhodamine, cyanines, quinolones, indoles, imidazoles, stilbene, phenathridines, squarine, phthalocyanines and oxazines.[14]

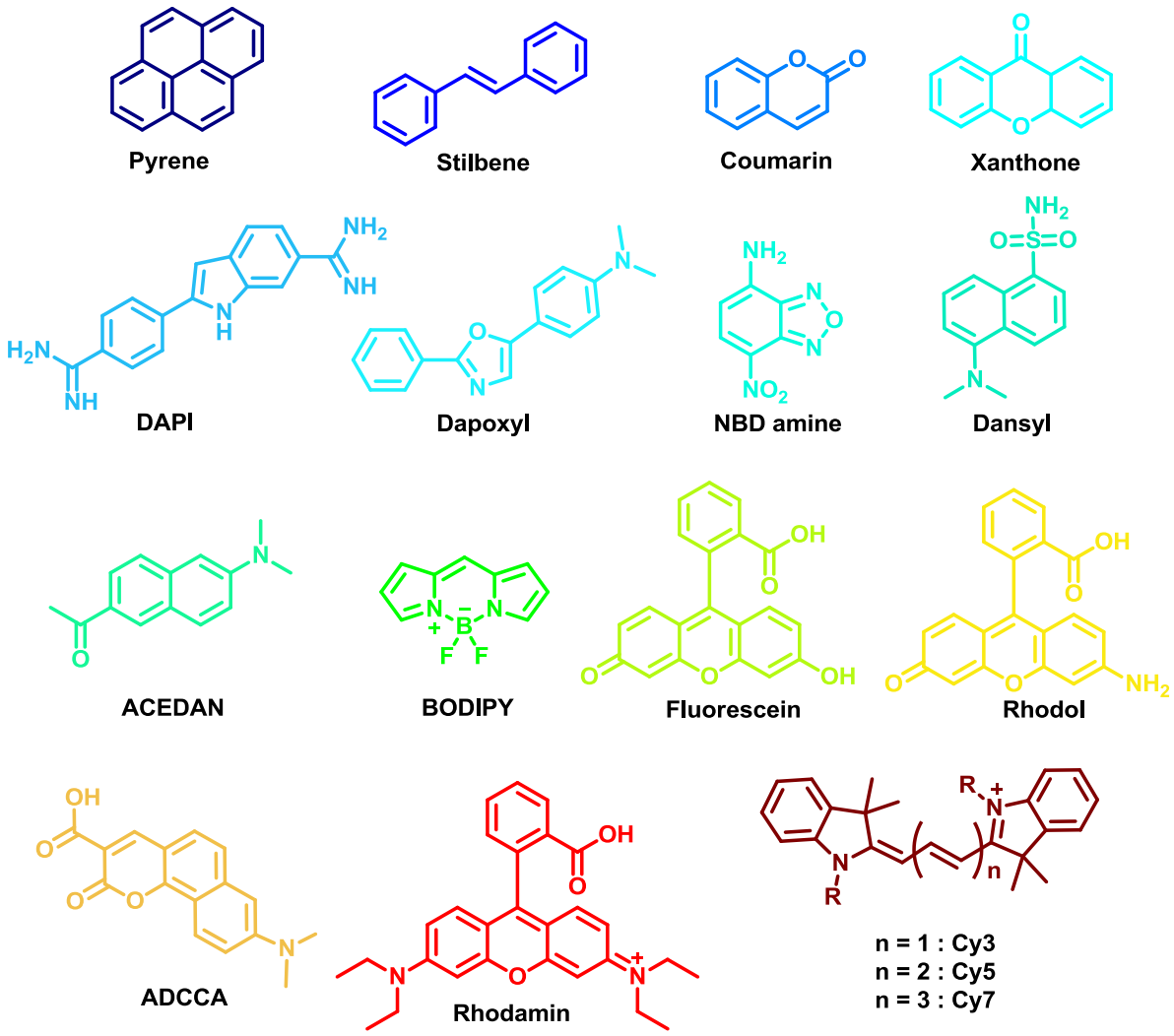

Figure 1.1 Representative Fluorophores with emission ranging from blue to NIR

1.4 Sensor development strategies

1.4.1 Design based approach

A sensor is an analytical device, which can detect or measure the physical quantity of an analyte or substance or otherwise responds to it. Among the various classes of sensors in use, optical sensors have received much attention recently. The optical sensors can be broadly categorized as absorbance sensor or fluorescence sensor. While absorbance sensor respond by change in absorbance, resulting visual color change. The fluorescence sensor can respond to the presence of analyte by either change in fluorescence intensity or by shift in emission wavelength. The classic example of absorbance sensor in use is Litmus papers, which show gradual color change with change in pH, uses colorimetric dyes which are responsive to different pH. Similarly various fluorescent dyes has been developed which show change in fluorescent intensity with change in pH.[15,16,17,18]

"Designed based approach" is one of the general technique for sensor development which utilizes a known molecular recognition motif for legend detection and a fluorophore for signal amplification. This knowledge-based architectural design has led the development of numerous sensors. The most robust pH-sensitive dyes are based on fluorescein (carboxyfluorescein, BCECF[19], SNARF[20]). Furthermore, various ion sensors are developed based on the known binding motifs.[21] Numerous sensors with different fluorescent core has been developed for Zn^{2+}, Fe^{2+}, Fe^{3+}, Mn^{2+}, Ni^{2+}, Co^{2+}, Pb^{2+}, Cd^{2+}, Hg^{2+} and more.[21,22] For ions like calcium and magnesium, large number of probes has been developed using BAPTA based chelator (quin2[23], indo-1[24], fura-2[25]). The

sodium selective SBFI[26] and potassium-selective PBFI[27] (crown ethers with slightly different cavity size suitable for each ion) have utilized to develop ion selective fluorescent probes. These known binding ligands have been efficiently used to develop numerous fluorescent sensors for selective ion sensing and imaging.

Similarly, based on the nature of cellular organelle and selective targeting motifs various organelle targeting fluorescent probes have been developed. Fatty acids has been efficiently utilized for the development of membrane probes.[28] Conventional positively charged fluorescent dyes Rhodamine 123 and tetramethyl-rosamine were mitochondria targeting.[29] Various more cationic probes have been developed with positively charged triphenylphosphonium and were found to target mitochondria.[30] Whereas the weakly basic amines are known to accumulate in the cellular compartment with low internal pH and has been used for developing various lysosome targeting probes.[31] These developments made various useful probes for specific organelle labeling and imaging.

However, the designed based approach can develop sensors or probes for targets which has been explored and studied earlier. Based on the experience and available knowledge new probes are developed with different fluorescent scaffold with similar sensing property. Whereas in biological research there are numerous proteins, enzymes and targets has not been explored yet. The knowledge based sensor development can provide the exact mechanism however; it is difficult to develop new probes for vast majority of new/unknown biological targets.

1.4.2 Diversity based approach

To overcome the difficulty of Target Oriented Approach, Diversity Oriented Synthesis (DOS) has recently been developed as a powerful tool for drug discovery.[32, 33,34,35,36] In this strategy; a lead molecule is modified by combinatorial chemistry to obtain large pool of compounds. Further screening of this diverse compounds against a variety of analytes by high-throughput manner may lead the rapid discovery of several potential molecules.[37] High-Throughput Screening (HTS) are of different type, such as enzymatic assay or cell line based and result in rapid discovery of novel active compounds.[37, 38] Due to the success of DOS in rapid drug discovery, several research groups including ours has adopted this approach for swift development of novel fluorescent sensors. We have named it Diversity Oriented Fluorescent Library Approach (DOFLA).[39, 40] In this approach one fluorescent scaffold is modified by combinatorial chemistry to generate huge pool of fluorescent compounds. These compounds were used in HTS with various sets of analytes or with panel of cell lines to discover selective probes[40] or sensors[41]. Within limited period of time DOFLA has generated numerous useful fluorescent sensors (e.g. GTP[42], DNA[43], green-RNA,[44] Glutathione,[45] Heparin,[46] β-amyloid,[47] chymotrypsin,[39] human serum albumin,[48] caffeine[49]) and bio-imaging probes from cell based screening (muscle differentiation inhibitor: B25**,** embryonic stem cell probe: CDy1,[50,51] human pluripotent stem cell probe,[52] microglia specific probe,[53] Neural stem cell selective probe,[54,55]) and more. Fluorescent imaging probes for such diverse and complex targets can be discovered rapidly by the use of combinatorial fluorescent libraries. These examples are evidence of the efficiency and power of DOFLA in rapid fluorescent sensor and bio-imaging probe development.

1.5 Two-photo fluorescence

Laser Scanning Microscopy (LSM) has revolutionized the bio-imaging studies. In LSM, the laser is focused to a diffraction-limited beam <1 μm in diameter and is scanned across the specimen. Confocal LSM provides depth discrimination and improves spatial resolution by the use of a pin-hole in front of detector, which rejects the out-off focus emissions. LSM images with impressive resolution have been obtained with the use of fluorescent probes that absorbs and emit visible light. But LSM images with ultraviolet (UV) absorbing fluorophore remain a challenge largely because of (i) lack of suitable microscopic lenses with good chromatic correction and transparency at UV region. (ii) photo-damage induced by the UV light to living cells and (iii) limited availability of UV lasers. For tissue imaging the excitation light wavelength dictate the depth of imaging. Near infra-red excitation are more suitable for deep tissue imaging or *in vivo* imaging because of the longer wave-length and deeper tissue penetration. Maria Goeppert-Mayer suggested in her doctoral dissertation in 1931 that, "by two-photon absorption the UV or visible absorbing compounds could be excited using longer wave length excitation light" (**Figure 1.2**).[56]

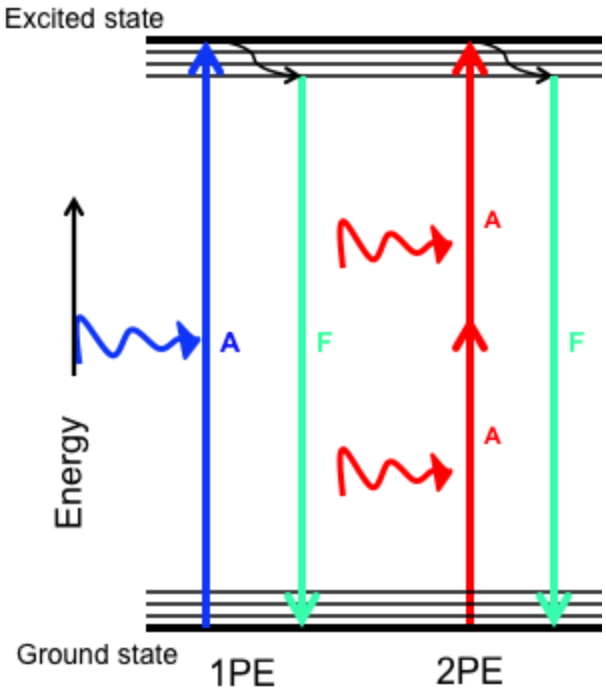

Figure 1.2 Jablonski diagram of single-photon and two-photon excitation.

The electronic energy levels and their vibrational substructure are shown with horizontal lines and the physical processes that cause transitions between these levels are depicted by vertical arrows; absorption-A, Fluorescence-F.

Two-photon (TP) excitation is possible by the very high local instantaneous intensity provided by focused femtosecond (fs) pulsed laser using LSM (**Figure 1.3 A**). With the invention of colliding mode-locked dye laser producing stream of pulses with duration of 100 fs at repetition rate of 80 MHz the TP excitation became a reality. With such high intensity and high repetition rate pulses the dye preset at the focal point have appreciable probability to absorb two long wavelength photons simultaneously and attain the excited state (**Figure 1.3 B**). With two-photon excitation (TPE) possible, the various UV and visible absorbing dyes can be used for deep tissue imaging (because of deeper penetration of longer wavelength light). But the high repetition resulted in higher photo bleaching, also different dyes show different two-photon absorption cross section

(TPACS). Molecules with large TPACS, δ, has suddenly become the center of demand for variety of applications with TP-excited fluorescence microscopy. These applications take advantages of the TPA feature, the ability to create excited states with photons of half excitation energy (this provides improved penetration in absorbing or scattering media). Unfortunately the most of the commercially available organic dyes have relatively small δ. The design strategies and structure property studies of TP absorption dyes has resulted in the synthesis of fluorescent molecules with unprecedented δ values (**Figure 1.4, 1.5** and **1.6**).[57]

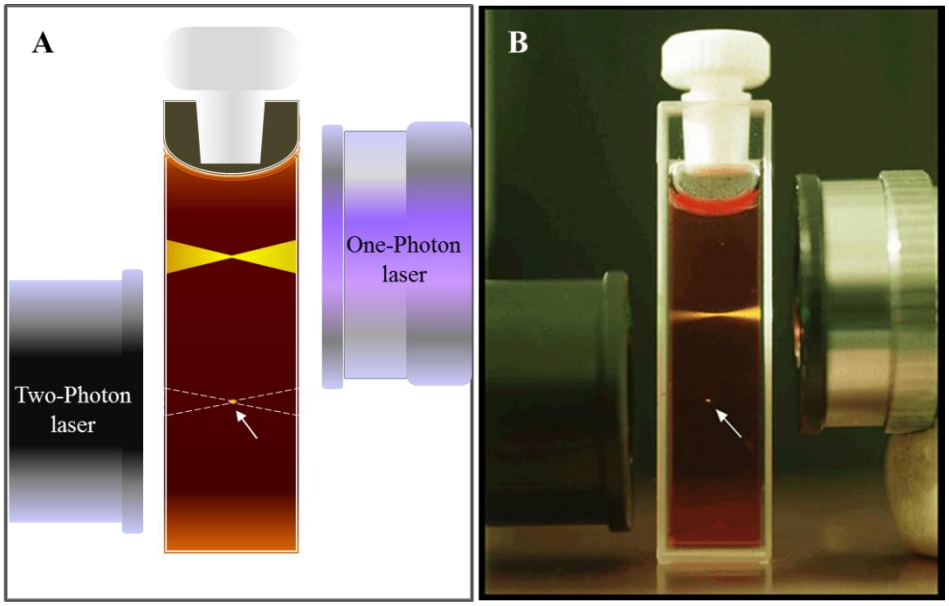

Figure 1.3 Comparison of one-photon and two-photon focal point

(A) The schematic illustration and (B) image; show the difference between ordinary single-photon excitation and two-photon excitation. The cuvette contains a solution of the dye *Safranin O*, which normally emits yellow light when excited by green. The upper lens focuses green (543 nm) light from a continuous-wave (CW) helium-neon laser into the cuvette (one-photon) and produces the expected conical pattern of excitation, fading to the left due the self-absorption in the concentrated dye solution. The lower objective lens focuses a pulsed infrared (1046 nm) beam from a neodymium-YLF laser (two-photon). One infrared photon alone is not sufficiently energetic to excite fluorescence, so that two photons need to team up and join their energies. This focal volume (**arrowed**) can be raster-scanned to anywhere in the cuvette thereby creating a point-wise, sequential

3-D representation of fluorescence intensity. (Image credit: Brad Amos/Science Photo Library, London).

On the molecular level, δ can be increased by combining three different structural elements: electron donating group (D), electron accepting group (A) and conjugated π-bridges that connects the acceptor and donor. As shown in the **Figure 1.4**, based on the spatial arrangement, the architecture can be simple dipolar or symmetric quadrupolar architecture. Moreover, the architecture are not limited to straight line, it can be more complex even 3D designs. All these architectures are designed to maximize the degree of charge transfer upon excitation while maintaining a strong dipole moment.

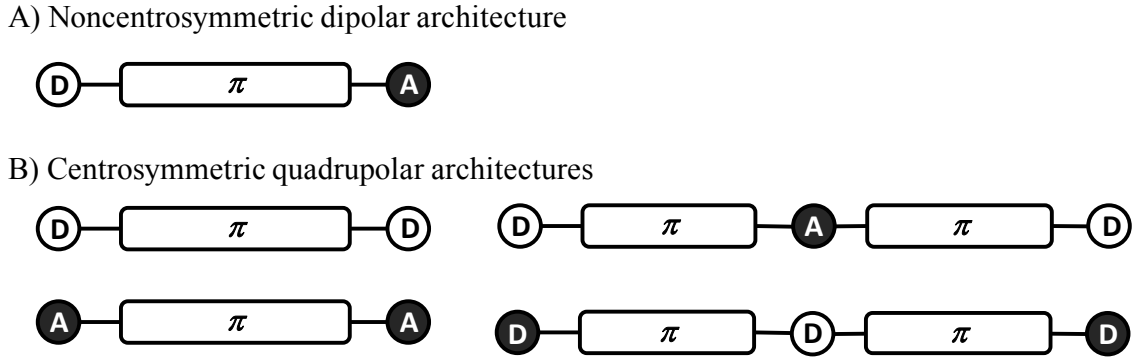

Figure 1.4 Molecular design of two-photon fluorophore

The structure property relationships for various designs approach are extensively reviewed[57, 58] some representative structures with large TPACS are showed in **Figure 1.5** and **Figure 1.6**.

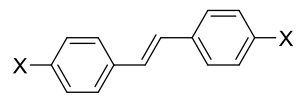

1, X = H, δ = 12 GM at 514 nm
2, X = NBu_2, δ = 110 GM at 620 nm
3, X = NPh_2, δ = 340 GM at 680 nm

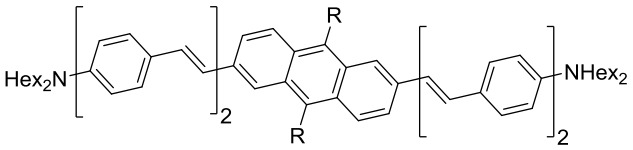

13, R = H, δ = 1100 GM at 800 nm
14, X = CN, δ = 5500 GM at 980 nm

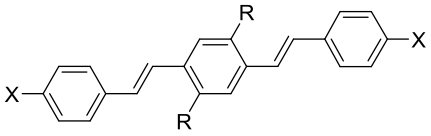

4, X = NBu_2, R = H, δ = 995 GM at 730 nm
5, X = NBu_2, R = OMe, δ = 900 GM at 730 nm
6, X = NPh_2, R = CN, δ = 1940 GM at 835 nm
7, X = NPh_2, R = Br, δ = 450 GM at 800 nm

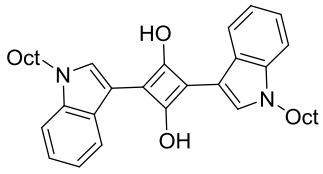

15, δ = 450 GM at 730 nm

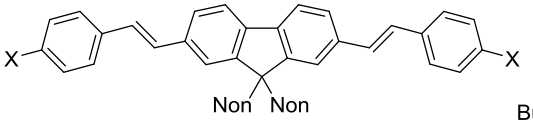

8, X = OMe, δ = 110 GM at 750 nm
9, X = NBu_2, δ = 1300 GM at 740 nm

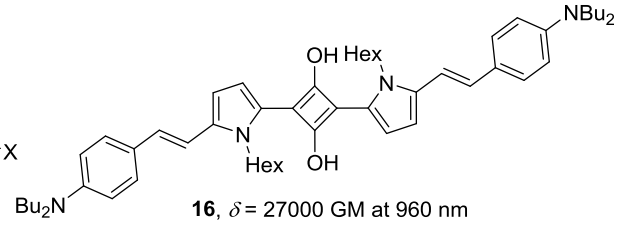

16, δ = 27000 GM at 960 nm

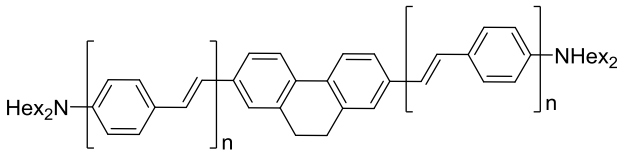

17,n = 1, δ = 1700 GM at 740 nm
18, n = 2, δ = 3300 GM at 740 nm

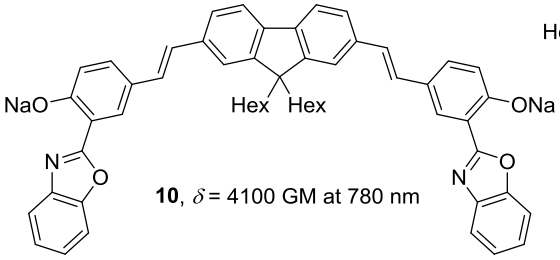

10, δ = 4100 GM at 780 nm

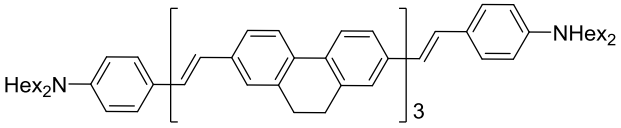

19, δ = 3800 GM at 740 nm

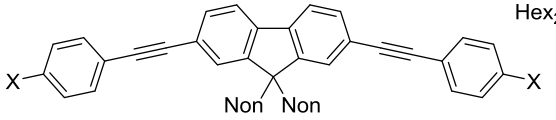

11, X = $NHex_2$, δ = 1200 GM at 705 nm
12, X = SO_2CF_3, δ = 83 GM at 705 nm

Figure 1.5 Representative examples of Two-photon fluorescent molecules with large TPACS-I

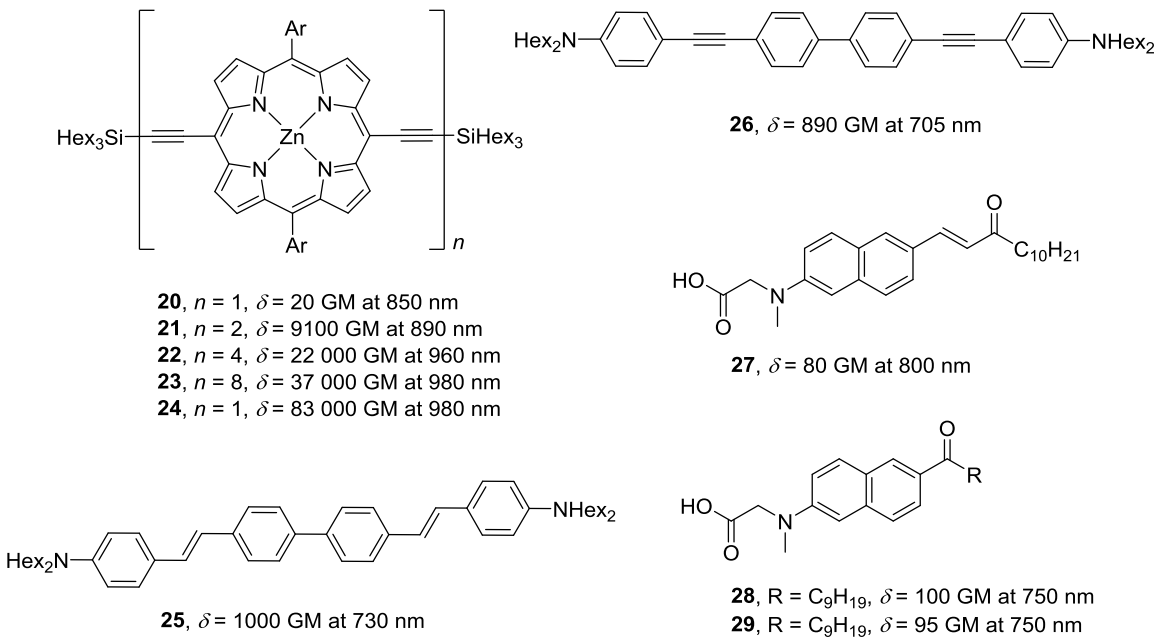

Figure 1.6 Representative examples of Two-photon fluorescent molecules with large TPACS -II

1.6 Scope and Outline

High-throughput screening in combination with diversity-oriented fluorescent library has become a robust way for discovery of novel fluorescent probes and sensors. Selective imaging probes for novel biological targets like neuronal stem cell, pluripotent stem cells have been discovered rapidly with DOFLA. Whereas traditional methods are more suitable for probes development aimed at well-studied targets, with exact mechanism of action known. In this thesis we explored both the DOFLA based approach and traditional targeted oriented approach for tissue imaging probe development. We began with the DOFLA based approach, and constructed combinatorial TP fluorescent dye libraries on solid support. From the cell based screening a novel alpha cell selective fluorescent probe was discovered. We develop this probe for TP pancreatic islet imaging. We used designed based approach for pancreatic beta cell selective probe development.

Insulin producing beta cells are well studied because of their involvement in diabetes and are known to have higher GLUT2 expression. We used 2-Glucosamine which is a high affinity GLUT2 ligand, for design and synthesis of beta cell selective probe.

The aim of this thesis:

1) Longer excitation wavelength is a key requirement for deeper tissue imaging. To develop two-photon fluorescent dye library, **TPG** and **TPC** library has been designed and synthesized based on ACEDAN scaffold. Solid phase synthesis technique was utilized as an efficient approach for the rapid development of TP libraries.
2) To discover novel pancreatic TP imaging probe, we established a cell based screening system with commercially available pancreatic cell lines. By screening **TPG** and **TPC** library we found one alpha cell selective probe **TP-α**. We further evaluated the selectivity of **TP-α** in mouse pancreatic islet cells. TP imaging of **TP-α** stained live pancreatic islet show the 3D distribution of alpha cells on the surface of the islet.
3) After the discovery of glucagon producing alpha cell selective probe, we aimed for the insulin producing beta cell probe development. Beta cells are known to have higher expression of GLUT2 on its cell surface. GLUT2 have higher affinity to D-Glucosamine over D-Glucose. By utilizing this fact, we synthesized Glucosamine conjugated TP probes. But, GLUTs mediated uptake may be affected by the distance between the TP fluorophore and D-Glucosamine. Among the various linker sized evaluated we found C6 have best uptake. We further used this probe for TP pancreatic tissue imaging.

4) Polyphosphate (polyP) is a polymer composed of many orthophosphates linked together by phosphoanhydride bonds. Recent investigations show, polyP have multiple important role in cellular metabolism both in eukaryotes and mammalians. Here we present the identification of novel fluorescent probes that allow for specific labeling of synthetic polyP *in vitro* as well as endogenous polyP in living cells. These probes demonstrate high selectivity for the labeling of polyP that was not sensitive to a number of ubiquitous organic polyphosphates, notably RNA. Use of these probes allowed us to demonstrate the real time detection of polyP release from lysosomes in live cells. Furthermore, we have been able to detect the increased levels of polyP in cells with Parkinson's disease related mutations.

1.7 Reference

1. Lemasters, B. H. a. J. J., Optical Microscopy: Emerging Methods and Applications. *Elsevier Inc.* **1993**.

2. R. W. Horobin, J. A. K., Conn's Biological Stains: A Handbook of Dyes, Stains and Fluorochromes for Use in Biology and Medicine. *bios.co.uk* **2002,** (10th Edition).

3. Kohen, E., Cell Structure and Function by Microspectrofluorometry. Elsevier Inc. 1989, (ISBN: 978-0-12-417760-4).

4. The Nobel Prize in Chemistry 2014. *Nobelprize.org. Nobel Media AB 2014. Web.* **2014,** (<http://www.nobelprize.org/nobel_prizes/chemistry/laureates/2014/>).

5. Chen, B. C.; Legant, W. R.; Wang, K.; Shao, L.; Milkie, D. E.; Davidson, M. W.; Janetopoulos, C.; Wu, X. S.; Hammer, J. A., 3rd; Liu, Z.; English, B. P.; Mimori-Kiyosue, Y.; Romero, D. P.; Ritter, A. T.; Lippincott-Schwartz, J.; Fritz-Laylin, L.; Mullins, R. D.; Mitchell, D. M.; Bembenek, J. N.; Reymann, A. C.; Bohme, R.; Grill, S. W.; Wang, J. T.; Seydoux, G.; Tulu, U. S.; Kiehart, D. P.; Betzig, E., Lattice light-sheet microscopy: imaging molecules to embryos at high spatiotemporal resolution. *Science* **2014,** *346* (6208), 1257998.

6. Lakowicz, J. R., *Principles of fluorescence spectroscopy*. Plenum Press: New York, 1983; p xiv, 496 p.

7. (a) Slavik, J., Fluorescent Probes in Cellular and Molecular Biology **1994**; (b) Mason, W. T., Fluorescent and Luminescent Probes for Biological Activity (Second Edition), A Practical Guide to Technology for Quantitative Real-Time Analysis, A volume in Biological Techniques Series. *Elsevier Ltd.* **1999**.

8. Chalfie, M.; Tu, Y.; Euskirchen, G.; Ward, W. W.; Prasher, D. C., Green fluorescent protein as a marker for gene expression. *Science* **1994,** *263* (5148), 802-5.

9. Miyawaki, A.; Sawano, A.; Kogure, T., Lighting up cells: labelling proteins with fluorophores. *Nature cell biology* **2003,** *Suppl*, S1-7.

10. Ekimov, A., Growth and optical properties of semiconductor nanocrystals in a glass matrix. *J. Lumin.* **1996,** (70), 1-20.

11. Delehanty, J. B.; Bradburne, C. E.; Susumu, K.; Boeneman, K.; Mei, B. C.; Farrell, D.; Blanco-Canosa, J. B.; Dawson, P. E.; Mattoussi, H.; Medintz, I. L., Spatiotemporal multicolor labeling of individual cells using peptide-functionalized quantum dots and mixed delivery techniques. *Journal of the American Chemical Society* **2011,** *133* (27), 10482-9.

12. Lovric, J.; Cho, S. J.; Winnik, F. M.; Maysinger, D., Unmodified cadmium telluride quantum dots induce reactive oxygen species formation leading to multiple organelle damage and cell death. *Chemistry & biology* **2005,** *12* (11), 1227-34.

13. Giepmans, B. N.; Adams, S. R.; Ellisman, M. H.; Tsien, R. Y., The fluorescent toolbox for assessing protein location and function. *Science* **2006,** *312* (5771), 217-24.

14. Lavis, L. D.; Raines, R. T., Bright ideas for chemical biology. *ACS chemical biology* **2008,** *3* (3), 142-55.

15. Bassnett S, R. L., Beebe DC, Intracellular pH measurement using single excitation-dual emission fluorescence ratios. *Am. J. Physiol.* **1990,** *258*, C171-C178.

16. Kermis, H. R.; Kostov, Y.; Harms, P.; Rao, G., Dual excitation ratiometric fluorescent pH sensor for noninvasive bioprocess monitoring: development and application. *Biotechnology progress* **2002,** *18* (5), 1047-53.

17. Wang, Z.; Zheng, G.; Lu, P., 9-(cycloheptatrienylidene)-fluorene derivative: remarkable ratiometric pH sensor and computing switch with NOR logic gate. *Organic letters* **2005,** *7* (17), 3669-72.

18. Niu, C. G.; Gui, X. Q.; Zeng, G. M.; Guan, A. L.; Gao, P. F.; Qin, P. Z., Fluorescence ratiometric pH sensor prepared from covalently immobilized porphyrin and benzothioxanthene. *Analytical and bioanalytical chemistry* **2005,** *383* (2), 349-57.

19. Ozkan, P.; Mutharasan, R., A rapid method for measuring intracellular pH using BCECF-AM. *Biochimica et biophysica acta* **2002,** *1572* (1), 143-8.

20. Tsien, R. Y., Fluorescent indicators of ion concentrations. *Methods in cell biology* **1989,** *30*, 127-56.

21. Carter, K. P.; Young, A. M.; Palmer, A. E., Fluorescent sensors for measuring metal ions in living systems. *Chemical reviews* **2014,** *114* (8), 4564-601.

22. Zhang, J. F.; Zhou, Y.; Yoon, J.; Kim, J. S., Recent progress in fluorescent and colorimetric chemosensors for detection of precious metal ions (silver, gold and platinum ions). *Chemical Society reviews* **2011,** *40* (7), 3416-29.

23. Tsien, R.; Pozzan, T., Measurement of cytosolic free Ca2+ with quin2. *Methods in enzymology* **1989,** *172*, 230-62.

24. Grynkiewicz, G.; Poenie, M.; Tsien, R. Y., A new generation of Ca2+ indicators with greatly improved fluorescence properties. *The Journal of biological chemistry* **1985,** *260* (6), 3440-50.

25. Poenie, M.; Tsien, R., Fura-2: a powerful new tool for measuring and imaging [Ca2+]i in single cells. *Progress in clinical and biological research* **1986,** *210*, 53-6.

26. Minta, A.; Tsien, R. Y., Fluorescent indicators for cytosolic sodium. *The Journal of biological chemistry* **1989,** *264* (32), 19449-57.

27. Kasner, S. E.; Ganz, M. B., Regulation of intracellular potassium in mesangial cells: a fluorescence analysis using the dye, PBFI. *The American journal of physiology* **1992,** *262* (3 Pt 2), F462-7.

28. Thumser, A. E.; Storch, J., Characterization of a BODIPY-labeled fluorescent fatty acid analogue. Binding to fatty acid-binding proteins, intracellular localization and metabolism. *Molecular and cellular biochemistry* **2007,** *299* (1-2), 67-73.

29. Johnson, L. V.; Walsh, M. L.; Chen, L. B., Localization of mitochondria in living cells with rhodamine 123. *Proceedings of the National Academy of Sciences of the United States of America* **1980,** *77* (2), 990-4.

30. Dhanasekaran, A.; Kotamraju, S.; Kalivendi, S. V.; Matsunaga, T.; Shang, T.; Keszler, A.; Joseph, J.; Kalyanaraman, B., Supplementation of endothelial cells with mitochondria-targeted antioxidants inhibit peroxide-induced mitochondrial iron uptake, oxidative damage and apoptosis. *The Journal of biological chemistry* **2004,** *279* (36), 37575-87.

31. Liu, T.; Xu, Z.; Spring, D. R.; Cui, J., A lysosome-targetable fluorescent probe for imaging hydrogen sulfide in living cells. *Organic letters* **2013,** *15* (9), 2310-3.

32. Spandl, R. J.; Diaz-Gavilan, M.; O'Connell, K. M.; Thomas, G. L.; Spring, D. R., Diversity-oriented synthesis. *Chemical record* **2008,** *8* (3), 129-42.

33. Galloway, W. R.; Isidro-Llobet, A.; Spring, D. R., Diversity-oriented synthesis as a tool for the discovery of novel biologically active small molecules. *Nature communications* **2010,** *1*, 80.

34. Tan, D. S., Diversity-oriented synthesis: exploring the intersections between chemistry and biology. *Nature chemical biology* **2005,** *1* (2), 74-84.

35. CJ, O. C.; Beckmann, H. S.; Spring, D. R., Diversity-oriented synthesis: producing chemical tools for dissecting biology. *Chemical Society reviews* **2012,** *41* (12), 4444-56.

36. Hung, A. W.; Ramek, A.; Wang, Y.; Kaya, T.; Wilson, J. A.; Clemons, P. A.; Young, D. W., Route to three-dimensional fragments using diversity-oriented synthesis. *Proceedings of the National Academy of Sciences of the United States of America* **2011,** *108* (17), 6799-804.

37. Ibbeson, B. M.; Laraia, L.; Alza, E.; CJ, O. C.; Tan, Y. S.; Davies, H. M.; McKenzie, G.; Venkitaraman, A. R.; Spring, D. R., Diversity-oriented synthesis as a tool for identifying new modulators of mitosis. *Nature communications* **2014,** *5*, 3155.

38. Kuruvilla, F. G.; Shamji, A. F.; Sternson, S. M.; Hergenrother, P. J.; Schreiber, S. L., Dissecting glucose signalling with diversity-oriented synthesis and small-molecule microarrays. *Nature* **2002,** *416* (6881), 653-7.

39. Wang, S.; Kim, Y. K.; Chang, Y. T., Diversity-oriented fluorescence library approach (DOFLA) to the discovery of chymotrypsin sensor. *Journal of combinatorial chemistry* **2008,** *10* (3), 460-5.

40. Yun, S. W.; Kang, N. Y.; Park, S. J.; Ha, H. H.; Kim, Y. K.; Lee, J. S.; Chang, Y. T., Diversity oriented fluorescence library approach (DOFLA) for live cell imaging probe development. *Accounts of chemical research* **2014,** *47* (4), 1277-86.

41. Kang, N. Y.; Ha, H. H.; Yun, S. W.; Yu, Y. H.; Chang, Y. T., Diversity-driven chemical probe development for biomolecules: beyond hypothesis-driven approach. *Chemical Society reviews* **2011,** *40* (7), 3613-26.

42. Wang, S.; Chang, Y. T., Combinatorial synthesis of benzimidazolium dyes and its diversity directed application toward GTP-selective fluorescent chemosensors. *Journal of the American Chemical Society* **2006,** *128* (32), 10380-1.

43. Feng, S.; Kim, Y. K.; Yang, S.; Chang, Y. T., Discovery of a green DNA probe for live-cell imaging. *Chem. Commun.* **2010,** *46* (3), 436-8.

44. Li, Q.; Kim, Y.; Namm, J.; Kulkarni, A.; Rosania, G. R.; Ahn, Y. H.; Chang, Y. T., RNA-selective, live cell imaging probes for studying nuclear structure and function. *Chemistry & biology* **2006,** *13* (6), 615-23.

45. Ahn, Y. H.; Lee, J. S.; Chang, Y. T., Combinatorial rosamine library and application to *in vivo* glutathione probe. *Journal of the American Chemical Society* **2007,** *129* (15), 4510-1.

46. Wang, S.; Chang, Y. T., Discovery of heparin chemosensors through diversity oriented fluorescence library approach. *Chem. Commun.* **2008,** (10), 1173-5.

47. Li, Q.; Min, J.; Ahn, Y. H.; Namm, J.; Kim, E. M.; Lui, R.; Kim, H. Y.; Ji, Y.; Wu, H.; Wisniewski, T.; Chang, Y. T., Styryl-based compounds as potential *in vivo* imaging agents for beta-amyloid plaques. *Chembiochem : a European journal of chemical biology* **2007,** *8* (14), 1679-87.

48. Ahn, Y. H.; Lee, J. S.; Chang, Y. T., Selective human serum albumin sensor from the screening of a fluorescent rosamine library. *Journal of combinatorial chemistry* **2008,** *10* (3), 376-80.

49. Xu, W.; Kim, T. H.; Zhai, D.; Er, J. C.; Zhang, L.; Kale, A. A.; Agrawalla, B. K.; Cho, Y. K.; Chang, Y. T., Make caffeine visible: a fluorescent caffeine "traffic light" detector. *Scientific reports* **2013,** *3*, 2255.

50. Im, C. N.; Kang, N. Y.; Ha, H. H.; Bi, X.; Lee, J. J.; Park, S. J.; Lee, S. Y.; Vendrell, M.; Kim, Y. K.; Lee, J. S.; Li, J.; Ahn, Y. H.; Feng, B.; Ng, H. H.; Yun, S. W.; Chang, Y. T., A fluorescent rosamine compound selectively stains pluripotent stem cells. *Angewandte Chemie* **2010,** *49* (41), 7497-500.

51. Kang, N. Y.; Yun, S. W.; Ha, H. H.; Park, S. J.; Chang, Y. T., Embryonic and induced pluripotent stem cell staining and sorting with the live-cell fluorescence imaging probe CDy1. *Nature protocols* **2011,** *6* (7), 1044-52.

52. Hirata, N.; Nakagawa, M.; Fujibayashi, Y.; Yamauchi, K.; Murata, A.; Minami, I.; Tomioka, M.; Kondo, T.; Kuo, T. F.; Endo, H.; Inoue, H.; Sato, S.; Ando, S.; Kawazoe, Y.; Aiba, K.; Nagata, K.; Kawase, E.; Chang, Y. T.; Suemori, H.; Eto, K.; Nakauchi, H.; Yamanaka, S.; Nakatsuji, N.; Ueda, K.; Uesugi, M., A chemical probe that labels human pluripotent stem cells. *Cell reports* **2014,** *6* (6), 1165-74.

53. Leong, C. L., S. C.; Ock, J.; See, P.; Park, S. J.; Ginhoux, F.; Yun, S. W. Chang, Y. T., Microglia specific fluorescent probe for live cell imaging. *Chem. Commun.* **2014,** *50*, 1089-1091

54. Leong, C.; Zhai, D.; Kim, B.; Yun, S. W.; Chang, Y. T., Neural stem cell isolation from the whole mouse brain using the novel FABP7-binding fluorescent dye, CDr3. *Stem cell research* **2013,** *11* (3), 1314-22.

55. Yun, S. W.; Leong, C.; Zhai, D.; Tan, Y. L.; Lim, L.; Bi, X.; Lee, J. J.; Kim, H. J.; Kang, N. Y.; Ng, S. H.; Stanton, L. W.; Chang, Y. T., Neural stem cell specific fluorescent chemical probe binding to FABP7. *Proceedings of the National Academy of Sciences of the United States of America* **2012,** *109* (26), 10214-7.

56. M, G.-M., Über Elementarakte mit zwei Quantensprüngen. *Annals of Physics* **1931,** *9* (3), 273-295.

57. Albota, M.; Beljonne, D.; Bredas, J. L.; Ehrlich, J. E.; Fu, J. Y.; Heikal, A. A.; Hess, S. E.; Kogej, T.; Levin, M. D.; Marder, S. R.; McCord-Maughon, D.; Perry, J. W.; Rockel, H.; Rumi, M.; Subramaniam, G.; Webb, W. W.; Wu, X. L.; Xu, C., Design of organic molecules with large two-photon absorption cross sections. *Science* **1998,** *281* (5383), 1653-6.

58. Pawlicki, M.; Collins, H. A.; Denning, R. G.; Anderson, H. L., Two-photon absorption and the design of two-photon dyes. *Angewandte Chemie* **2009,** *48* (18), 3244-66.

Chapter: 2

Solid phase synthesis of two-Photon Fluorescent dye libraries

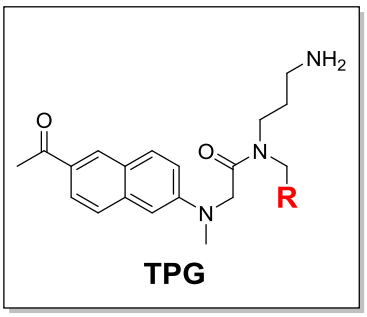

TPG

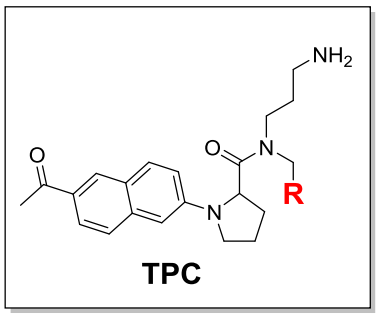

TPC

Chapter 2

2.1 Introduction

Two-photon laser scanning microscopy (TPLSM) uses high-pulsed TP excitation laser to induce fluorescence and has been known as a powerful technique for three-dimensional (3D) imaging of cell and tissue. This technique provides deeper tissue penetration and higher resolution by localized excitation. At near infra-red (NIR) wavelength region (700-1100 nm) the tissue remains comparatively transparent.[1] The localized excitation also significantly decreases the photo-bleaching and photo-degradation of the TP probes in biological sample due to tiny localized excitation of sub-femtoliter volume, which results in high contrast three-dimensional images.[2]

These applications are subject to the availability of fluorescent probes with large two-photo absorption cross section (TPACS). But the number of TP fluorophore is limited. Webb et al. have done a systematic study of TP absorption property of various commercially available fluorescent probes.[3] A general observation is that, even though the probes have been useful in one-photon bio-imaging application but their TP absorption cross sections are low ranging from several GM to tens of GM. Very few commercial probes, such as Rhodamine B has a maximum TPACS of 200 GM, but for it photo-stability is low.[3] With the advancement and availability of TP laser scanning microscopy, the development of improved fluorophore with better TP absorption cross section has begun.[4,5]

The availability of new TP fluorescent probe will enable cell and tissue imaging with higher sensitivity, greater penetration depth, better resolution and lower photo damage.[1, 2] However most of the early developed high TPA probes were highly hydrophobic in nature and have higher molecular mass.[6,7,8,9] Among the various TPA

scaffold reported, we focus on 2-acetyl-6-dimethylamino-naphtalene (ACEDAN) for systematic library generation. So far ACEDAN scaffold has been successfully demonstrated for TP imaging probe for cell membrane and for various metal ion detection in live cell and tissue.[10] This scaffold exhibited good photo physical properties such as, optimum TPA (100 GM), excellent photo stability, good quantum yield, low pH-dependence and good solubility in various solvents.[11] With an intention to develop, more novel TP fluorescent probes, we designed and synthesized ACEDAN based combinatorial fluorescent dye libraries (**TPG** and **TPC**).

2.2 Objective

Here we developed the solid phase diversity methodology of ACEDAN derived TP libraries **TPG** and **TPC**. These TP libraries compounds were further diversified to their corresponding acetyl (**TPGAC** and **TPCAC**) and chloro-acetyl (**TPGCA** and **TPCCA**) derivatives using a simple but powerful solid phase activated ester chemistry. This chapter mainly covers the synthesis and photo-physical characterization of **TPG** and **TPC** library compounds and its future prospect for development of TP bio-imaging probe.

2.3 Result and discussion

2.3.1 Design and synthesis of TPG library on solid support

For **TPG** library synthesis (**Scheme 2.1**), carboxylic acid containing ACEDAN scaffold was used as the key intermediate. The general synthetic strategy of TPG acid include four steps (43 % overall yield). First, methyl 2-((6-acetylnaphthalen-2-yl)(methyl)amino)acetate **D** was synthesized according to reported procedure (Cho et al.), then followed by basic hydrolysis of that ester provide the key intermediate **TPG acid**.[11] The structurally diverse TPG library was synthesized using previously

reported robust solid phase synthesis technique.[13] Here the wide structural diversity was introduced by the use of solid phase secondary amines **G** utilizing a simple reaction between the bromopropylamine loaded resins with the series of primary amines (**Chart 2.1**). Then the key intermediate **TPG acid** was coupled to the solid phase amine building block by using a standard acid-amine coupling protocol.[13-14] The final step of acid cleavage from the solid supported compounds **H** yield 80 pure members of the **TPG library** (average purity 90 % without further purification at 350 nm, **Table 2.1, Table 2.2 and Table 2.3**).

Scheme 2.1 General synthetic scheme of **TPG** library.

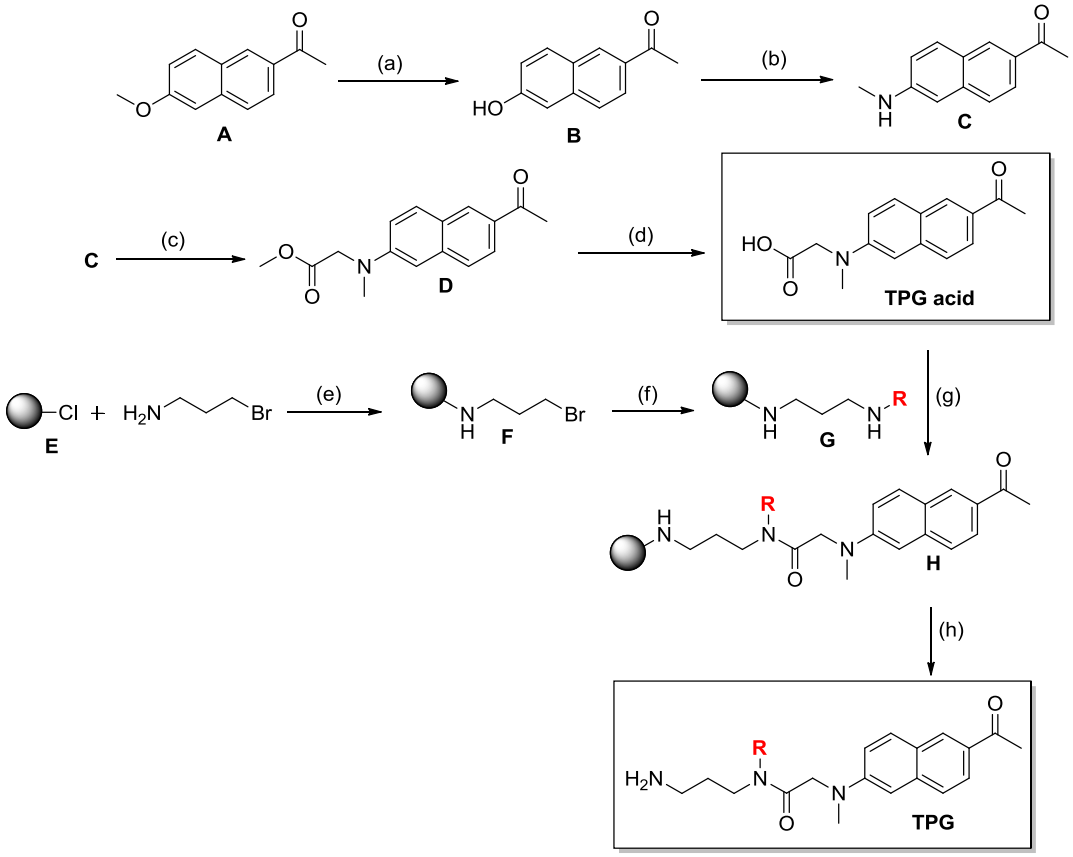

Reagents and conditions: (a) Conc. HCl, DCM, TEA, 2 h at 110 °C. (b) Methylamine, $Na_2S_2O_5$, H_2O, 4 h at 140° C (Microwave). (c) Methylbromoacetate, Na_2HPO_4, NaI, Acetonitrile, MW, 2 h at 140 °C. (d) KOH, EtOH, 5 h at rt. (e) DIEA, THF, 12 h at rt. (f) DIEA, RNH_2 (amine building blocks), NMP, 12 h at 70 °C. (g) HATU, DIEA, DMF, 24 h at rt. (h) 5 % TFA in DCM, 15 min at rt. R is 80 different amines (**Chart 2.1**)

Scheme 2.2 **TPGAC** and **TPGCA** library synthesis

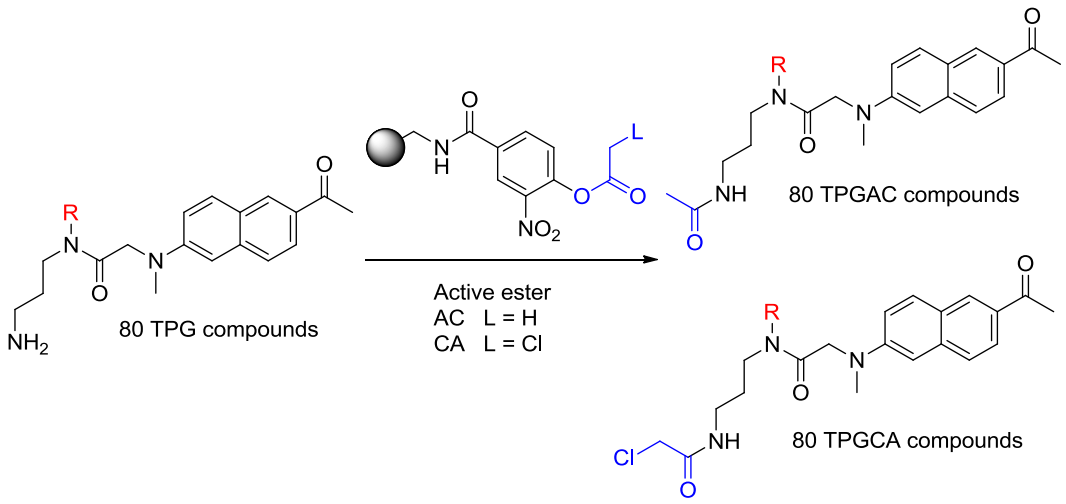

Reagents and conditions: (a) DCM/ACN (7:1), (2 μL) catalytic amount of saturated $NaHCO_3$, 2 h at rt. R is 80 different amines (**Chart 2.1**)

2.3.1.1 Photo-physical property measurement

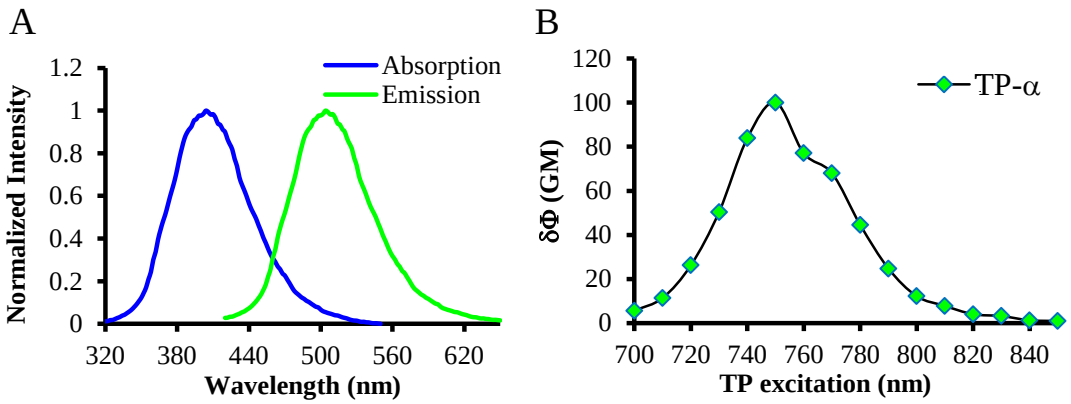

Figure 2.1 One-photon and two-photon optical property of TPG-456.

(A) One-photon absorption and emission spectra for TPG-456 1 μM in PBS buffer (pH = 7.4). (B) Two-photon action cross section of TPG-456 measured in ethanol at 10 μM concentration.

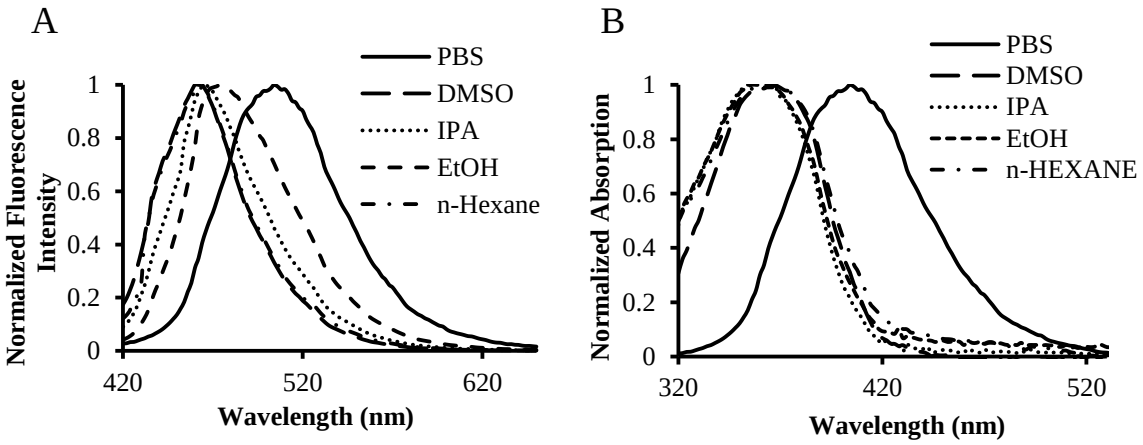

Figure 2.2 Absorption and emission spectra of TPG-456 in different solvents.

(A) Solvent dependent fluorescence shift of TPG-456 with various polar and non-polar solvents. (B) Solvent dependent absorption shift of TPG-456. All optical property measured using 10 μM of compounds in Phosphate Buffer (PBS) pH.7.4, DMSO, Isopropyl alcohol, Ethanol and n-Hexane.

Chart 2.1 Amine building blocks for TPG library

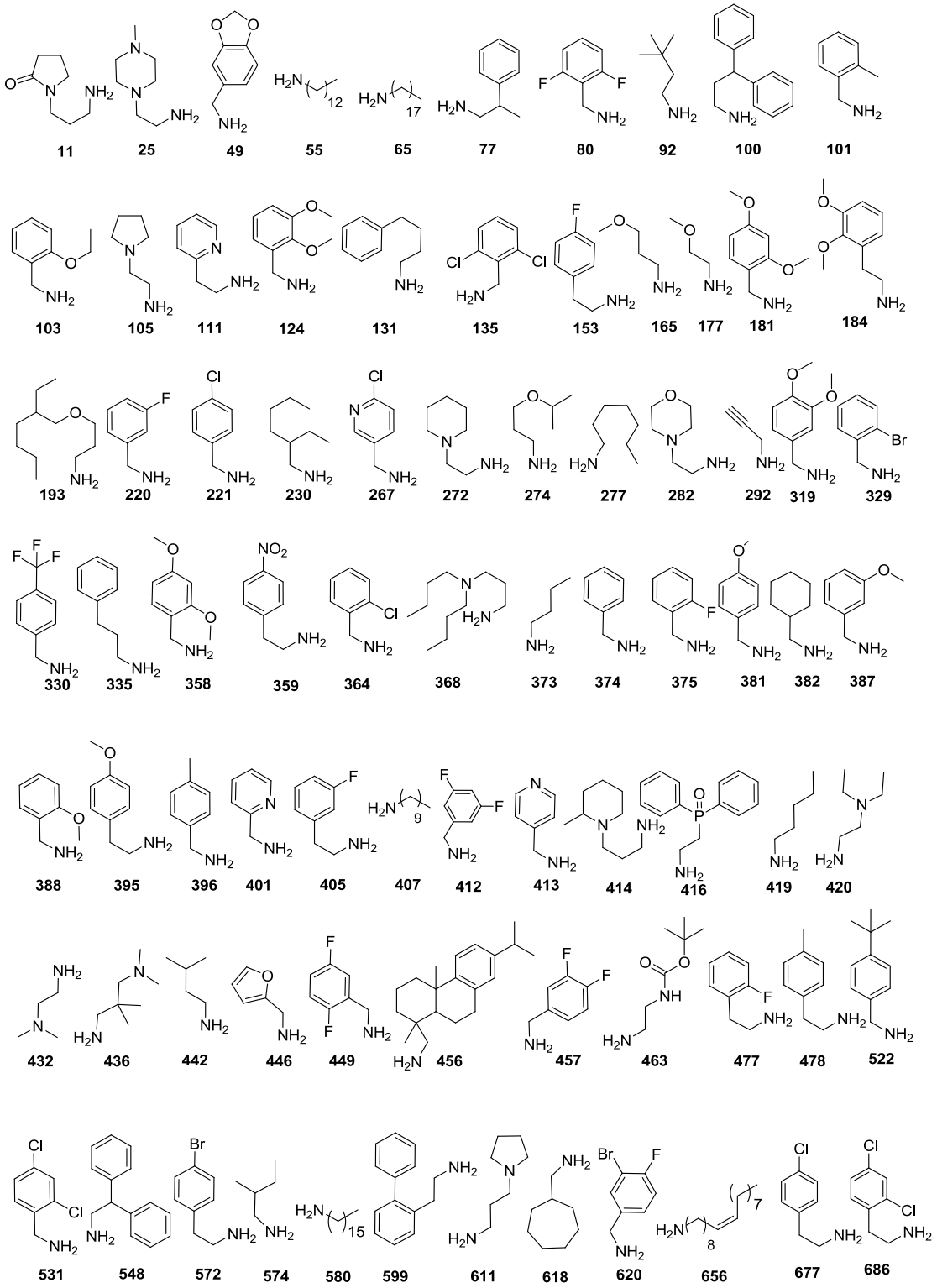

Table 2.1 Spectroscopic properties and purity table for **TPG** library

Calculated mass, experimental mass, absorbance maximum (λ_{abs}), fluorescent emission maximum (λ_{em}), quantum yield (Φ) and purity.

UC	**M**$^{+}$ (cal)	**M**$^{+}$**1**(exp.)	**Abs**(nm)	**Em**(nm)	***QY**(Φ)	[a]**Purity** (%)
TPG-11	438.26	439.26	363	460	0.49	98
TPG-25	439.29	440.29	361	460	0.42	93
TPG-49	447.22	448.22	361	461	0.48	85
TPG-55	495.38	496.38	361	461	0.37	91
TPG-65	565.46	566.46	355	460	0.44	85
TPG-77	431.26	432.26	367	460	0.60	98
TPG-80	439.21	440.21	363	460	0.49	98
TPG-92	397.27	398.27	359	460	0.38	98
TPG-100	507.29	508.29	360	460	0.52	97
TPG-101	417.24	418.24	361	462	0.48	99
TPG-103	447.25	448.25	363	460	0.43	95
TPG-105	410.27	411.27	362	460	0.50	97
TPG-111	418.24	419.24	363	462	0.29	95
TPG-124	463.25	464.25	359	461	0.39	97
TPG-131	445.27	446.27	363	460	0.23	98
TPG-135	471.15	472.15	358	460	0.53	96
TPG-153	471.21	472.21	364	461	0.44	97
TPG-165	385.24	386.24	352	464	0.30	98
TPG-177	371.22	372.22	369	461	0.31	98
TPG-181	463.25	464.25	361	460	0.65	99
TPG-184	477.26	478.26	358	460	0.78	97
TPG-193	483.35	484.35	361	463	0.35	92
TPG-220	421.22	422.22	362	460	0.63	96
TPG-221	437.19	438.19	360	460	0.36	97
TPG-230	425.30	426.30	361	460	0.59	95
TPG-266	477.26	478.26	368	460	0.59	95
TPG-267	438.18	439.18	360	461	0.42	91
TPG-274	413.27	414.27	366	460	0.29	99
TPG-277	411.29	412.29	369	462	0.32	97
TPG-282	426.26	427.26	363	460	0.38	91
TPG-292	351.19	352.19	359	455	0.66	81
TPG-319	463.25	464.25	359	461	0.59	96
TPG-329	517.11	518.11	353	458	0.42	89
TPG-330	471.21	472.21	360	460	0.68	95
TPG-335	431.26	432.26	369	460	0.34	97
TPG-358	499.22	500.22	362	460	0.48	98
TPG-359	498.20	499.20	376	450	0.17	92
TPG-364	437.19	438.19	361	462	0.54	97

TPG-368	482.36	483.36	361	460	0.36	93
TPG-373	369.24	370.24	363	460	0.41	97
TPG-374	403.23	404.23	358	460	0.52	98
TPG-375	421.22	422.22	363	462	0.44	94
TPG-381	433.24	434.24	369	460	0.68	95
TPG-382	409.27	410.27	368	460	0.45	92
TPG-387	433.24	434.24	360	460	0.40	97
TPG-388	433.24	434.24	361	462	0.43	97
TPG-395	447.25	448.25	367	461	0.62	98
TPG-396	417.24	418.24	359	461	0.32	98
TPG-401	404.22	405.22	360	462	0.42	91
TPG-405	435.23	436.23	358	461	0.35	92
TPG-407	453.34	454.34	361	460	0.56	96
TPG-412	439.21	440.21	359	460	0.72	98
TPG-413	404.22	405.22	361	461	0.95	92
TPG-414	452.32	453.32	365	460	0.39	93
TPG-416	541.25	542.25	371	460	0.43	85
TPG-419	383.26	384.26	369	464	0.39	93
TPG-420	412.28	413.28	377	455	0.56	85
TPG-432	384.25	385.25	363	460	0.59	86
TPG-436	426.30	427.30	363	460	0.34	81
TPG-442	383.26	384.26	361	460	0.65	96
TPG-446	393.21	394.21	364	460	0.42	98
TPG-449	439.21	440.21	363	460	0.47	97
TPG-456	581.40	582.40	357	464	0.69	75
TPG-457	439.21	440.21	360	460	0.73	95
TPG-463	456.27	457.27	374	460	0.44	96
TPG-477	435.23	436.23	367	460	0.53	98
TPG-478	431.26	432.26	362	460	0.71	97
TPG-522	459.29	460.29	358	460	0.66	98
TPG-531	471.15	472.15	363	460	0.47	97
TPG-548	493.27	494.27	361	460	0.56	97
TPG-572	495.15	496.15	362	460	0.76	98
TPG-574	383.26	384.26	362	460	0.81	99
TPG-580	537.43	538.43	362	462	0.81	97
TPG-599	493.27	494.27	363	461	0.69	98
TPG-611	424.28	425.28	357	462	0.94	91
TPG-618	423.29	424.29	365	460	0.78	96
TPG-620	499.13	500.13	358	459	0.91	93
TPG-656	563.45	564.45	363	460	0.65	95
TPG-677	451.20	452.20	377	460	0.58	99
TPG-686	485.16	486.16	361	460	0.69	98

Table 2.2 Spectroscopic properties and purity table for **TPGAC** library

UC	M^+(cal)	M^+1(exp.)	Abs(nm)	Em(nm)	QY(Φ)	Purity (%)
TPGAC11	480.60	481.2	359	467	0.50	95
TPGAC25	481.63	482.3	369	466	0.31	82
TPGAC49	489.56	490.2	354	466	0.43	90
TPGAC55	537.78	538.2	337	472	0.28	80
TPGAC65	607.91	608.4	360	466	0.24	85
TPGAC77	473.61	474.2	366	466	0.45	80
TPGAC80	481.53	482.2	360	466	0.33	95
TPGAC92	439.59	440.2	360	467	0.29	95
TPGAC100	549.70	550.2	363	465	0.33	96
TPGAC101	459.58	460.2	368	465	0.32	95
TPGAC103	489.61	490.2	355	466	0.35	90
TPGAC105	452.59	453.4	360	466	0.47	96
TPGAC111	460.57	461.2	366	466	0.29	91
TPGAC124	505.61	506.2	361	466	0.32	95
TPGAC131	487.63	488.2	363	464	0.24	97
TPGAC135	514.44	514.2	359	464	0.38	96
TPGAC153	514.03	478.2	359	466	0.37	95
TPGAC165	427.54	428.2	363	467	0.31	95
TPGAC177	413.51	414.2	362	467	0.26	90
TPGAC181	505.61	506.2	359	466	0.41	95
TPGAC184	519.63	520.2	368	467	0.51	96
TPGAC193	525.72	526.2	357	467	0.33	92
TPGAC220	463.54	464.2	366	465	0.42	97
TPGAC221	480.00	480.2	356	465	0.35	95
TPGAC230	467.64	468.2	369	465	0.47	97
TPGAC266	519.63	420.2	367	465	0.43	95
TPGAC267	480.99	482.2	360	465	0.35	89
TPGAC274	455.59	456.2	366	466	0.30	94
TPGAC277	453.62	454.2	366	465	0.27	96
TPGAC282	468.59	469.2	359	465	0.33	91
TPGAC292	393.48	394.2	349	465	0.24	77
TPGAC319	505.61	506.2	359	465	0.47	96
TPGAC329	560.91	560.2	310	446	0.21	80
TPGAC330	513.55	514.2	359	465	0.44	93
TPGAC335	473.61	474.2	360	467	0.34	97
TPGAC358	542.07	506.2	359	465	0.39	96
TPGAC359	541.04	505.2	310	466	0.08	89
TPGAC364	479.20	480.2	359	466	0.44	95
TPGAC368	525.75	526.0	360	465	0.40	90
TPGAC373	411.54	412.2	365	466	0.27	96

TPGAC374	445.55	446.2	369	465	0.48	94
TPGAC375	463.54	464.2	360	466	0.33	92
TPGAC381	475.58	476.2	366	466	0.47	95
TPGAC382	451.60	452.2	366	465	0.34	90
TPGAC387	475.58	476.2	360	466	0.35	96
TPGAC388	475.58	476.2	360	467	0.38	96
TPGAC395	489.61	490.2	362	465	0.40	97
TPGAC396	459.58	460.2	313	466	0.21	94
TPGAC401	446.54	447.2	346	465	0.29	89
TPGAC405	477.57	478.2	359	466	0.32	92
TPGAC407	495.70	496.4	367	466	0.53	95
TPGAC412	481.53	482.2	366	465	0.48	94
TPGAC413	446.54	447.2	371	465	0.43	89
TPGAC414	495.68	495.4	359	465	0.48	90
TPGAC416	583.66	584.2	357	465	0.39	82
TPGAC419	425.56	542.2	367	465	0.28	91
TPGAC420	454.60	454.2	310	445	0.20	76
TPGAC432	426.55	427.2	310	446	0.07	77
TPGAC436	468.63	469.2	369	466	0.33	70
TPGAC442	425.56	426.2	367	466	0.46	95
TPGAC446	435.52	43.2	361	466	0.32	95
TPGAC449	481.53	482.2	367	467	0.36	95
TPGAC456	623.87	624.2	310	466	0.23	70
TPGAC457	481.53	482.2	362	466	0.46	95
TPGAC463	498.61	499.2	324	465	0.19	70
TPGAC477	477.57	478.2	368	465	0.38	96
TPGAC478	473.61	474.2	366	467	0.50	97
TPGAC522	501.66	502.2	363	465	0.47	95
TPGAC531	514.44	514.2	363	465	0.37	95
TPGAC548	535.68	536.2	359	465	0.37	96
TPGAC572	538.48	538.2	367	466	0.52	97
TPGAC574	425.56	426.4	368	465	0.50	94
TPGAC580	579.86	508.4	367	463	0.62	93
TPGAC599	535.68	536.2	367	466	0.54	95
TPGAC611	466.62	467.4	359	466	0.57	90
TPGAC618	465.63	466.4	365	467	0.45	92
TPGAC620	542.44	543.2	310	466	0.47	90
TPGAC656	605.89	606.4	366	466	0.49	90
TPGAC677	494.03	494.2	369	476	0.39	96
TPGAC686	528.47	528.2	366	466	0.45	95

Table 2.3 Spectroscopic properties and purity table for **TPGCA** library

UC	M^+(cal)	M^+1(exp.)	Abs(nm)	Em(nm)	QY(Φ)	Purity (%)
TPGCA11	515.04	515.2	344	470	0.47	100
TPGCA25	516.08	516.2	357	467	0.28	81
TPGCA49	524.01	524.2	363	466	0.36	91
TPGCA55	572.22	573.2	362	468	0.29	74
TPGCA65	642.35	642.2	362	468	0.52	73
TPGCA77	508.05	508.2	361	468	0.41	97
TPGCA80	515.98	516.2	363	467	0.29	93
TPGCA92	474.04	474.2	362	468	0.27	89
TPGCA100	584.15	584.2	366	467	0.44	96
TPGCA101	494.03	494.2	358	467	0.39	94
TPGCA103	524.05	524.2	361	468	0.31	92
TPGCA105	487.03	487.2	360	465	0.52	81
TPGCA111	495.01	495.2	365	468	0.18	93
TPGCA124	540.05	540.2	357	467	0.38	94
TPGCA131	522.08	522.2	363	466	0.27	85
TPGCA135	548.89	548.0	357	467	0.40	96
TPGCA153	548.48	512.2	361	467	0.32	94
TPGCA165	461.98	462.0	367	468	0.28	96
TPGCA177	447.96	448.0	365	466	0.26	93
TPGCA181	540.05	540.2	361	466	0.51	96
TPGCA184	554.08	554.2	364	466	0.52	93
TPGCA193	560.17	560.2	363	468	0.29	91
TPGCA220	497.99	498.2	370	466	0.42	89
TPGCA221	514.44	514.2	358	466	0.31	92
TPGCA230	502.09	502.0	363	466	0.52	91
TPGCA266	554.08	554.2	361	466	0.59	92
TPGCA267	515.43	515.2	357	466	0.31	91
TPGCA274	490.04	490.2	362	468	0.30	96
TPGCA277	488.06	488.2	362	467	0.27	87
TPGCA282	503.03	503.2	358	467	0.30	83
TPGCA292	427.92	427.2	310	465	0.21	77
TPGCA319	540.05	540.2	360	467	0.49	92
TPGCA329	595.36	594.0	349	468	0.29	81
TPGCA330	548.00	548.2	360	466	0.57	92
TPGCA335	508.05	508.2	361	468	0.23	88
TPGCA358	576.51	540.2	359	467	0.34	86
TPGCA359	575.48	539.2	310	464	0.06	92
TPGCA364	514.44	514.2	359	466	0.46	91
TPGCA368	560.19	560.3	360	468	0.37	91
TPGCA373	445.98	446.2	363	467	0.24	89

TPGCA374	480.00	480.2	360	466	0.45	91
TPGCA375	497.99	498.2	365	467	0.31	88
TPGCA381	510.02	510.2	363	468	0.40	96
TPGCA382	486.05	486.2	364	467	0.35	92
TPGCA387	510.02	510.2	359	466	0.47	91
TPGCA388	510.02	510.2	363	467	0.44	94
TPGCA395	524.05	524.2	362	468	0.40	92
TPGCA396	494.03	494.2	356	466	0.24	88
TPGCA401	480.99	481.2	347	469	0.17	92
TPGCA405	512.02	512.2	355	466	0.23	91
TPGCA407	530.14	530.2	369	467	0.49	91
TPGCA412	515.98	516.2	362	466	0.59	96
TPGCA413	480.99	481.2	357	466	0.25	82
TPGCA414	529.12	529.2	363	468	0.37	78
TPGCA416	618.10	618.2	347	466	0.53	91
TPGCA419	460.01	460.2	363	467	0.24	93
TPGCA420	489.05	489.2	310	466	0.13	82
TPGCA432	461.00	460.2	355	468	0.39	86
TPGCA436	503.08	503.2	361	467	0.30	91
TPGCA442	460.01	406.2	365	468	0.63	93
TPGCA446	469.96	470.2	360	466	0.15	95
TPGCA449	515.98	516.2	363	467	0.38	89
TPGCA456	658.31	658.4	352	468	0.33	91
TPGCA457	515.98	516.2	361	468	0.53	96
TPGCA463	533.06	533.2	310	467	0.28	82
TPGCA477	512.02	512.2	362	466	0.43	94
TPGCA478	508.05	508.2	365	466	0.52	95
TPGCA522	536.11	536.2	363	467	0.65	93
TPGCA531	548.89	548.2	361	466	0.43	91
TPGCA548	570.12	570.2	358	468	0.35	95
TPGCA572	572.92	572.2	359	468	0.53	94
TPGCA574	460.01	560.2	365	466	0.61	90
TPGCA580	614.30	614.2	365	467	0.56	87
TPGCA599	570.12	570.2	361	466	0.47	91
TPGCA611	501.06	501.2	356	470	0.47	94
TPGCA618	500.07	500.2	361	467	0.61	95
TPGCA620	576.89	576.2	310	467	0.40	88
TPGCA656	640.34	640.2	362	467	0.26	81
TPGCA677	528.47	528.2	363	467	0.56	96
TPGCA686	562.92	562.2	365	467	0.47	94

*Quantum yields were measured in DMSO, using Coumarin-1 as a standard (Φ = 0.58) in DMSO as reference compound.[14] [a]Purities were determined according to UV absorption at 365 nm. All absorbance and fluorescence excitation and emission data were recorded by SpectraMax M2, Molecular Devices, fluorescent plate reader (10 μM compounds in DMSO (100 μL) for λ_{abs}, 10 μM compounds in EtOH (100 μL) for λ_{em}) in 96-well polypropylene plates. Mass was calculated as (M) and found in ESI-MS (M+H) in the positive mode scan, or found mass (M-H) in the negative mode scan; Purity data was calculated on the basis of the integration in HPLC trace at 365 nm.

2.3.2 Design and synthesis of TPC library on solid support

Among the various TP scaffold reported ACEDAN is one of the most successful core, with numerous examples of metal sensors with cell and deep tissue imaging. After successful completion of the first ACEDAN based TP fluorescent library **TPG** we plan for the next TP library development. Recently Cho group have published another ACEDAN based core but with a Proline linker.[15] In this core, the N-dialkyl group was replaced by cyclic Pyrrolidine ring with a carboxyl group attached at 2nd position. This new core also preserve necessary properties like i) significant TPA cross-section for bright TP imaging, ii) appreciable water solubility for cell and tissue imaging, iii) pH resistant and iv) high photo stability.[16] To develop our next TP library, we decide to utilize this new ACEDAN core with Proline. The presence of carboxylic group on the core makes it suitable for our robust solid phase synthesis. Due to the presence of cyclic linker in the structure we named this library **TPC** (two-photon -cyclic).

For the TPC library synthesis (**Scheme 2.3**) Proline containing ACEDAN scaffold **TPC acid** was used as key intermediate. The general synthetic strategy of **TPC acid** involved two steps (40 % overall yield) reaction process. First, **1** was synthesized by demethylation of 6-methoxy-2-acetylnaphthanlene, followed by Bucherer reaction of naphthalene with Proline to get **TPC acid**. Then the structurally diverse TPC library was synthesized using previously reported robust solid phase synthesis technique.[13] Here the wide structural diversity was introduced by the use of

solid phase secondary amines **3** utilizing the simple reaction between the bromopropylamine loaded resins **2** with the series of primary amines (**Chart 2.2**). Then the key intermediate **TPC acid** was coupled to the solid phase amine building block by using a standard acid-amine coupling protocol. The final step of the acidic cleavage from the solid supported compound yielded 80 very pure members of TPC library (average purity is 90 % without further purification at 350 nm, **Table 2.4, Table 2.5 and Table 2.6**).

Scheme 2.3 General synthetic scheme of **TPC** library

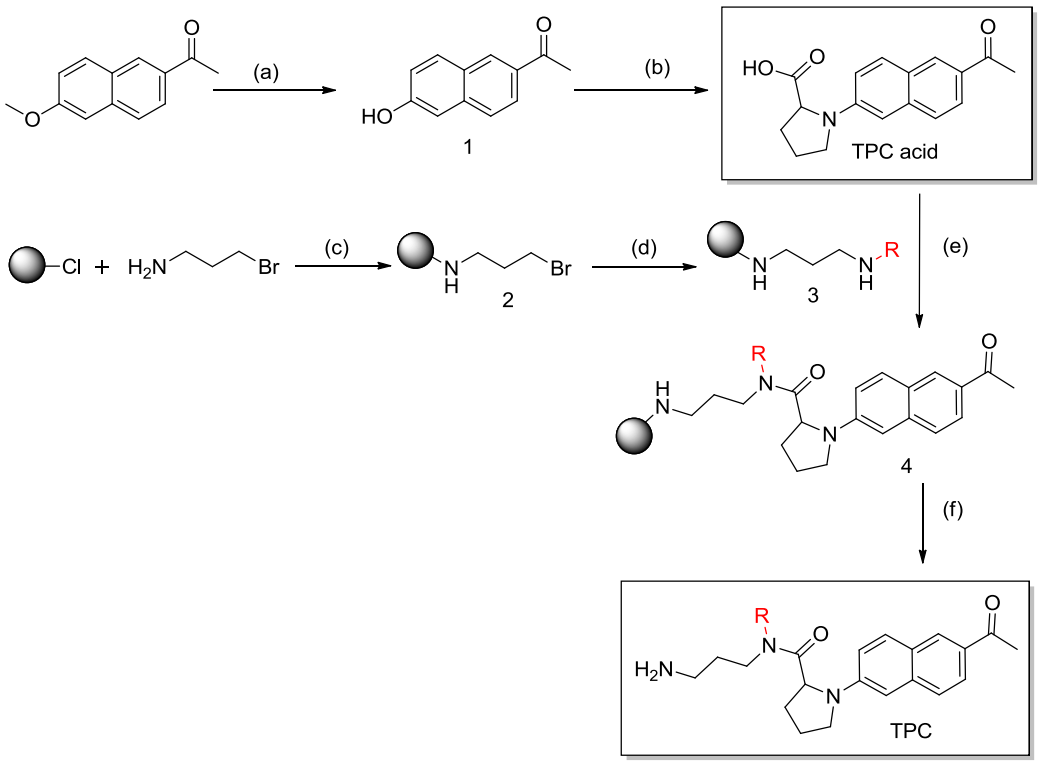

Reagents and conditions: (a) Conc. HCl, TEA, 2 h at 90° C. (b) Proline, $Na_2S_2O_5$, H_2O, 4 h at 140° C (Microwave). (c) DIEA, THF, 3-bromopropylamine, 12 h at rt. (d) DIEA, RNH_2, NMP, 12 h at 70° C. (e) DMF, HATU, DIEA, 24 h at rt. (f) 5 % TFA in DCM, 40 min at rt. R is 80 different amines (**Chart 2.2**)

Then, **TPCAC** and **TPCCA** compounds were synthesized according to the previously reported protocol. All the compounds in the library were characterized by HPLC-MS and 80 relatively pure compounds (average purity ~90 %, measured at 350 nm (**Table 2.4, Table 2.5 and Table 2.6)** were collected for further studies.

Scheme 2.4 **TPCAC** and **TPCCA** library synthesis

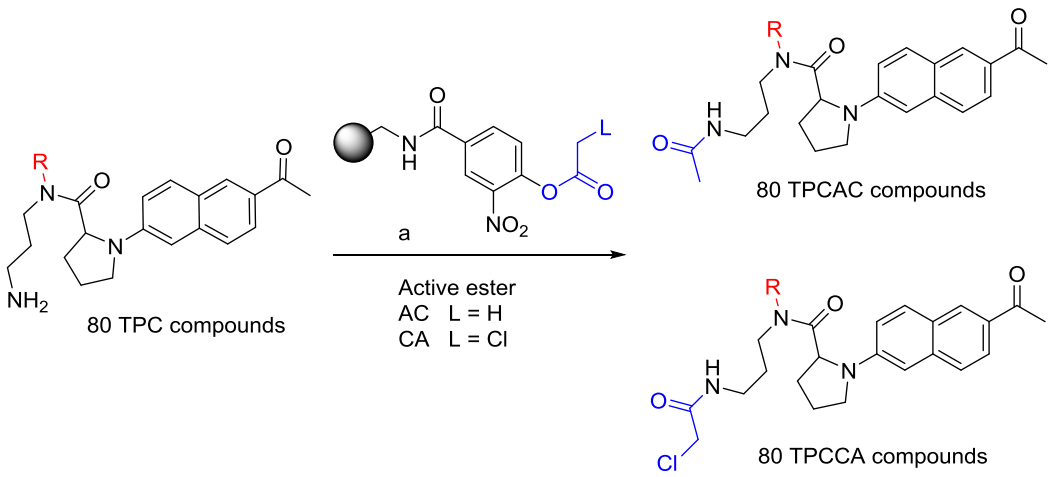

Reagents and conditions: (a) DCM/ACN (7:1), (2 μL) catalytic amount of sat. $NaHCO_3$, 2 h at rt. R is 80 different amines (**Chart 2.2**)

Chart 2.2 Amine building blocks for TPC library

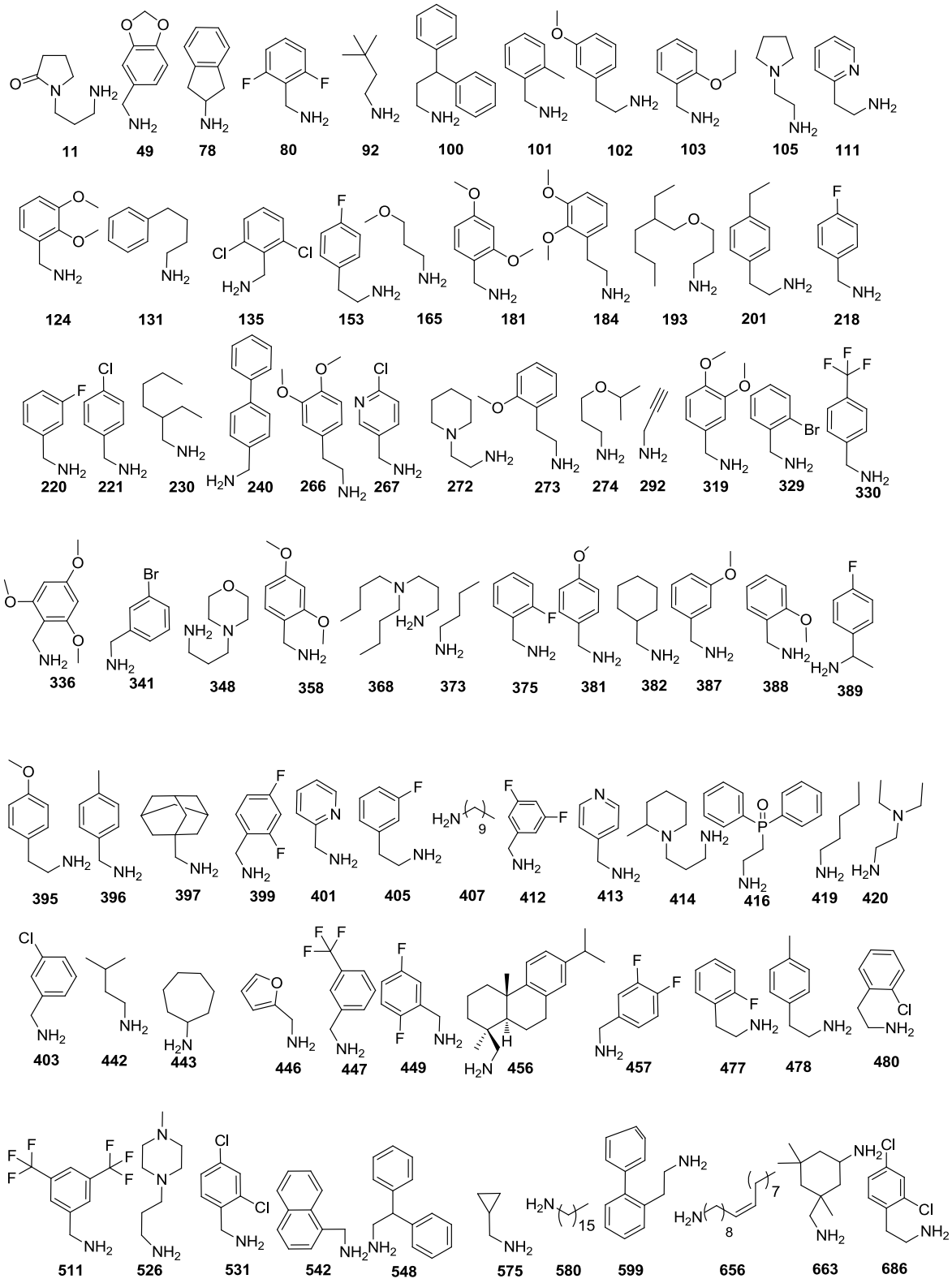

Table 2.4 Spectroscopic properties and purity table for **TPC** library

UC	**M**$^{+}$(cal)	**M**$^{+}$**1**(exp.)	**Abs**(nm)	**Em**(nm)	**QY**(Φ)	**Purity** (%)
TPC11	466.29	465.2	371	465	0.46	98
TPC49	473.23	474.2	371	465	0.53	99
TPC78	455.25	456.2	373	465	0.54	99
TPC80	465.22	466.2	372	465	0.60	99
TPC92	423.28	424.2	375	465	0.41	99
TPC100	533.30	534.2	372	465	0.50	94
TPC101	443.25	444.2	371	464	0.46	99
TPC102	473.26	474.2	370	465	0.36	93
TPC103	473.26	474.2	374	471	0.46	99
TPC105	436.28	437.2	370	465	0.43	82
TPC111	444.25	445.2	372	465	0.50	99
TPC124	489.26	490.2	371	465	0.52	98
TPC131	471.28	472.2	374	465	0.46	98
TPC135	497.16	498.0	370	465	0.57	98
TPC153	461.24	462.2	372	471	0.53	90
TPC165	411.25	412.2	372	465	0.60	99
TPC181	489.26	490.2	370	465	0.52	98
TPC184	503.27	504.2	370	464	0.49	99
TPC193	509.36	510.2	372	464	0.47	99
TPC201	471.28	472.2	371	465	0.41	96
TPC218	447.23	448.2	370	465	0.47	99
TPC220	447.23	448.2	370	465	0.46	99
TPC221	463.20	464.2	370	464	0.49	99
TPC230	451.32	452.2	371	465	0.51	98
TPC240	505.27	506.2	370	464	0.55	98
TPC266	503.27	504.2	373	465	0.57	99
TPC267	464.19	465.2	370	465	0.58	98
TPC272	450.29	451.2	370	465	0.56	90
TPC273	473.26	474.2	372	465	0.38	95
TPC274	439.28	440.2	372	465	0.45	99
TPC292	377.21	378.2	376	467	0.58	87
TPC319	489.26	490.2	371	465	0.56	99
TPC329	507.15	478.0	303	464	0.75	97
TPC330	497.22	498.2	370	465	0.57	99
TPC336	519.27	520.2	375	465	0.61	96
TPC341	507.15	508.2	372	464	0.57	95
TPC348	466.29	467.2	373	465	0.49	92
TPC358	489.26	490.2	373	465	0.62	98
TPC368	508.37	509.2	371	464	0.45	95
TPC373	395.25	396.2	371	467	0.52	98
TPC375	447.23	448.2	371	464	0.59	99

TPC381	459.25	460.2	373	465	0.54	98
TPC382	435.28	436.2	372	467	0.52	99
TPC387	459.25	460.2	370	464	0.49	97
TPC388	459.25	460.2	373	464	0.59	98
TPC389	461.24	462.2	361	464	0.52	87
TPC395	473.26	474.2	373	464	0.51	99
TPC396	443.25	444.2	371	465	0.58	99
TPC397	487.32	488.3	372	465	0.56	99
TPC399	465.22	466.2	370	465	0.59	98
TPC401	430.23	431.3	376	465	0.58	95
TPC403	463.20	464.2	370	465	0.53	99
TPC405	461.24	462.2	373	465	0.50	99
TPC407	479.35	480.2	370	465	0.33	99
TPC412	465.22	466.2	370	464	0.49	99
TPC413	430.23	431.2	371	464	0.41	80
TPC414	478.33	479.2	371	465	0.36	90
TPC416	567.26	568.2	370	465	0.52	98
TPC419	409.27	410.2	372	465	0.57	82
TPC420	438.29	439.2	372	465	0.52	92
TPC442	409.27	410.2	373	465	0.49	98
TPC443	435.28	436.2	374	465	0.53	98
TPC446	419.22	420.2	373	465	0.47	90
TPC447	497.22	498.2	372	470	0.48	99
TPC449	465.22	466.2	370	464	0.62	97
TPC456	607.41	608.2	370	465	0.59	80
TPC477	461.24	462.2	370	465	0.50	99
TPC478	457.27	458.2	373	465	0.35	99
TPC480	477.21	478.2	373	465	0.38	99
TPC511	565.21	566.2	370	464	0.50	97
TPC526	479.32	480.2	371	465	0.59	80
TPC531	497.16	498.2	370	464	0.62	99
TPC542	479.25	480.2	369	471	0.58	98
TPC548	519.28	520.2	375	464	0.54	99
TPC575	393.24	394.2	374	465	0.44	99
TPC580	563.44	564.2	373	465	0.49	97
TPC599	519.28	520.2	376	465	0.58	99
TPC656	589.46	589.2	373	465	0.38	92
TPC663	492.34	492.2	370	475	0.46	93
TPC686	511.17	512.0	373	465	0.42	99

Table 2.5 Spectroscopic properties and purity table for **TPCAC** library

UC	M^+(cal)	M^+1(exp.)	**Abs**(nm)	**Em**(nm)	**QY**(Φ)	**Purity** (%)
TPCAC11	506.28	507.2	369	465	0.54	80
TPCAC49	515.24	516.2	369	465	0.45	86
TPCAC78	497.26	498.2	365	465	0.50	80
TPCAC80	507.23	508.2	369	465	0.53	91
TPCAC92	465.29	466.2	369	465	0.40	96
TPCAC100	575.31	576.2	366	465	0.49	87
TPCAC101	485.26	486.2	363	464	0.44	88
TPCAC102	515.27	516.2	362	465	0.39	90
TPCAC103	515.27	516.2	363	467	0.45	87
TPCAC105	478.29	479.2	368	465	0.41	84
TPCAC111	486.26	487.2	369	465	0.47	95
TPCAC124	531.27	532.2	369	464	0.46	88
TPCAC131	513.29	514.2	371	465	0.49	93
TPCAC135	539.17	540	365	465	0.50	80
TPCAC153	503.25	504.2	369	465	0.45	95
TPCAC165	453.26	454.2	362	464	0.54	80
TPCAC181	531.27	532.2	363	464	0.44	90
TPCAC184	545.28	546.2	365	464	0.45	91
TPCAC193	551.37	552.2	369	465	0.53	92
TPCAC201	513.29	514.2	363	465	0.45	95
TPCAC218	489.24	490.2	369	465	0.47	92
TPCAC220	489.24	490.2	368	465	0.45	93
TPCAC221	505.21	506.2	365	464	0.44	90
TPCAC230	493.33	494.2	369	465	0.43	97
TPCAC240	547.28	548.2	369	465	0.50	91
TPCAC266	545.28	546.2	369	464	0.49	93
TPCAC267	506.20	507.2	360	464	0.54	85
TPCAC272	492.31	493.2	365	464	0.48	95
TPCAC273	515.27	516.2	364	465	0.44	70
TPCAC274	481.29	482.2	369	464	0.37	95
TPCAC292	419.22	420.2	360	465	0.53	75
TPCAC319	531.27	532.2	368	464	0.47	92
TPCAC329	549.16	520	300	460	0.35	70
TPCAC330	539.24	540.2	366	465	0.46	86
TPCAC336	561.28	562.2	369	465	0.55	93
TPCAC341	549.16	550.2	368	465	0.52	85
TPCAC348	508.30	509.2	369	465	0.43	95
TPCAC358	531.27	532.2	369	465	0.51	92
TPCAC368	550.38	551.2	362	465	0.47	95
TPCAC373	437.26	438.2	369	464	0.43	95

TPCAC375	489.24	490.2	369	464	0.58	95
TPCAC381	501.26	502.2	369	465	0.46	88
TPCAC382	477.29	478.2	369	465	0.47	93
TPCAC387	501.26	502.2	369	464	0.46	91
TPCAC388	501.26	502.2	369	465	0.51	94
TPCAC389	503.25	504.2	300	464	0.46	75
TPCAC395	515.27	516.2	369	465	0.46	95
TPCAC396	485.26	486.2	369	464	0.47	90
TPCAC397	529.33	530.3	368	464	0.51	94
TPCAC399	507.23	508.2	369	465	0.53	94
TPCAC401	472.24	473.3	369	465	0.54	90
TPCAC403	505.21	506.2	368	465	0.48	90
TPCAC405	503.25	504.2	369	465	0.44	95
TPCAC407	521.36	522.2	369	465	0.35	97
TPCAC412	507.23	508.2	369	465	0.45	93
TPCAC413	472.24	473.2	363	464	0.43	90
TPCAC414	520.34	521.2	365	465	0.45	95
TPCAC416	609.27	610.2	366	465	0.50	95
TPCAC419	451.28	452.2	369	465	0.48	82
TPCAC420	480.31	481.2	368	465	0.47	92
TPCAC442	451.28	452.2	369	465	0.41	92
TPCAC443	477.29	478.2	369	466	0.46	90
TPCAC446	461.23	462.2	369	465	0.38	90
TPCAC447	539.24	540.2	368	464	0.47	95
TPCAC449	507.23	508.2	369	465	0.54	90
TPCAC456	649.42	650.2	364	465	0.52	60
TPCAC477	503.25	504.2	369	465	0.41	93
TPCAC478	499.28	500.2	373	465	0.30	96
TPCAC480	519.22	520.2	369	465	0.35	95
TPCAC511	607.22	608.2	369	463	0.44	99
TPCAC526	521.33	522.2	369	465	0.48	90
TPCAC531	539.17	540.2	366	464	0.49	85
TPCAC542	521.26	522.2	367	465	0.51	90
TPCAC548	561.29	562.2	369	465	0.47	97
TPCAC575	435.25	436.2	369	464	0.33	96
TPCAC580	605.45	606.2	369	465	0.39	85
TPCAC599	561.29	562.2	371	464	0.43	95
TPCAC656	631.47	631.2	369	464	0.30	87
TPCAC663	534.35	534.2	369	465	0.39	60
TPCAC686	553.19	554	369	465	0.31	96

Table 2.6 Spectroscopic properties and purity table for **TPCCA** library

UC	M^+(cal)	M^+1(exp.)	**Abs**(nm)	**Em**(nm)	**QY**(Φ)	**Purity** (%)
TPCCA11	540.25	541.2	361	467	0.46	90
TPCCA49	549.20	550.2	357	466	0.39	90
TPCCA78	531.22	532.2	310	467	0.22	91
TPCCA80	541.19	542.2	310	470	0.29	89
TPCCA92	499.26	500.2	369	465	0.44	92
TPCCA100	609.27	610.2	356	465	0.34	89
TPCCA101	519.22	520.2	360	466	0.47	89
TPCCA102	549.23	550.2	358	465	0.36	85
TPCCA103	549.23	550.2	369	466	0.45	89
TPCCA105	512.25	513.2	357	465	0.37	87
TPCCA111	520.22	521.2	364	469	0.39	89
TPCCA124	565.23	566.2	356	465	0.34	91
TPCCA131	547.26	548.2	369	465	0.51	93
TPCCA135	573.13	574	310	465	0.19	82
TPCCA153	537.21	538.2	361	466	0.41	91
TPCCA165	487.22	488.2	310	466	0.21	76
TPCCA181	565.23	566.2	352	465	0.31	87
TPCCA184	579.25	580.2	357	466	0.39	89
TPCCA193	585.33	586.2	357	471	0.39	95
TPCCA201	547.26	548.2	358	465	0.43	90
TPCCA218	523.20	524.2	362	467	0.49	89
TPCCA220	523.20	524.2	360	466	0.41	88
TPCCA221	539.17	540.2	359	465	0.37	90
TPCCA230	527.29	528.2	357	465	0.44	92
TPCCA240	581.24	582.2	356	465	0.35	88
TPCCA266	579.25	580.2	353	469	0.36	85
TPCCA267	540.16	541.2	354	465	0.38	90
TPCCA272	526.27	527.2	310	466	0.21	93
TPCCA273	549.23	550.2	310	464	0.17	70
TPCCA274	515.25	516.2	364	467	0.39	95
TPCCA292	453.18	454.2	310	449	0.23	71
TPCCA319	565.23	566.2	359	468	0.42	85
TPCCA329	583.12	554	310	443	0.13	78
TPCCA330	573.20	574.2	357	465	0.38	83
TPCCA336	595.24	596.2	310	465	0.28	87
TPCCA341	583.12	584.2	358	465	0.45	90
TPCCA348	542.26	543.2	368	466	0.51	95
TPCCA358	565.23	566.2	357	465	0.44	89
TPCCA368	584.34	585.2	310	466	0.25	82
TPCCA373	471.22	472.2	361	465	0.41	92

TPCCA375	523.20	524.2	356	467	0.46	91
TPCCA381	535.22	536.2	356	465	0.45	93
TPCCA382	511.26	512.2	369	467	0.52	95
TPCCA387	535.22	536.2	361	465	0.47	91
TPCCA388	535.22	536.2	358	465	0.50	89
TPCCA389	537.21	538.2	310	443	0.14	70
TPCCA395	549.23	550.2	364	466	0.49	86
TPCCA396	519.22	520.2	356	465	0.49	93
TPCCA397	563.29	564.3	356	466	0.37	95
TPCCA399	541.19	542.2	358	465	0.39	90
TPCCA401	506.20	507.3	357	466	0.40	86
TPCCA403	539.17	540.2	358	467	0.41	93
TPCCA405	537.21	538.2	363	467	0.47	94
TPCCA407	555.32	556.2	369	465	0.42	98
TPCCA412	541.19	542.2	362	465	0.44	94
TPCCA413	506.20	507.2	328	442	0.14	84
TPCCA414	554.30	555.2	310	450	0.31	76
TPCCA416	643.23	644.2	356	466	0.34	91
TPCCA419	485.24	486.2	358	467	0.44	87
TPCCA420	514.27	515.2	357	465	0.39	88
TPCCA442	485.24	486.2	362	467	0.47	89
TPCCA443	511.26	512.2	356	467	0.37	91
TPCCA446	495.19	496.2	364	465	0.49	92
TPCCA447	573.20	574.2	362	467	0.53	94
TPCCA449	541.19	542.2	357	466	0.45	91
TPCCA456	683.38	684.2	310	467	0.25	60
TPCCA477	537.21	538.2	364	465	0.48	94
TPCCA478	533.24	534.2	369	467	0.43	95
TPCCA480	553.19	554.2	368	465	0.46	93
TPCCA511	641.18	642.2	364	466	0.52	93
TPCCA526	555.29	556.2	353	465	0.26	85
TPCCA531	573.13	574.2	350	464	0.38	89
TPCCA542	555.22	556.2	353	465	0.37	88
TPCCA548	595.26	596.2	357	469	0.42	95
TPCCA575	469.21	470.2	368	465	0.49	92
TPCCA580	639.41	640.2	362	466	0.51	81
TPCCA599	595.26	596.2	368	467	0.50	88
TPCCA656	665.43	665.2	369	465	0.45	85
TPCCA663	568.31	568.2	343	466	0.42	78
TPCCA686	587.15	588.2	369	467	0.48	95

*Quantum yields were measured in DMSO, using Coumarin-1 as a standard (Φ = 0.58) in DMSO as reference compound.[14] [a]Purities were determined according to UV absorption at 365 nm. All absorbance and fluorescence excitation and emission data

were recorded by SpectraMax M2, Molecular Devices, fluorescent plate reader (10 μM compounds in DMSO (100 μL) for λ_{abs}, 10 μM compounds in EtOH (100 μL) for λ_{em}) in 96-well polypropylene plates. Mass was calculated as (M) and found in ESI-MS (M+H) in the positive mode scan, or found mass (M-H) in the negative mode scan; Purity data was calculated on the basis of the integration in HPLC trace at 365 nm.

2.4 Conclusion

We have successfully synthesized Two TP fluorescent dye libraries named **TPG** and **TPC** based on ACEDAN scaffold in solid phase. Both the library is made up off 80 compounds each. Member of these libraries have good one photon quantum yield (~50 %) and also optimum two-photon action cross-section (~100 GM). Both these libraries were further modified to acetyl (**TPGAC**, **TPCAC**) and chloroacetyl (**TPGCA**, **TPCCA**) versions. Combining both **TPG** and **TPC** libraries a total of 480 TP fluorescent probes have been developed. These compounds were used to explore in both *in-vitro* screening and cell based fluorescent screening for development of useful imaging sensors.

2.5 Experimental Section

2.5.1 Reagents and Solvents

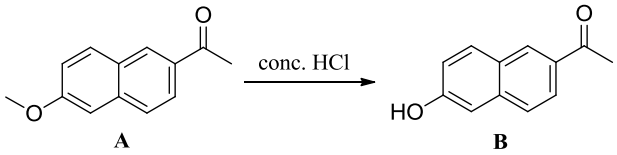

A **B**

Synthesis of compound B: To a stirred suspension of 1-(6-methoxy-2-naphthyl)-1-ethanone, (**A)** (10.0 g, 50 mmol) in 80 mL of Conc. HCl in presence of DCM (2 mL), 15 drops of (~ 0.75 mL) triethlyamine was added in a 100 mL three-neck round bottom flask equipped with a reflux condenser and an isobaric dropping funnel. The stirred mixture was heated to boil and then reflux for 2 h at 90° C.[17] Monitoring the reaction using LCMS, revealed complete consumption of the starting material The hot solution was filtered through a mineral wool plug to remove the oily residue. After cooling the solid was filtered out through a glass frit. Then the solid was dissolved in 20 mL of ethyl acetate and was washed with brine. Organic layer was separated and dried over anhydrous magnesium sulfate. The solvent was removed under reduced pressure to give the crude demethylated product. The crude product was dissolved in 1N NaOH solution and then 1N HCl was added till a yellow precipitate was formed at 0 °C. The solid was filtered out to afford pure compound **B** as a yellow solid (8.09 g, 81 % yield). ^{1}H NMR (CD_3OD, 500 MHz), δ (ppm): 8.44 (s, 1H), 7.89 (dd, J = 8.5, 4 Hz, 2H), 7.67 (d, J = 8.5 Hz, 1H), 7.15 (d, J = 8.5 Hz, 2H), 4.88 (br s, 1H), 3.02 (s, 3H); ^{13}C NMR (CD_3OD, 125 MHz), δ (ppm): 200.58, 159.52, 139.36, 133.13, 132.73, 132.06, 128.69, 127.70, 125.21, 120.51, 110.11, 26.63. m/z ($C_{12}H_{10}O_2$) calcd: 186.07; found 187.2.

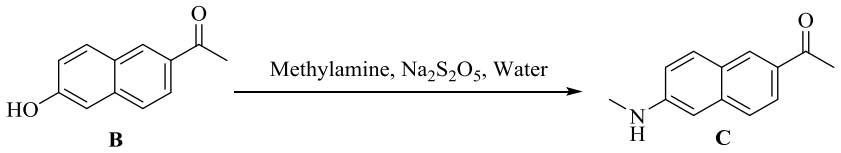

Synthesis of compound C. To a stirred suspension of 2-hydroxy-6-acetylnaphthlene (**B**) (1.0 g, 5.37 mmol) in 30 mL H_2O, $Na_2S_2O_5$ (2 g, 10.74 mmol) and 40 % methylamine solution in water (0.8 g, 27 mmol) were added. The mixture was heated for 4h at 140^o C under microwave conditions.[11] The reactor was allowed to cool gradually to attain room temperature. Monitoring the reaction using LCMS, revealed complete consumption of the starting material. The reaction mixture was filtered and washed thoroughly with copious amount of cold water. The solid obtained was crystallized from $CHCl_3$/EtOH (3:1) to afford pure compound **C** as pale yellow crystals (0.67 g, 67 %). ^{1}H NMR ($CDCl_3$, 300 MHz); δ (ppm): 8.28 (s, 1H), 7.92 (dd, J = 8.5, 3 Hz, 1H), 7.71 (d, J = 8.5 Hz, 1H), 7.63 (d, J = 8.5 Hz, 1H), 6.93 (dd, J = 8.5 Hz, 2H), 6.7 (s, 1H), 2.94 (s, 3H), 2.65 (s, 3H); ^{13}C NMR ($CDCl_3$, 75 MHz); δ (ppm): 198.14, 148.90, 138.15, 131.01, 130.88, 130.55, 126.19, 124.88, 118.62, 103.77, 30.70, 26.52. m/z ($C_{13}H_{13}NO$) calcd: 199.1; found 200.1.

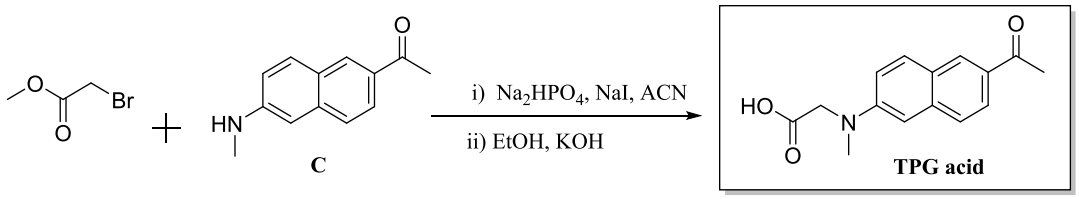

Synthesis of TPG acid. To a mixture of **C** (3.0 g, 8.8 mmol) in ACN, methyl bromoacetate (2.0 g, 13 mmol), Na_2HPO_4 (1.9 g, 13 mmol) and NaI (0.5 g, 3.5 mmol) (50 mL) was added and heated for 4 h at 140° C under microwave condition.[11] Monitoring the reaction using LCMS, revealed complete consumption of the starting material. The reaction mixture was cooled to room temperature, water was added

followed by ethylacetate and the layers were separated. The organic layer was washed with water followed by brine and was evaporated to dryness to give the crude compound. The crude compound was purified by crystallization from EtOH to obtain a light yellow powder; yield 2.5 g (70 % yield). To this ester intermediate (2.0 g, 4.9 mmol), KOH (0.70 g, 12 mmol) in EtOH (50 mL) was added and stirred for 5 h at room temperature. The resultant solution was diluted with ice cold water (100 mL) and was acidified slowly using conc. HCl (aq) to pH 3. The resulting precipitate was filtered, washed with distilled water and purified by crystallization from chloroform/petroleum ether to afford dark yellow solid (1.5 g, 63 %). ^{1}H NMR **TPG acid** (CD_3OD, 500 MHz), δ (ppm): 8.34 (s, 1H), 7.82 (dd, J = 9, 3 Hz, 2H), 7.61 (d, J = 9.0 Hz, 1H), 7.15 (d, J = 9.0 Hz, 1H), 6.89 (s, 1H), 4.22 (s, 2H), 3.14 (14 (s, 3H), 2.60 (s, 3H); ^{13}C NMR **TPG acid** (CD_3OD, 125 MHz), δ (ppm): 200.42, 174.35, 150.94, 139.32, 132.02, 131.97, 131.92, 127.46, 125.19, 117.11, 106.57, 54.85, 39.82, 26.45. m/z ($C_{15}H_{15}NO_3$) calcd: 257.11; found 256.1.

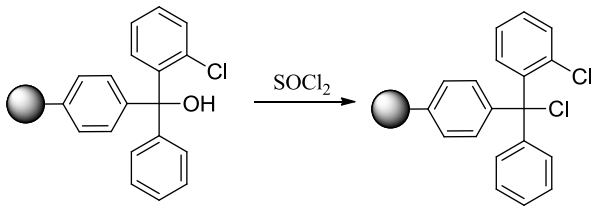

E

Synthesis of E. Thionyl chloride (1.2 mL, 16.48 mmol) was added to 2-Chlorotrityl alcohol resin (4g, 5.48mmol, 1.37 mmol/g) suspended in 40 mL of anhydrous DCM. The reaction mixture was shaken using a shaker for 10 h at room temperature. Then the resin was filtered, washed thoroughly with DMF (3 x 40 mL) followed by DCM (3 x 40 mL). The obtained resin was dried under high vacuum till a free flowing solid was obtained.

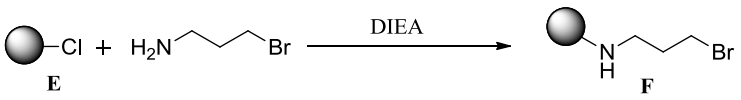

E F

Synthesis of compound F. To 3-bromopropylamine (3.5 g, 15.75 mmol, 5 eq) THF (5 mL/g), DIPEA (6 mL, 32.5 mmol, 10 eq) was added. The resulting solution was then added to 2-chlorotrityl chloride resin (2.5 g, 3.25 mmol, 1 eq, 1.3 mmol/g) suspended in dichloromethane (10 mL/g). After shaking for 12 h, the resin was filtered through 10 mL cartridge, washed with DMF (5 x 40 mL), methanol (5 x 40 mL) and dichloromethane (10 x 40 mL). The unreacted resin was then capped using 10 mL of 20 % MeOH in DMF for 2h. The resin obtained was again washed with DMF (5 x 40 mL), methanol (5 x 20 mL) and dichloromethane (5 x 20 mL) and was dried under high vacuum till a free flowing solid was obtained.

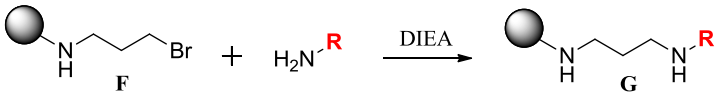

F G

Synthesis of compound G. (loading of amine building blocks to the resin). For each reaction, resin (solid supported 3-bromopropylamine) (100 mg, 0.1 mmol, 1 eq, 1mmol/g) was suspended in 2 mL of N-Methyl-2-pyrrolidone (NMP) in a 20 mL of glass vial. 7 eq of each amine (0.7 mmol) and 14 eq of DIEA (1.4 mmol) were then added in 2 mL of the same solvent. The reaction mixture was shaken for 12 h at 70 °C on a heating block. The reaction mixture was cooled and the resin was filtered through 10 mL cartridge and washed with DMF (5 x 5 mL), methanol (5 x 5mL) and dichloromethane (5 x 5mL). The solid supported secondary amine resins obtained, were dried under high vacuum and used for next steps.

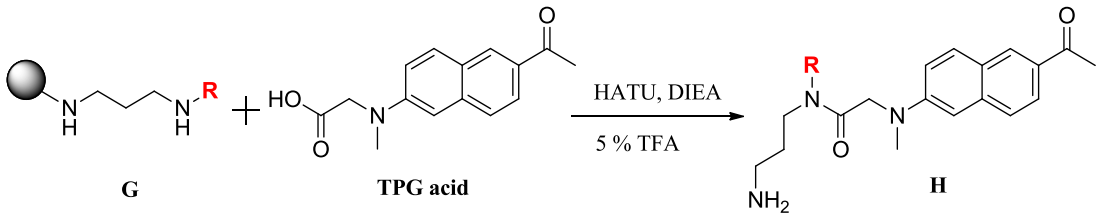

Synthesis of compound H (coupling of TPG acid to the amine containing resin). To synthesize **TPG** library, each of (solid supported secondary amine) resin (50 mg, 0.035 mmol, 1eq, 0.7 mmol/g) was suspended in 3 mL of DMF in a 10 mL syringe then **TPG acid** (28 mg, 0.07 mmol, 1 eq), HATU (30 mg, 0.77 mmol, 2.2 eq) and DIEA (30 μL, 0.168 mmol, 4.8 eq) were added. At a time 40 individual reaction mixtures were placed on orbital shaker for 24 h at room temperature. After which, the resin was filtered through a 10 mL cartridge and washed with DMF (5 x 5 mL), methanol (5 x 5 mL) and dichloromethane (5 x 5mL). The resin was dried under high vacuum to afford solid supported compounds resin and then the subsequently the dried resin of 50 mg was treated with 5 % TFA in dichloromethane (5 mL) for 10 min. The solution was drained to the 20 mL vial and then organic layer was washed with the saturated $NaHCO_3$ solution and then the organic layer was separated and dried using vacuum to afford the **TPG** library products. Each of **TPG** compound was solid and primarily characterized by LC-MS.

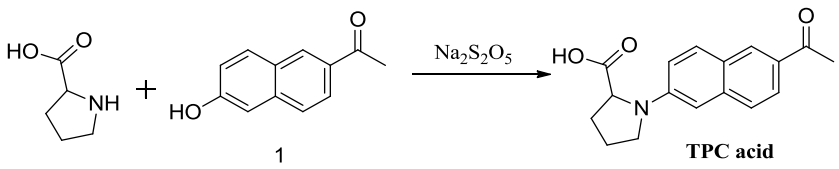

1-(6-acetylnaphthalen-2-yl)pyrrolidine-2-carboxylic acid (TPC acid):

A mixture of 2-acetyl-6-hydroxynapthalene (1.5 g, 8.1 mmol), L-Proline (4.5 g, 39 mmol), $Na_2S_2O_5$ (3.1 g, 16 mmol), NaOH (1.6 g, 39 mmol) and water (25 ml) was stirred in the microwave reactor for 4 h at 140° C.[15] The mixture was cooled at

room temperature, washed with water and acidified with dilute HCl to pH 2-3 in an ice bath. The precipitate was collected by filtration, washed with water and purified by column chromatography on silica gel ($CHCl_3$ / MeOH 4:1) yield 1.7 g (78 %). ^{1}H NMR (DMSO-d_6, 300 MHz,), δ (ppm): 8.29 (s, 1H), 7.75 (d, J = 9 Hz, 1H), 7.69 (dd, J = 9, 1.5 Hz, 1H), 7.49 (d, J = 9 Hz, 1H), 6.93 (dd, J = 9, 2.1 Hz, 1H), 6.63 (d, J = 2.1 Hz, 1H), 4.16 (d, J = 7.5 Hz, 1H), 3.42 (m, 1H), 2.50 (m, 3H), 2.09 (m, 1H), 1.99 (m, 4H). ^{13}C NMR (DMSO-d_6, 75 MHz), δ (ppm): 196.82, 175.49, 147.20, 137.32, 130.64, 130.58, 129.48, 125.45, 124.21, 123.89, 116.68, 104.14, 61.63, 48.04, 30.59, 26.30, 23.46. m/z ($C_{17}H_{17}NO_3$) calcd: 283.12; found 282.2.

2.5.2 Quantum yield measurements.

Quantum yield were calculated by measuring the integrated area of emission spectra for **TPG** and **TPC** library compounds in comparison with the same measurement for Coumarin-1 (Φ = 0.58) in DMSO as reference compound.[14] Both library compounds and Coumarin 1 were excited at 370 nm and emission spectra were collected from 420-600 nm. Quantum yields were calculated suing Equation 2.1, where F represents the area of fluorescent emission, n is reflective index of the solvent and Abs is absorbance at excitation wavelength selected for standards and samples. Emission was integrated between 420 to 600 nm.

Equation 2.1 Quantum yield measurements

$$\Phi_{(sample)} = \Phi_{(ref)} \frac{F_{(sample)}}{F_{(\mathrm{ref})}} \frac{\eta_{(sample)}}{\eta_{(\mathrm{ref})}} \frac{Abs_{(\mathrm{ref})}}{Abs_{(sample)}} \qquad (1)$$

2.5.3 Two-photon absorption cross sections measurement.

The TP emission spectra of **TPG** library compounds were determined over a broad spectral region by the two-photon induced fluorescence method with Rhodamine B in

methanol as a reference.[18], A PTI, Quanta Master™ spectro-fluorimeter and femtosecond Ti: Sapphire laser (Mira 900F, 220 fs pulse width, 76 MHz repetition rate, tuning range 740 - 840 nm, Coherent (USA) were used. TP fluorescence measurements were performed in 10 mm fluorometric quartz cuvettes with 10 μM of represented TPG and TPC compounds in Methanol and 10 μM Rhodamine B as reference in same solvent.[18] The experimental fluorescence excitation and detection conditions were conducted with negligible reabsorption processes which can effect TPA measurements. The two-photon absorption cross section of the probes was calculated at each wavelength according to equation 2.2.[19]

Equation 2.2 Two-photon absorption cross sections measurement

$$\delta_{sample} = \delta_{reference} \frac{\Phi_{(ref)} I_{(sample)} C_{(ref)} \eta_{(sample)}^{2} P_{(ref)}^{2}}{\Phi_{(sample)} I_{(ref)} C_{(sample)} \eta_{(ref)}^{2} P_{(sample)}^{2}} \qquad (2)$$

Where I is the integrated fluorescence intensity, C is the concentration, η is the refractive index, Φ is the quantum yield and P is the incident power on the sample, subscript ‘ref’ stands for reference samples, ‘sample’ stands for samples. The uncertainty in the measured cross sections was about ± 10 %.

2.6 Reference:

1. Helmchen, F.; Denk, W., Deep tissue two-photon microscopy. *Nature methods* **2005,** *2* (12), 932-40.

2. Denk, W.; Strickler, J. H.; Webb, W. W., Two-photon laser scanning fluorescence microscopy. *Science* **1990,** *248* (4951), 73-6.

3. Xu, C.; Zipfel, W.; Shear, J. B.; Williams, R. M.; Webb, W. W., Multiphoton fluorescence excitation: new spectral windows for biological nonlinear microscopy. *Proceedings of the National Academy of Sciences of the United States of America* **1996,** *93* (20), 10763-8.

4. Le Droumaguet, C.; Mongin, O.; Werts, M. H.; Blanchard-Desce, M., Towards "smart" multiphoton fluorophores: strongly solvatochromic probes for two-photon sensing of micropolarity. *Chem. Commun.* **2005,** (22), 2802-4.

5. Schafer-Hales, K. J.; Belfield, K. D.; Yao, S.; Frederiksen, P. K.; Hales, J. M.; Kolattukudy, P. E., Fluorene-based fluorescent probes with high two-photon action cross-sections for biological multiphoton imaging applications. *Journal of biomedical optics* **2005,** *10* (5), 051402.

6. Albota, M.; Beljonne, D.; Bredas, J. L.; Ehrlich, J. E.; Fu, J. Y.; Heikal, A. A.; Hess, S. E.; Kogej, T.; Levin, M. D.; Marder, S. R.; McCord-Maughon, D.; Perry, J. W.; Rockel, H.; Rumi, M.; Subramaniam, G.; Webb, W. W.; Wu, X. L.; Xu, C., Design of organic molecules with large two-photon absorption cross sections. *Science* **1998,** *281* (5383), 1653-6.

7. Pawlicki, M.; Collins, H. A.; Denning, R. G.; Anderson, H. L., Two-photon absorption and the design of two-photon dyes. *Angewandte Chemie* **2009,** *48* (18), 3244-66.

8. Kim, D.; Ryu, H. G.; Ahn, K. H., Recent development of two-photon fluorescent probes for bioimaging. *Organic & biomolecular chemistry* **2014,** *12* (26), 4550-66.

9. Myung Kim, H.; Rae Cho, B., Two-photon materials with large two-photon cross sections. Structure-property relationship. *Chem. Commun.* **2009,** (2), 153-64.

10. (a) Kim, H. M.; Cho, B. R., Two-photon fluorescent probes for metal ions. *Chemistry, an Asian journal* **2011,** *6* (1), 58-69; (b) Lim, C. S.; Cho, B. R., Two-photon probes for biomedical applications. *BMB reports* **2013,** *46* (4), 188-94.

11. Kim, H. M.; Jung, C.; Kim, B. R.; Jung, S. Y.; Hong, J. H.; Ko, Y. G.; Lee, K. J.; Cho, B. R., Environment-sensitive two-photon probe for intracellular free magnesium ions in live tissue. *Angewandte Chemie* **2007,** *46* (19), 3460-3.

12. Metten, B.; Smet, M.; Boens, N.; Dehaed, W., Synthesis of APTRA derivatives as building blocks for low-affinity fluorescent Ca2+ indicators. *Synthesis-Stuttgart* **2005,** (11), 1838-1844.

13. Das, R. K.; Samanta, A.; Ha, H. H.; Chang, Y. T., Solid phase synthesis of ultra-photostable cyanine NIR dye library. *Rsc Adv* **2011,** *1* (4), 573-575.

14. Ghosh, K. K.; Ha, H. H.; Kang, N. Y.; Chandran, Y.; Chang, Y. T., Solid phase combinatorial synthesis of a xanthone library using click chemistry and its application to an embryonic stem cell probe. *Chem. Commun.* **2011,** *47* (26), 7488-90.

15. Kang, M. Y.; Lim, C. S.; Kim, H. S.; Seo, E. W.; Kim, H. M.; Kwon, O.; Cho, B. R., Detection of nickel in fish organs with a two-photon fluorescent probe. *Chemistry* **2012,** *18* (7), 1953-60.

16. Seo, E. W.; Han, J. H.; Heo, C. H.; Shin, J. H.; Kim, H. M.; Cho, B. R., A small-molecule two-photon probe for nitric oxide in living tissues. *Chemistry* **2012,** *18* (39), 12388-94.

17. Li, J. R.; Zhang, G., Synthesis and crystal structure of 2-acetylnaphthalen-6-yl 4-methylbenzosulfonate. *J Chem Crystallogr* **2005,** *35* (10), 789-793.

18. Makarov, N. S.; Drobizhev, M.; Rebane, A., Two-photon absorption standards in the 550-1600 nm excitation wavelength range. *Optics express* **2008,** *16* (6), 4029-47.

19. Lee, S. K.; Yang, W. J.; Choi, J. J.; Kim, C. H.; Jeon, S. J.; Cho, B. R., 2,6-Bis[4-(p-dihexylaminostyryl)styryl]anthracene derivatives with large two-photon cross sections. *Organic letters* **2005,** *7* (2), 323-6.

Chapter: 3

Discovery of Alpha Cell Selective Two-Photon Fluorescent Probe TP-α

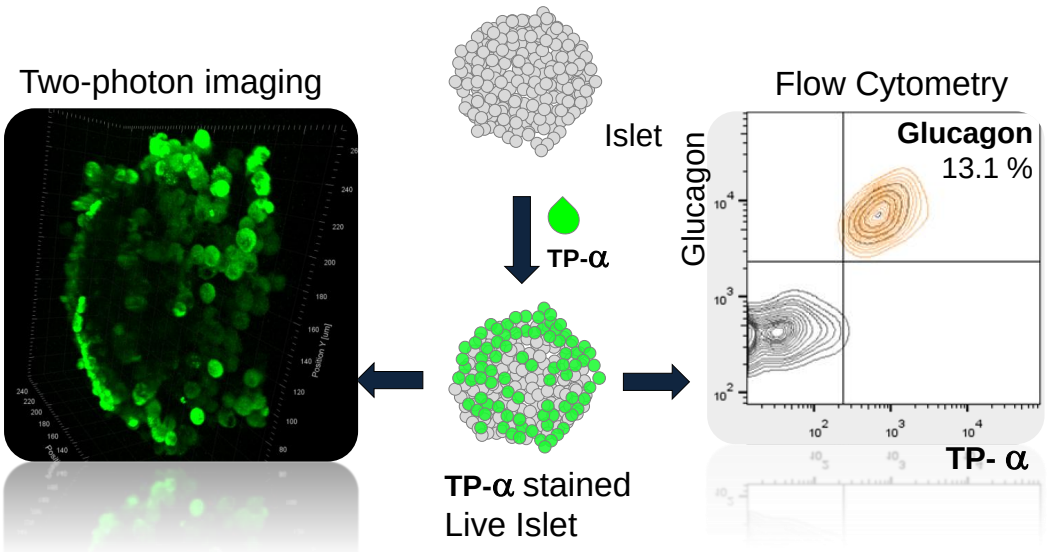

Chapter 3

3.1 Introduction

Pancreatic alpha cells secrete glucagon in response to low blood glucose level. Glucagon counter-regulates the hypoglycemic effect of insulin by glycogenolysis and gluconeogenesis.[1] Studies over the last decade showed that the human islets not only have architectural differences with the well-studied rodent islets, but also varied endocrine cell population.[2] These studies revealed that the proportion of beta cells in human islet is much less than the murine islets (approximately 55 % versus 77 %). On the contrary, the fraction of alpha cells is greater in human islet than murine islet (approximately 35 % versus 15 %).[2] Together, the higher alpha cell proportion and the unique association of alpha and beta cells in human islets have drawn more research interests to study pancreatic alpha cells for understanding their function and influence on diabetes. Although several beta cell imaging probes in use,[3,4,5] imaging of alpha cells is still in its infancy. The conventional technique for imaging alpha cells is based on glucagon immunostaining of pancreatic tissue sections or by the use of transgenic mouse models with a fluorescent reporter gene linked to the glucagon promoter.[6]

In addition, the metabolic status of pancreatic islets has also been determined via auto fluorescence imaging of NADPH[7,8] or cytosolic calcium imaging.[9] Previously, an OP small molecule probe, Glucagon Yellow (GY), was reported by our group as an alpha cell selective fluorescent probe (GY: **Figure 3.2 B**).[10] Despite the fact that GY has alpha cell selectivity, the negligible TP optical property (**Figure 3.2 C**) has limited its application as an efficient TP imaging probe. As such TP microscopy offers benefit over

OP microscopy for deep tissue imaging due to the utilization of high power pulsed near-infra-red excitation laser light.[11] GY showed high photo bleaching properties (**Figure 3.2 D**), which further limits its suitability as a TP imaging probe. Even though a few small molecule one photon fluorescent probes has been reported for islet imaging, no two-photon alpha cell imaging till date has been demonstrated with whole islet in live conditions.

TP microscopy utilizes two near-infrared photons as the excitation source and offers a number of advantages over OP microscopy including deeper penetration depth, localized excitation and longer observation time.[11] TP imaging is suitable for live deep tissue imaging and has been used for various types of tissues including brain imaging.[11] TP imaging technique has also been assessed for pancreatic islets either with auto-fluorescence imaging[7] or with various hydrophilic and hydrophobic agents.[12] Development of more novel TP probes suitable for live islet imaging will therefore be of great value to future bio imaging research.

New technological advancement in the TP microscopic techniques has created a high demand for the development of novel TP bio-imaging probes.[11,13] Although the fluorescent proteins have TP fluorescent excitation property,[14] their expression in target cells is expensive and tedious. Hence, small molecule fluorescent probes offer a better alternative. Cell based screening of fluorescent compound libraries has resulted in the discovery of various useful bio-imaging probes.[15,16,17,18,19,20] Herein, we report the discovery of a novel alpha cell selective TP fluorescent probe using cell-based screening of TP fluorescent dye libraries.

3.2 Objective

In this chapter, I discuss the discovery of a novel alpha cell selective probe, TPG-456. We screened the 480 compounds from two TP dye libraries (TPG: 240 compounds and TPC: 240 compounds) against three different pancreatic cell lines. One compound from TPG library (TPG-456) was found out to be a selective hit for alpha TC1 cell line. We named this TP alpha cell probe as **TP-α**. This probe was found to labels alpha cells quickly and effectively in live conditions and offers significant advantages over conventional glucagon antibody labeling which requires fixations and permeabilization. **TP-α** enables real-time staining and observation of alpha cells in live intact islet with TP imaging.

3.3 Result and Discussion

3.3.1 Discovery of TP-α: an alpha TC1 selective probe

The cell-based screening with fluorescent dye library has led to the rapid discovery of various cell-specific imaging probes.[15,16,17,18,19,20] To expedite the discovery of useful probes from synthesized TP libraries (**TPG** and TPC), we setup a cell-based screening system with three commercially available pancreatic cell lines; glucagon producing alpha TC1 cells, insulin producing beta TC6 cells and exocrine acinar 266-6 cells, as a model system (**Figure 3.1 A**). Primary image analysis based on relative fluorescent intensity revealed that one **TPG** compound has alpha cell-selective staining. After confirmatory tests and reproducibility in imaging and flow-cytometry the compound, **TPG**-456 ($\lambda_{abs}/\lambda_{em}$ = 370/510 nm, TP fluorescence action cross section = 107 GM, OP quantum yield Φ = 0.69) was selected to be the final alpha TC1 cell selective hit

(**TP-α**: **Figure 3.1A, B** and **Figure 3.2 C, D**). The MTT assay using alpha TC1 and beta TC6 cells revealed that the **TP-α** staining either at working (1 μM) or higher concentrations (2 μM) had minimal interference with the cell viability even up to 24 h (**Figure 3.11**). With these experiments, we confirmed the selectivity and non-toxicity of **TP-α** in alpha TC1 and beta TC6 cells in the working concentration range of the probe.

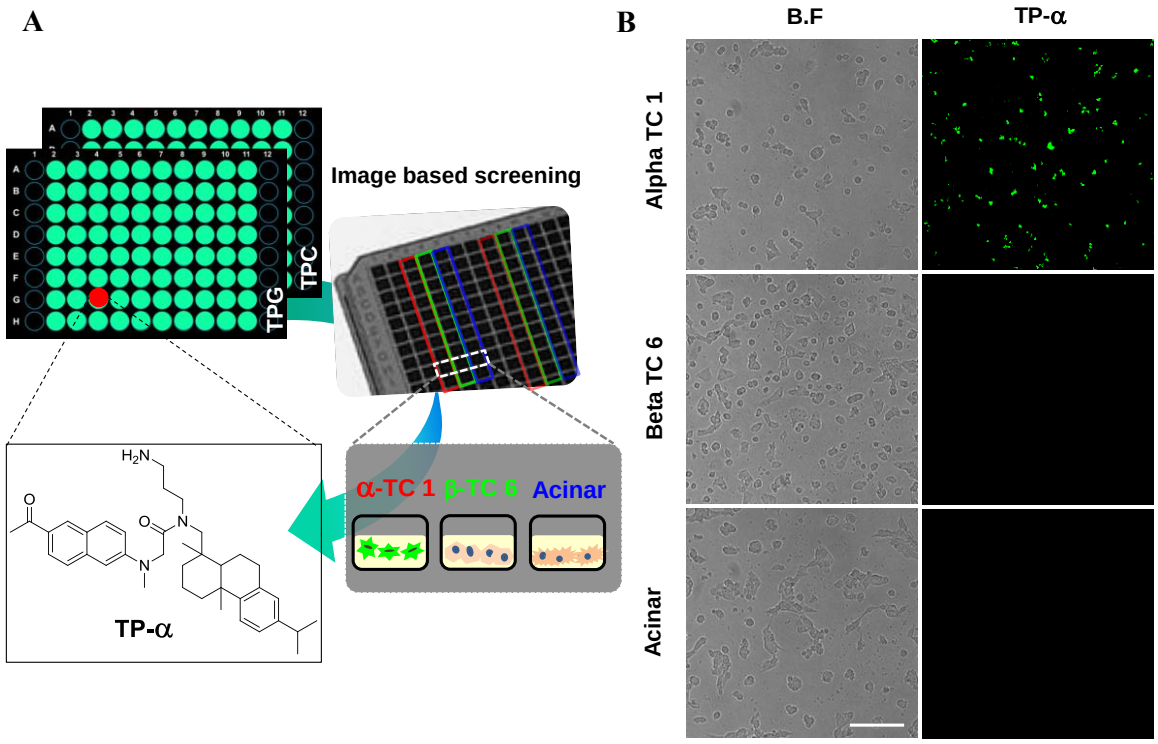

Figure 3.1 Cell based screening and hit discovery.

(A) Overview of image based screening for **TPG** library compounds. Three pancreatic cell lines Alpha TC1, Beta TC6 and Acinar 266-6 cells were used for discovery of pancreatic two photon imaging probe with 480 TP fluorescent dyes, lead to the discovery of Alpha TC1 cell selective probe: **TP-α**. (B) Selective staining of Alpha TC 1 cell by **TP-α**, in comparison with Beta TC6 and Acinar cells. Live cells were stained with 1 μM **TP-α** and incubated for 1 h at 37 °C before imaging. Images were captured with Image Xpress Micro system after PBS wash. Fluorescence data collected at 450-500 nm upon excitation at 370 nm. Scale bar 50 μm.

3.3.2 Photo physical property measurement of TP-α

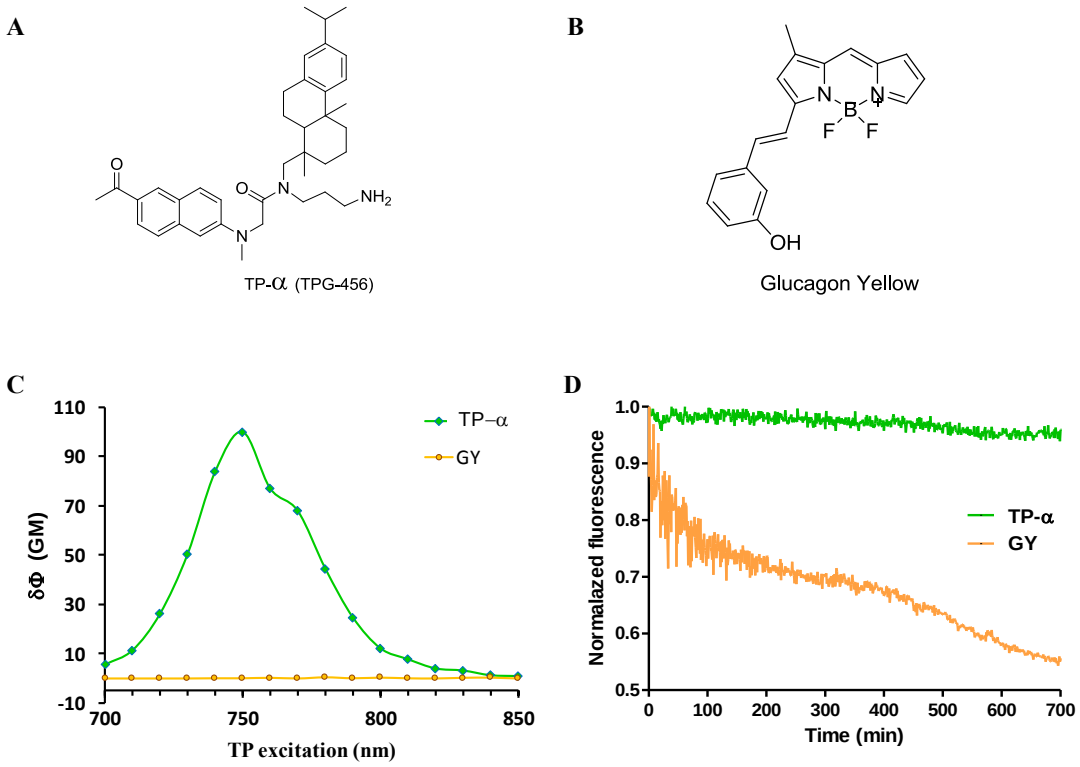

Figure 3.2 Chemical structure and optical property of **TP-α** and GY.

(A) Chemical structure of **TP-α** (B) Structure of Glucagon Yellow (C) Two-photon action cross section (δΦ in GM) of **TP-α** and Glucagon yellow (GY); measured at 10 μM in Methanol. (D) Photo-stability evaluation of **TP-α** and GY. Compounds were dissolved in PBS buffer (10 mM, pH 7.3) containing 1 % DMSO to a 10 μM final concentration and fluorescence measurements were recorded for 12 h at rt. Values are represented as means for sequential measurements every 1 min and fitted to a non-linear regression, one-phase exponential decay.

3.3.3 *In-vitro* fluorescence response of TP-α

Since **TP-α** selectively stains glucagon producing alpha cells in comparison with insulin producing beta cells in islets, we evaluated the fluorescence response of **TP-α** with glucagon and insulin first. We found that, **TP-α** not only have concentration dependent fluorescence response with glucagon (**Figure 3.3 A**), but also have more than 8 fold fluorescence intensity with Glucagon in comparison with Insulin (**Figure 3.3 C**).

The fractional saturation curve of **TP-α** (6 μM) with glucagon revealed a dissociation constant of 65.44 μM (**Figure 3.3 B**). We also evaluated the fluorescence response of **TP-α** with pancreatic signaling molecules like acetylcholine,[21] dopamine[22] and found no response with them. Moreover the *in vitro* study with 23 other biological analytes revealed excellent glucagon selectivity of **TP-α** (**Figure 3.3 C**).

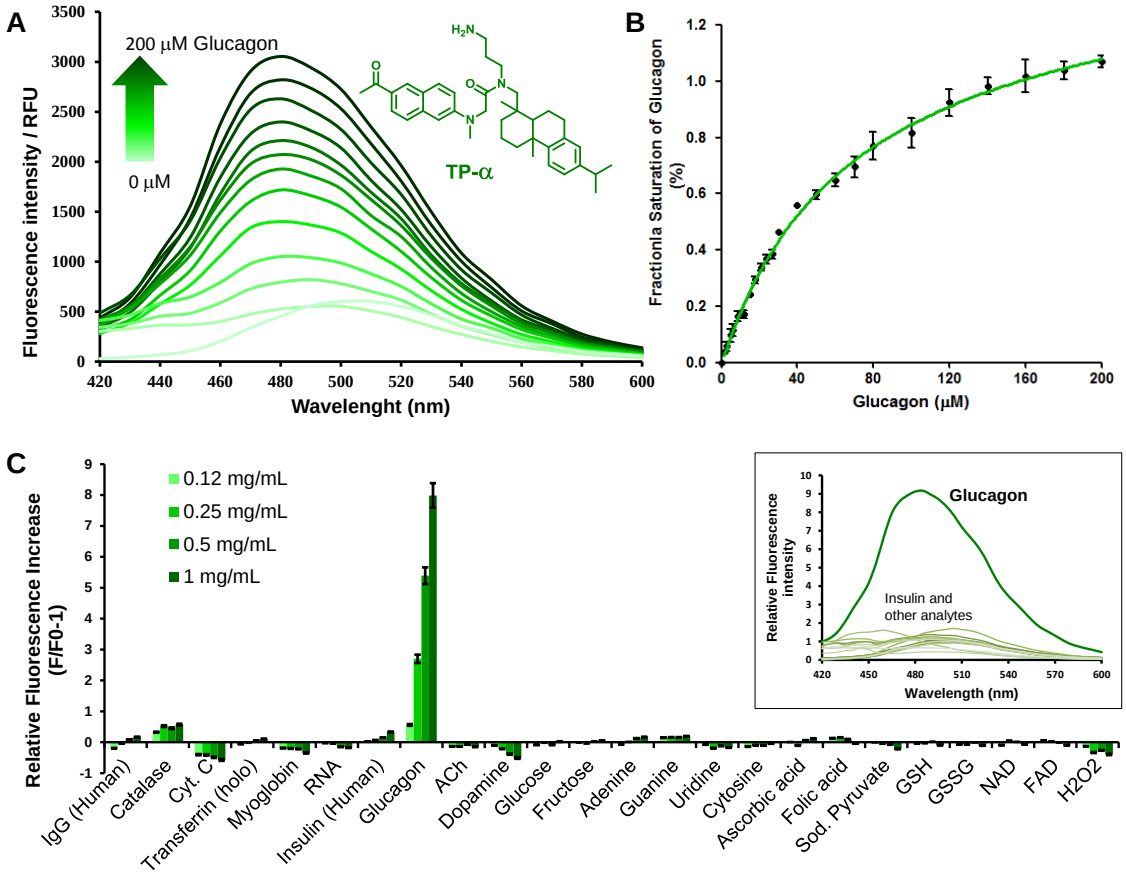

Figure 3.3 *In vitro* fluorescence responses of **TP-α**.

(A) Fluorescence spectra of **TP-α** (10 μM) without glucagon and upon incubation with different concentration of glucagon (from 10 μM to 200 μM) in 10 mM phosphate buffer (1 % DMSO, pH 7.4) under excitation of 370 nm light. Insert is the structure of **TP-α**. (B) Fractional saturation curve of glucagon with **TP-α**. Various concentration of glucagon were incubated with 6 μM **TP-α** for 30 min on ice in 10 mM phosphate buffer (pH 7.3, 1 % DMSO), followed by measurement of fluorescent emission. Experimental K_D = 65.44 μM. (C) Selectivity of **TP-α** (10 μM) for glucagon in comparison with insulin, other proteins and small molecule analytes (H_2O_2 30 % solution in water). Insert

show the selective increase in fluorescent emission of **TP-α** with glucagon in comparison to other analytes. Values are represented as mean and error bars are standard deviation (n = 3).

3.3.4 TP-α stains primary alpha cell selectively

The alpha TC1 cell selective **TP-α** still require reconfirmation in primary alpha cells.[23] Alpha cells are an integral component of the pancreatic islet of Langerhans. Islet tissues are scarce and represent only about 1-2 % of the whole pancreas.[24,25] The scarceness of these cells in mice pancreatic islet makes selective alpha cell imaging a challenging task. To avoid the hassle of isolating the rare primary alpha cells from islets, we decided to use whole islets for further studies. Islets were partially dissociated[26] and cultured over a week for imaging and immunostaining studies (**Figure 3.5 A** and **Figure 3.8A, B**). Staining with **TP-α** showed small populations (~13 ± 4 %) of the islet cells with bright fluorescence signal (**Figure 3.5, 3.6** and **3.8**) and as expected, this population fell within the range of alpha cell population (10 - 20 %).[2,24] Based on the image analysis and flow cytometry data, the **TP-α** positive cells showed higher fluorescent signal than other dim islet cells (**Figure 3.4, 3.6** and **3.8**). Further validation was carried out with the glucagon immunostaining of cultured islet cells and it was noticed that the **TP-α** bright population were glucagon positive (**Figure 3.5**).

Likewise, flow cytometry also revealed the **TP-α** bright population was merged with glucagon antibody positive alpha cells (**Figure 3.5 B**). These data illustrate that **TP-α** not only stained alpha TC1 cell selectively but also selectively stains the mouse primary alpha cells in comparison with the other islet cells.

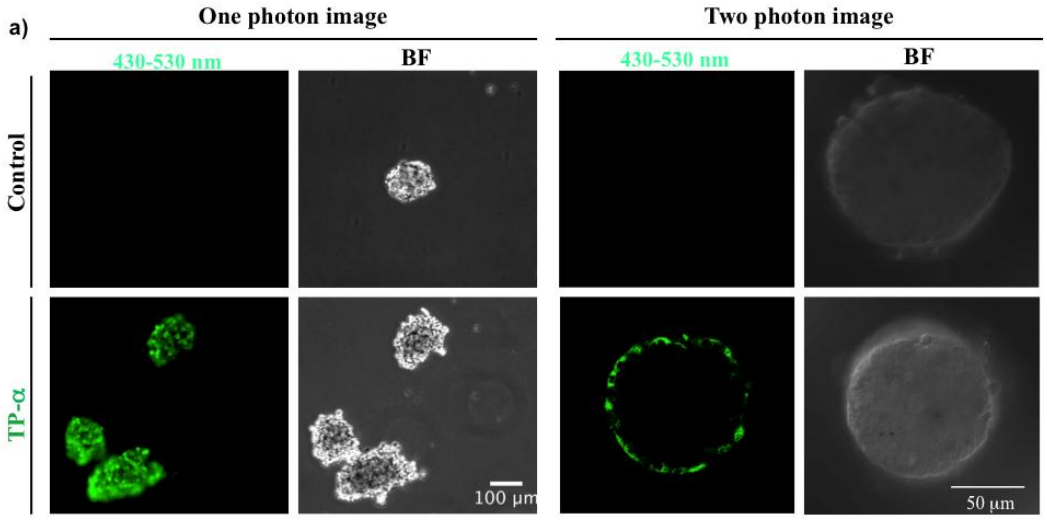

Figure 3.4 One-photon and two-photon live islet imaging.

Freshly isolated islet stained by **TP-α** 1 μM, Incubation for 1 h at 37 °C, images taken after washing with fresh media. One-photon images were taken by 10X objective with Nikon Ti microscope. ($\lambda_{abs}/\lambda_{em}$ = 370/ 490-510 nm). Two photon Images were captured using 40Xwater immersion objective by Leica TCS SP5x MP. ($\lambda_{abs}/\lambda_{em}$ = 750 fs/430-530 nm).

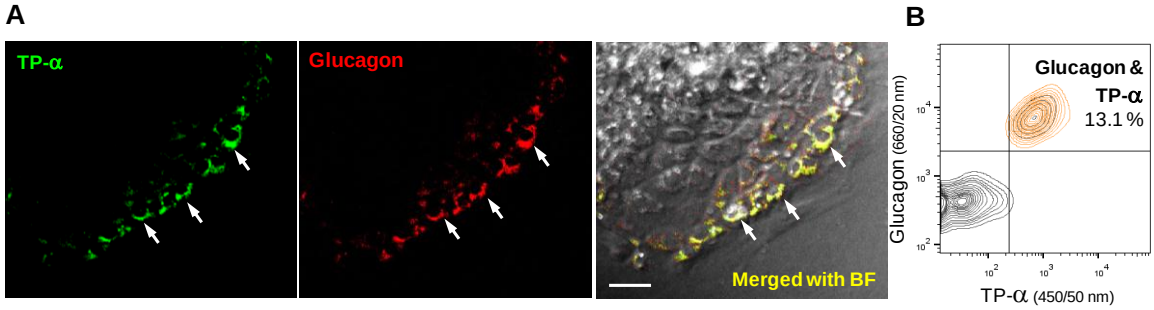

Figure 3.5 Antibody confirmation of **TP-α** selectivity

(A) Over one week cultured pancreatic islets stained with 1 μM **TP-α** followed by immunostaining with glucagon antibody (Cy5 secondary antibody signal at 650-670 nm). Merged image demonstrates the **TP-α** stained cells to be glucagon positive alpha cells. White arrow indicates some representative **TP-α** and glucagon positive cells. **TP-α** Ex/Em: 750 nm (fs)/ 430-530 nm and Glucagon ab. signal Ex/Em 630 nm/ 650-670nm. The images captured with monochrome detector and color used is false color. Scale bar 50 μm. (B) Dual parametric contour plot for **TP-α** and glucagon antibody stained pancreatic islet cells shows, **TP-α** positive subpopulation to be glucagon antibody positive (13.1 % dual positive).

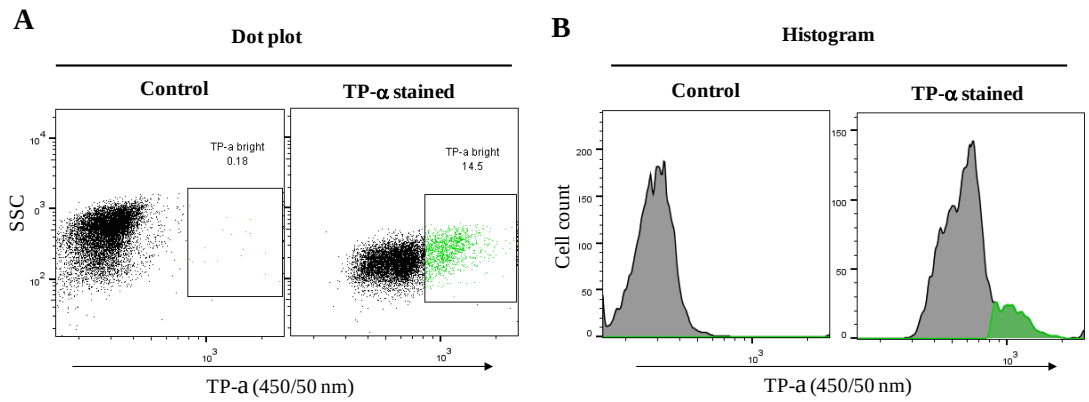

Figure 3.6 Flow cytometry for **TP-α** stained and control islet cells.

Freshly isolated mice islets control and 0.5 μM **TP-α** stained, were dissociated and analyzed with flow cytometry. (A) Dot plots (B) histograms for control (showing 0.1 % bright cell) and **TP-α** stained (14.5 % bright cells) in the gated region. Dim populations marked in black/grey color and **TP-α** bright cells (the population within the gatting region) marked as green color.

3.3.5 Alpha cell enrichment with TP-α staining

The appearance of the brightly stained alpha cell sub population of **TP-α** stained live islet cells was seen from the flow cytometry data (**Figure 3.5 B** and **3.6 A, 3.6 B**). This inspired us to assess the utility of this probe for the isolation and enrichment of brightly stained alpha cells. When we performed Fluorescence-activated cell sorting (FACS) to sort out the **TP-α** bright cells (15 %) from the **TP-α** stained islet cells suspension and monitor them with the glucagon immunostaining. The sorted out **TP-α** positive population were about five times enriched with alpha cells than in the native alpha cell population (**Figure 3.7**). Hence, by simple one step sorting based on **TP-α** bright cells gating ($\lambda_{abs}/\lambda_{em}$ = 405/485 ± 15 nm), we can enrich the mouse primary alpha cell.

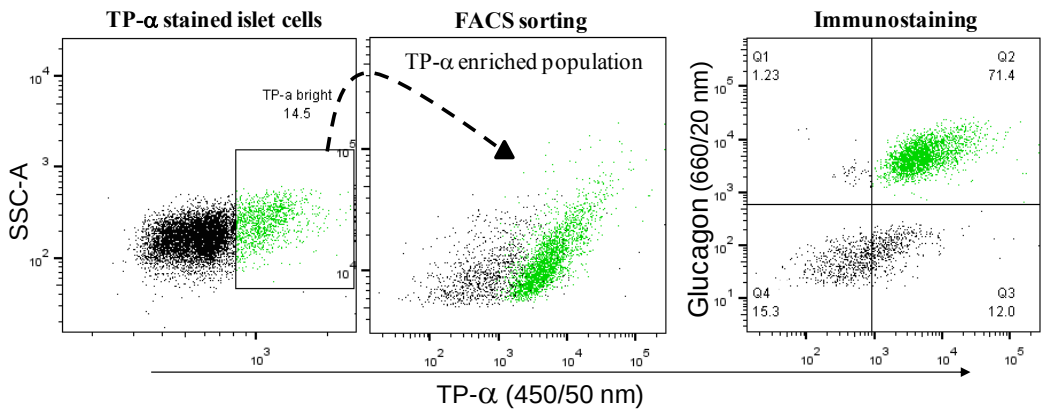

Figure 3.7 FACS sorting and enrichment of alpha cells with **TP-α** staining.

Dissociated islet cells from mice were stained with 0.5 μM **TP-α** followed by FACS sorting. 15 % **TP-α** bright cells were sorted and analyzed with glucagon antibody immunostaining. Dual parametric dot-plot show 71.4 % populations from the shorted cells are glucagon positive alpha cells.

3.3.6 TP-α stains alpha cells in live fresh islet.

Finally, we applied **TP-α** staining for alpha cell imaging on freshly isolated intact islet. **TP-α** stained pancreatic islets (**Figure 3.8 C-F**) showed three-dimensional distribution of brightly stained alpha cells on the surface of mice pancreatic islets in live condition (**Figure 3.9 A-B**). We found that, 1 μM **TP-α** staining for 1 h was the optimal staining for both OP and TP imaging (**Figure 3.4** and **3.8**). By evaluating the optical property of **TP-α** using TP spectral images, we found 750 nm (fs excitation light) and 430-530 nm (emission channel) to be the most suitable excitation light and emission channels for **TP-α** imaging. Likewise, TP optical sections of **TP-α** stained live islet even at the middle plane (~50 μm depth from the bottom of islet on the coverslip) showed good contrast between bright and dim cells (**Figure 3.8 C-F**). The discontinuous distribution of **TP-α** stained alpha cells at the mantle position on the islets displayed the native distribution of alpha cells (**Figure 3.8 C-F**) and matches with previous report.[27]

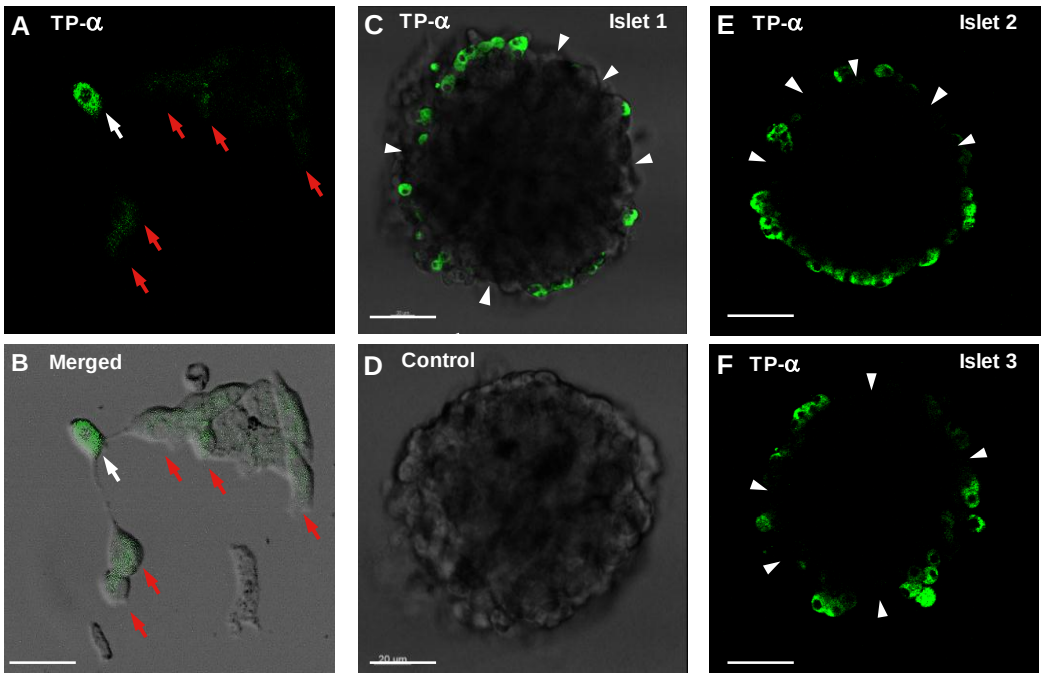

Figure 3.8 Two Photon imaging of **TP-α** stained live islet.

(A) Selective staining of alpha cell by **TP-α** in the cultured dissociated islet cells in live condition. Two-photon fluorescent live imaging of cultured islet cells after incubation with 1 μM **TP-α** for 1 h at 37 °C. (B) Merged image with bright field showing the both TP-α bright alpha cell (white arrow) and **TP-α** dim other islet cells (red arrow). Scale bar 15 μm. (C) Overlay of bright field and two-photon fluorescence image of islet treated with 1 μM **TP-α** for 1 h at 37 °C. Shows distribution of **TP-α** brightly stained alpha cells on the edge of the islet. Arrow head indicates absence of alpha cells in the mantle position. (~50 μm depth representative images) (D) For control DMSO 0.5 % for 1 h at 37 °C was used. Scale bar 50 μm. (E) and (F) Two-photon fluorescent optical section images of individual **TP-α** stained live islets.

The surface localization of alpha cells makes them susceptible to fall off during the enzymatic tissue digestion during islet isolation from the mice.[27] The isolated islets when stained with **TP-α**, we found that the over digested islets do not have **TP-α** bright cells on its surface. The simple **TP-α** staining can be a useful tool to examine the presence or absence of alpha cells on the isolated islets.

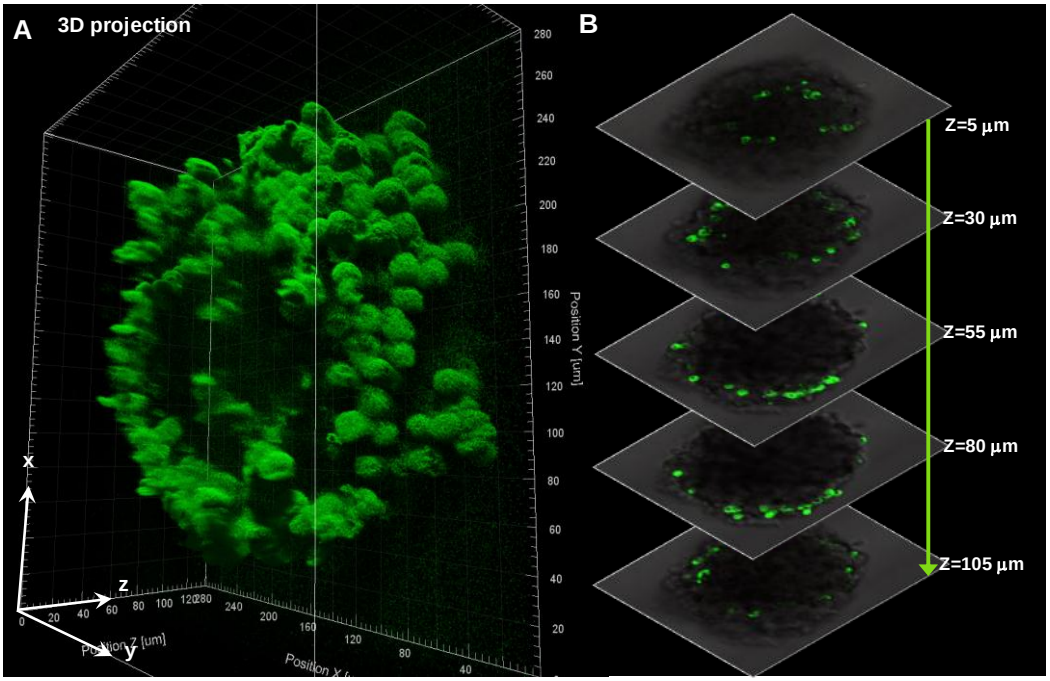

Figure 3.9 3D Projection of **TP-α** stained islet

(A) 3D Surface projection of the two-photon z-stack images for **TP-α** stained live islet (step size, 0.17 mm) using image processing software IMARIS (Supporting Video S1). (B) Representative sectional overlaid TPM images of **TP-α** stained live islet at the depth range of 5 μm to 105 μm. It reveals the natural distribution of alpha cells in the mouse pancreatic islet in live condition. Two-photon imaging was performed on 16 weeks old mouse pancreatic islet. All images taken with 40X water immersion objective using Leica TCS SP5X MP, Ex: 750 nm fs laser light, Em: 430-530 nm (images are represented from n = 30 islets).

In order to assure that this mantle staining is due to the selective staining of alpha cells and not due to impermeability of the fluorescent probe, we stained both intact islets and dissociated islet cells with **TP-α** and confirmed with flow cytometry. For both intact and dissociated islet staining conditions, we found similar **TP-α** stains similar sub-population of cells (15 ± 3 %, **Figure 3.10**). Similar sub-population staining with **TP-α** even in dissociated islet condition (18 ± 2 %) revealed that, **TP-α** staining of these cells is because of its intrinsic specificity to alpha cells and not due to surface localization. By far, this is the first demonstration where a selective alpha cell TP imaging in live

pancreatic islet is achieved with alpha cell specific small molecule fluorescent probe (**Figure 3.8** and **3.9**).

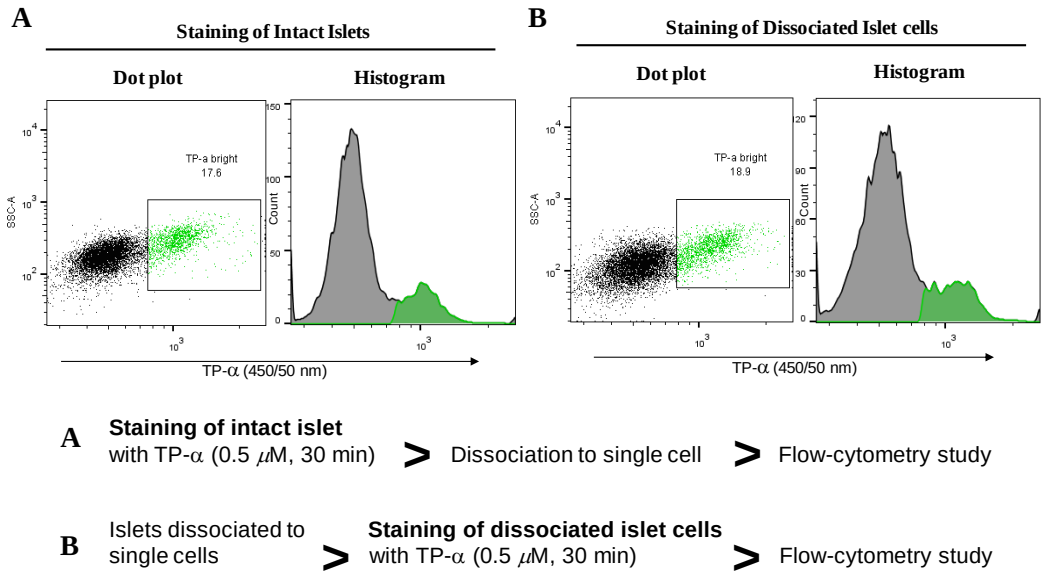

Figure 3.10 **TP-α** staining of islet in intact and dissociated condition.

Freshly isolated islets stained with 0.5 μM **TP-α** either directly intact islet (A) or after dissociation to single cell with trypsinization (B). Dim populations marked in black/grey color and **TP-α** bright cells (the population within the gating region) marked as green color.

3.4 Conclusion

In conclusion, the image-based screening of **TPG** and TPC libraries led to the discovery of a novel TP imaging probe **TP-α** for live alpha cell imaging in intact mice islets. **TP-α** is suitable for both TP islet imaging as well as the flow-cytometry study of scarce primary alpha cells from mice pancreatic islet tissue. Furthermore, *in vitro* fluorescence response test of **TP-α** with 23 relevant biological analytes displayed an excellent selectivity towards glucagon. The glucagon and alpha cell selective **TP-α** may

serve as a useful tool in pancreatic islet research for monitoring the survival or distribution of alpha cells during islet isolation and transplantation procedure.

3.5 Experimental details

3.5.1 Characterization of TP-α.

^{1}H NMR **TP-α** (**TPG-456**) (CD_3OD, 300 MHz), δ (ppm): 8.33 (dd, J = 18, 1.8 Hz, 1H), 7.84 (dd, J = 10.5, 1.8 Hz, 1H), 7.80 (s, 1H), 7.56 (dd, J = 8.4, 1.2 Hz, 1H), 7.05 (dd, J = 9, 2.1 Hz, 1H), 6.95 (m, 1H), 6.85 (d, J = 1.5 Hz, 1H), 6.74 (d, J = 1.5 Hz, 1H), 4.44 (s, 2H), 3.16 (s, 3H), 3.08 (s, 5H), 2.64 (s, 3H), 2.11 (m, 4H), 1.26 (s, 6H), 1.17 (m, 14H), 1.11 (s, 3H), 0.966 (s, 3H). ^{13}C NMR **TPG-M456** (CD_3OD, 75 MHz), δ (ppm): 198.22, 170.60, 161.26, 160.81, 149.03, 146.33, 145.63, 144.95, 133.15, 129.82, 125.57, 125.19, 124.43, 122.86, 117.86, 114.97, 114.00, 104.52, 59.18, 39.95, 39.22, 38.97, 37.24, 36.95, 36.76, 36.47, 36.19, 35.24, 34.54, 32.64, 29.09, 28.60, 28.41, 24.48, 23.47, 22.45, 18.49, 16.09. ESI-MS m/z (M+H) calcd: 582.39, found 582.20. ESI-HRMS of **TP-α** m/z (M+H) calcd: 582.4060 and found 582.4062.

3.5.2 *In vitro* fluorescence screening

TP-α (10 μM) was used for fluorescence property measurement and *in vitro* screening in 10 mM phosphate buffer (pH 7.3, 1 % DMSO). Fluorescence intensity was measured using SpectraMax M2 plate reader in 96 well plates. We used 370 nm wavelength light for excitation and emission was observed from 420 not to 600 nm. All analytes were tested in four concentration with serial dilution ranged from 1 mg/mL to 0.12 mg/mL. We used both macromolecules; IgG (human), Catalase, Cytochrome C, Transferrin (holo), Myoglobin, RNA, Insulin (human), Glucagon and small molecule analytes; Acetylcholine, Dopamine, Glucose, Fructose, Adenine, Guanine, Uridine, Cytosine, Ascorbic acid, Folic acid, Sod. Pyruvate, Glutathione, Glutathione reduced, β-

Nicotinamide adenine dinucleotide (NAD), Flavin adenine dinucleotide (FAD) and 30 % Hydrogen peroxide in the selectivity test. After the addition of dye the 96 well plates were incubated on ice for 30 min before fluorescence measurement.

3.5.3 Cell culture.

Insulin producing beta-TC6 (ATCC® CRL-11506™), glucagon producing alpha TC1 clone 6 (ATCC® CRL-2934™) and exocrine acinar cells 266-6 (ATCC® CRL-2151™) were obtained from the American Type Culture Collection (ATCC) and maintained according to ATCC protocols. Beta and acinar cells were cultured using Dulbecco's Modified Eagle's Medium (DMEM) with 4500 mg/L D-glucose, supplemented with 10 % fetal bovine serum (FBS) and 1 % penicillin-streptomycin. Alpha TC1 cells were cultured in DMEM with 1000 mg/L D-glucose, supplemented with 15 % heat inactivated FBS, 2.0 g/L D-glucose, 15 mM HEPES and 0.1 mM non-essential amino acids (GIBCO, Life Technologies, Carlsbad, CA, United States).

3.5.4 Image-based screening

A primary screening platform was established with the alpha TC1, beta-TC6 and acinar 266-6 cells. All three cell lines were seeded into 384 well plates and allowed to settle overnight before use. The cells were incubated with 0.5 and 1 μM of **TPG** library-80 compounds for 1 h. Wells were washed one time with fresh media to reduce the background before image acquisition. Automated imaging system ImageXpress® Micro with 10X objectives was used to capture the images.

3.5.5 Islet isolation, dissociation, culture and imaging

Primary pancreatic islets were isolated from the 16 week old C57BL/6 (WT) male mice. The animal handling and tissue harvesting is in accordance with the Institutional

Animal Care and Use Committee of Singapore Bio-imaging Consortium (Agency of Science, Technology and Research, Singapore). Pancreatic islets were isolated by Collagenase P digestion and islet picking methods as described earlier.[26] Briefly, fresh pancreas was cut into small pieces and digested with 1 mg/mL collagenase P (Roche, Indianapolis, IN, USA) solution in Hank's Balanced Salt Solution (HBSS; Invitrogen) for 10 minutes at 37 °C on a shaker, followed by 4 times buffer washing to remove the digested exocrine tissue. Manual picking of intact islets was carried out using Zeiss Stemi DV4 stereomicroscope. Islets were maintained in DMEM with 4500 mg/L glucose + 10 % FBS and 1 % penicillin-streptomycin (GIBCO, Life Technologies, Carlsbad, CA, United States) for 24 h before TP imaging. Islets were stained with 1 μM **TP-α** for 1 h at 37 °C and were transferred to fresh media for TP image acquisition. Primary pancreatic islet cells were dissociated by trypsinization and trituration method. Approximately 50 - 100 islets were dissociated by incubating with 0.25 % Trypsin-EDTA (1X), phenol red (GIBCO) for 2 minutes at 37 °C followed by trituration with repeated pipetting. Finally, the dissociated islet cells were transferred to the 4500 mg/L D-glucose DMEM with 10 % FBS and 1 % penicillin-streptomycin (GIBCO) for culture.[26] Dissociated cells were cultured for 1 week, with media change every 2-3 days. The cells were stained with 1 μM **TP-α** for 1 h at 37 °C and were transferred to fresh media before TP image acquisition.

3.5.6 OP and TP imaging

All confocal and TP imaging was done using Leica TCS SP5X MP (Leica Microsystems CMS GmbH, Mannheim, Germany) with 405 nm laser light for OP excitation and 750 nm femtosecond (fs) pulsed laser for TP excitation for **TP-α**. Images were taken using 10X dry, 40X water and 100X oil objectives. The TP excitation of **TP-α**

was achieved by titanium-sapphire laser light set at wavelength 750 nm and an output power of 2710 mW. To obtain the probe signal, internal photomultiplier tube was set at 430 to 530 nm. Image analysis and intensity measurements were carried out by Leica Application Suite Advanced Fluorescence (LAS AF). 3D projection of Z-stack TP images were processed with IMARIS software (Bitplane AG, Switzerland.) and the intensity is depicted as false color.

3.5.7 Immunostaining

Primary cells and islets were fixed in 4 % Paraformaldehyde and permeabilized with 0.1 % Triton-X 100. Fixed Cells were identified by primary antibodies against secretory markers at the respective dilutions: alpha cell - Glucagon (Sigma-Aldrich 3050 Spruce St. St. Louis, USA) 1:2000. For secondary antibody staining, Cy5® goat anti-mouse IgG (Invitrogen, Molecular Probes Inc, USA) was used. Images were scored using intensity analysis software MetaXpress® and confirmed by image-based visual analysis.

3.5.8 Cytotoxicity assays

Cytotoxicity assays were carried out using the MTS reagent kit (Promega) for 1-24h, with 1 and 2 μM **TP-α** treated alpha and beta cells in accordance with the manufacturer's instructions.

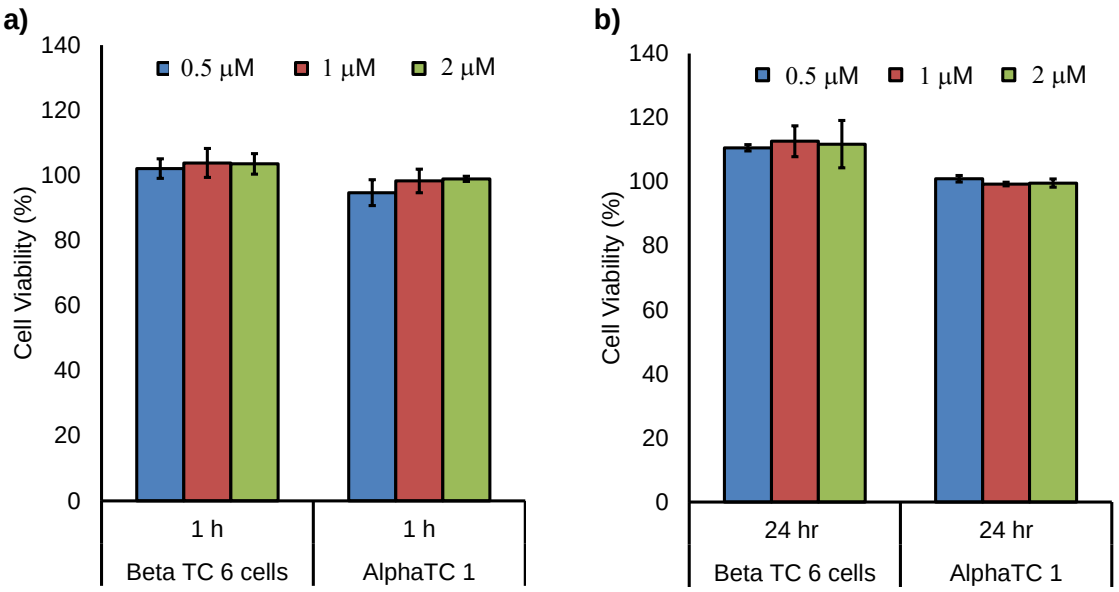

Figure 3.11 Cell viability study.

Cytotoxic effect of **TP-α** (**TPG-456**) in alpha TC1 and Beta TC6 cells. The cytotoxic effect of **TP-α** was tested by the MTS (3-(4,5-dimethylthiazol-2-yl)-5-(3-carboxymethoxyphenyl)-2-(4-sulfophenyl)-2H-tetrazolium, inner salt) assay using the Cell Titer 96 non-radioactive cell proliferation colorimetric assay kit (Promega) on alpha TC1 and beta TC6 cells. First, the alpha TC1 and beta TC6 cells (1 X 10^4cells in 100 μl of media) were seeded onto 96 well plate and then different concentrations (0 μM, 0.5 μM, 1 μM and 2 μM) of **TP-α** was added to the cells on the following day and incubated them for 1 h at 37 °C. After 1 h 20 μl of MTS solution was added to each well and incubated for another 2 hours before the absorbance was measured at 490 nm using Spectrometer. The same experiments were done for Day 1 (24 h). The control cells were 100 % alive without compound condition. At least 95 % of the **TP-α** treated cells were alive even after 24 h of incubation at 2 μM concentration. This indicates that the **TP-α** is nontoxic to alpha TC1 and beta TC6 cells.

3.5.9 Flow cytometry

Primary islet cell cultures were generated from the islets of C57BL/6 (WT) male mice as described above. Cells were stained with 0.5 μM of **TP-α** for 1 h at 37 °C and washed with Phosphate Buffer Saline (PBS) before acquisition on the BD LSR II analyzer. Cells were acquired using the appropriate filters for **TP-α** (Pacific blue; excitation laser light 405 nm and emission at 450/50 nm) and secondary antibody (Glucagon – Cy5).

3.5.10 Dissociation constant determination

The fluorescent emission spectra of **TP-α** was measured with various concentration of Glucagon by using SpectraMax M2 plate reader.[9] The fluorescent titration curve was fitted to the standard equation using Graphpad Prism 5 software. **TP-α** (6 μM) was titrated with different concentration of Glucagon (1-200 μM) in 1 mM phosphate buffer and the fluorescent intensity was measured at 480 nm (excitation at 370 nm). The bound fraction (X) of Glucagon at each concentration was determined using the eq. 3.1

Equation 3.1 Dissociation constant.

$$X = \frac{F_C - F_0}{F_C - F_0} \qquad (1)$$

Where *F*c and *F*o are the fluorescence intensities of a given concentration of **TP-α** with and without glucagon, respectively. *F*sat is the fluorescence intensity at the concentration of Glucagon when fully bound. The results were plotted according to nonlinear fitting curve eq. 3.2

Equation 3.2 Nonlinear fitting curve equation

$$F = F_0 + \frac{(F_{sat} - F_0)([\text{TP-}\alpha])}{K_D + [\text{TP-}\alpha]} \qquad (2)$$

Where K_D is the dissociation constant, [**TP-α**] is the concentration of **TP-α.**

3.6 References

1. Quesada, I.; Tuduri, E.; Ripoll, C.; Nadal, A., Physiology of the pancreatic alpha-cell and glucagon secretion: role in glucose homeostasis and diabetes. *The Journal of endocrinology* **2008,** *199* (1), 5-19.

2. Cabrera, O.; Berman, D. M.; Kenyon, N. S.; Ricordi, C.; Berggren, P. O.; Caicedo, A., The unique cytoarchitecture of human pancreatic islets has implications for islet cell function. *Proceedings of the National Academy of Sciences of the United States of America* **2006,** *103* (7), 2334-9.

3. Kang, N. Y.; Lee, S. C.; Park, S. J.; Ha, H. H.; Yun, S. W.; Kostromina, E.; Gustavsson, N.; Ali, Y.; Chandran, Y.; Chun, H. S.; Bae, M.; Ahn, J. H.; Han, W.; Radda, G. K.; Chang, Y. T., Visualization and isolation of Langerhans islets by a fluorescent probe PiY. *Angewandte Chemie* **2013,** *52* (33), 8557-60.

4. Latif, Z. A.; Noel, J.; Alejandro, R., A simple method of staining fresh and cultured islets. *Transplantation* **1988,** *45* (4), 827-30.

5. Lukowiak, B.; Vandewalle, B.; Riachy, R.; Kerr-Conte, J.; Gmyr, V.; Belaich, S.; Lefebvre, J.; Pattou, F., Identification and purification of functional human beta-cells by a new specific zinc-fluorescent probe. *The journal of histochemistry and cytochemistry : official journal of the Histochemistry Society* **2001,** *49* (4), 519-28.

6. Quoix, N.; Cheng-Xue, R.; Guiot, Y.; Herrera, P. L.; Henquin, J. C.; Gilon, P., The GluCre-ROSA26EYFP mouse: a new model for easy identification of living pancreatic alpha-cells. *FEBS letters* **2007,** *581* (22), 4235-40.

7. Bennett, B. D.; Jetton, T. L.; Ying, G.; Magnuson, M. A.; Piston, D. W., Quantitative subcellular imaging of glucose metabolism within intact pancreatic islets. *The Journal of biological chemistry* **1996,** *271* (7), 3647-51.

8. Patterson, G. H.; Knobel, S. M.; Arkhammar, P.; Thastrup, O.; Piston, D. W., Separation of the glucose-stimulated cytoplasmic and mitochondrial NAD(P)H responses in pancreatic islet beta cells. *Proceedings of the National Academy of Sciences of the United States of America* **2000,** *97* (10), 5203-7.

9. Asada, N.; Shibuya, I.; Iwanaga, T.; Niwa, K.; Kanno, T., Identification of alpha- and beta-cells in intact isolated islets of Langerhans by their characteristic cytoplasmic Ca2+ concentration dynamics and immunocytochemical staining. *Diabetes* **1998,** *47* (5), 751-7.

10. Lee, J. S.; Kang, N. Y.; Kim, Y. K.; Samanta, A.; Feng, S.; Kim, H. K.; Vendrell, M.; Park, J. H.; Chang, Y. T., Synthesis of a BODIPY library and its application to the development of live cell glucagon imaging probe. *Journal of the American Chemical Society* **2009,** *131* (29), 10077-82.

11. Helmchen, F.; Denk, W., Deep tissue two-photon microscopy. *Nature methods* **2005,** *2* (12), 932-40.

12. Takahashi, N.; Nemoto, T.; Kimura, R.; Tachikawa, A.; Miwa, A.; Okado, H.; Miyashita, Y.; Iino, M.; Kadowaki, T.; Kasai, H., Two-photon excitation imaging of pancreatic islets with various fluorescent probes. *Diabetes* **2002,** *51 Suppl 1*, S25-8.

13. Pawlicki, M.; Collins, H. A.; Denning, R. G.; Anderson, H. L., Two-photon absorption and the design of two-photon dyes. *Angewandte Chemie* **2009,** *48* (18), 3244-66.

14. Drobizhev, M.; Makarov, N. S.; Tillo, S. E.; Hughes, T. E.; Rebane, A., Two-photon absorption properties of fluorescent proteins. *Nature methods* **2011,** *8* (5), 393-9.

15. Kang, N. Y.; Ha, H. H.; Yun, S. W.; Yu, Y. H.; Chang, Y. T., Diversity-driven chemical probe development for biomolecules: beyond hypothesis-driven approach. *Chemical Society reviews* **2011,** *40* (7), 3613-26.

16. Yun, S. W.; Kang, N. Y.; Park, S. J.; Ha, H. H.; Kim, Y. K.; Lee, J. S.; Chang, Y. T., Diversity oriented fluorescence library approach (DOFLA) for live cell imaging probe development. *Accounts of chemical research* **2014,** *47* (4), 1277-86.

17. Ljosa, V.; Carpenter, A. E., High-throughput screens for fluorescent dye discovery. *Trends in biotechnology* **2008,** *26* (10), 527-30.

18. Yoo, J. S.; Lee, S. C.; Jow, Z. Y.; Koh, P. Y.; Chang, Y. T., A macrophage-specific fluorescent probe for intraoperative lymph node staging. *Cancer research* **2014,** *74* (1), 44-55.

19. Leong, C.; Zhai, D.; Kim, B.; Yun, S. W.; Chang, Y. T., Neural stem cell isolation from the whole mouse brain using the novel FABP7-binding fluorescent dye, CDr3. *Stem cell research* **2013,** *11* (3), 1314-22.

20. Feng, S.; Kim, Y. K.; Yang, S.; Chang, Y. T., Discovery of a green DNA probe for live-cell imaging. *Chem. Commun.* **2010,** *46* (3), 436-8.

21. Molina, J.; Rodriguez-Diaz, R.; Fachado, A.; Jacques-Silva, M. C.; Berggren, P. O.; Caicedo, A., Control of insulin secretion by cholinergic signaling in the human pancreatic islet. *Diabetes* **2014,** *63* (8), 2714-26.

22. Ustione, A.; Piston, D. W.; Harris, P. E., Minireview: Dopaminergic regulation of insulin secretion from the pancreatic islet. *Molecular endocrinology* **2013,** *27* (8), 1198-207.

23. Rouille, Y.; Westermark, G.; Martin, S. K.; Steiner, D. F., Proglucagon is processed to glucagon by prohormone convertase PC2 in alpha TC1-6 cells. *Proceedings of the National Academy of Sciences of the United States of America* **1994,** *91* (8), 3242-6.

24. Speier, S.; Nyqvist, D.; Cabrera, O.; Yu, J.; Molano, R. D.; Pileggi, A.; Moede, T.; Kohler, M.; Wilbertz, J.; Leibiger, B.; Ricordi, C.; Leibiger, I. B.; Caicedo, A.; Berggren, P. O., Noninvasive *in vivo* imaging of pancreatic islet cell biology. *Nature medicine* **2008,** *14* (5), 574-8.

25. Steiner, D. J.; Kim, A.; Miller, K.; Hara, M., Pancreatic islet plasticity: interspecies comparison of islet architecture and composition. *Islets* **2010,** *2* (3), 135-45.

26. Lernmark, A., The preparation of and studies on, free cell suspensions from mouse pancreatic islets. *Diabetologia* **1974,** *10* (5), 431-8.

27. Kharouta, M.; Miller, K.; Kim, A.; Wojcik, P.; Kilimnik, G.; Dey, A.; Steiner, D. F.; Hara, M., No mantle formation in rodent islets -- the prototype of islet revisited. *Diabetes research and clinical practice* **2009,** *85* (3), 252-7.

Chapter: 4

Synthesis and Assessment of Beta Cell Specific Glucosamine Based Two-Photon Probe

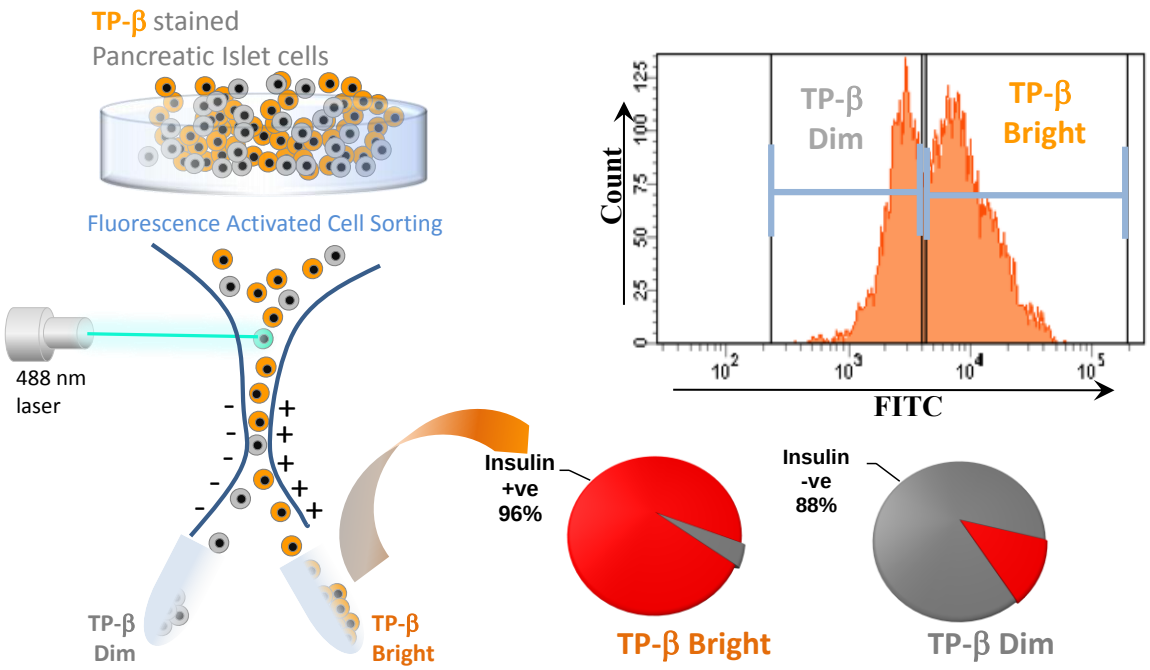

Chapter 4

4.1 Introduction

Diabetes mellitus one of the most common metabolic disorder in humans and is caused by impairment of glucose homeostasis.[1] Pancreatic beta cell is responsible for production, storage and release of insulin, the key hormone for maintaining the level of blood glucose.[2] Beta cells are located in pancreatic islets of Langerhans along with other endocrine cells. In type 1 diabetes mellitus (T1DM) the autoimmune destruction of insulin producing beta cells result in absolute deficiency of insulin in blood.[3] Whereas, in type 2 diabetes mellitus (T2DM) the relative insulin deficiency is caused by both; (i) the peripheral insulin resistance and (ii) beta cell secretory defect.[1-2,4] At present, the understanding of the reason behind the progression of diabetes mellitus is not completely understood. To monitor the onset and progress of disease, various non-invasive techniques like, computed tomography (CT), magnetic resonance imaging (MRI), positron emission tomography (PET) are under study for small animal imaging[5,6]. However, beta cells containing islet of Langerhans constitute only about 1 % of pancreatic mass and are distributed throughout the pancreatic tissue[7], which are less than the spatial resolution of these non-invasive imaging technologies.[8] In contrast to the above techniques, confocal[9] and two-photon laser scanning microscopy (TPLSM)[10] can be efficiently utilized for imaging at sub-cellular resolution, with high speed deep tissue imaging potential.[10] But, the *in vivo* studies with TPLSM are limited by shorter working distance and the penetration depth of excitation light (maximum ~1 mm).[11] Recently, *Speier et al.* has reported the noninvasive *in vivo* imaging of pancreatic islet cells

transplanted in to anterior chamber of mice eye.[12] The study utilized islets isolated from transgenic mice expressing Green Fluorescent Protein in beta cell for selective imaging.[12] Moreover, most of the beta cell related studies are done in isolated islet *in vitro*[13] or in transplantation condition *in vivo*[12-14] with the fluorescent protein expressed samples. The development of a beta cell selective TP probe could be of much value for future diabetic studies.

4.2 Beta cells and Streptozotocin

Streptozotocin (STZ) was first isolated from *Streptomyces achromogenes* in 1959[15] and was identified with antibiotic and anti-leukemic activity[16]. Herr et al. did the complete characterizations of STZ and reported its structure as 1-methyl-1-nitrosourea linked to C2 position of D-Glucose.[17] Sooner the efficacy of STZ for specific treatment of malignant islet cell tumor was discover.[18] The specific toxicity of STZ towards insulin producing beta cells[19,20] was assigned to the higher expression of Glucose transporter isoform GLUT2 on beta cell surface.[21,22,23] Mechanistic studies with GLUT2 expressing cell lines showed that, Gltu2 is a high affinity glucosamine transporter and uptake 2-Glucosamine in a higher rate over D-Glucose.[24] After two decades of investigation on STZ efficacy in cancer chemotherapy, in 1982 FDA approved STZ for the treatment of pancreatic islet cell cancer.[25,26] Subsequently there 2-deoxyglucose fluorescent probes were developed, either as radio labeled trackers such as [^{14}C] 2-deoxy-D-glucose[27], [^{18}F] fluoro-2-deoxy-D-glucose[28] and [^{14}C] or [^{3}H]3-Omethyl-D-glucose[29,30] or as one fluorescent probes 2-[N-(7-nitrobenz-2-oxa-1,3-diazol-4-yl)amino]-2-deoxy-Dglucose (2-NBDG)[31,32] However, 2-NBDG have poor photo stability in water and do not show good

competition in cellular uptake with D-Glucose in physiological condition. *Park et al.* have developed various D-Glucose conjugated fluorescent probes for tumor imaging and glucose uptake monitoring. These reports emphasize on various properties; such as linker size, rigidity of linker and total net charge on the molecule.[33,34,35] Also recently they have reported a TP glucose tracker AG2 and demonstrated glucose uptake in human cancerous tissue.[34] However, all these probes have fluorophore attached at α-anomeric position of D-Glucose: i.e. O-linked fluorophore. Hitherto, no TP 2-glucosamine based probe has been developed for beta cell imaging.

4.3 Objective

After the discovery of TP alpha cell selective probe: **TP-α** (Chapter 3), we aimed for the development of TP beta cell selective probe. We hypothesize that, "the GLUT2 targeting glucosamine analogues can be good beta cell probes". To evaluate this idea, we synthesized 2-Deoxy-2-amino-D-Glucose conjugated TP probes, but with different carbon chain length linkers between the fluorophore and glucosamine. Five derivatives with different linker size, starting from zero carbon, two-, four-, six- and fifteen carbons (PEG) were developed and evaluated for uptake in beta cells. We discovered that, TP-C6-Glucosamine compounds gave best uptake in mice primary beta cells comparison to other glucosamine probes. We named this probe as **TP-β** and was further assessed for *ex vivo* two photon imaging.

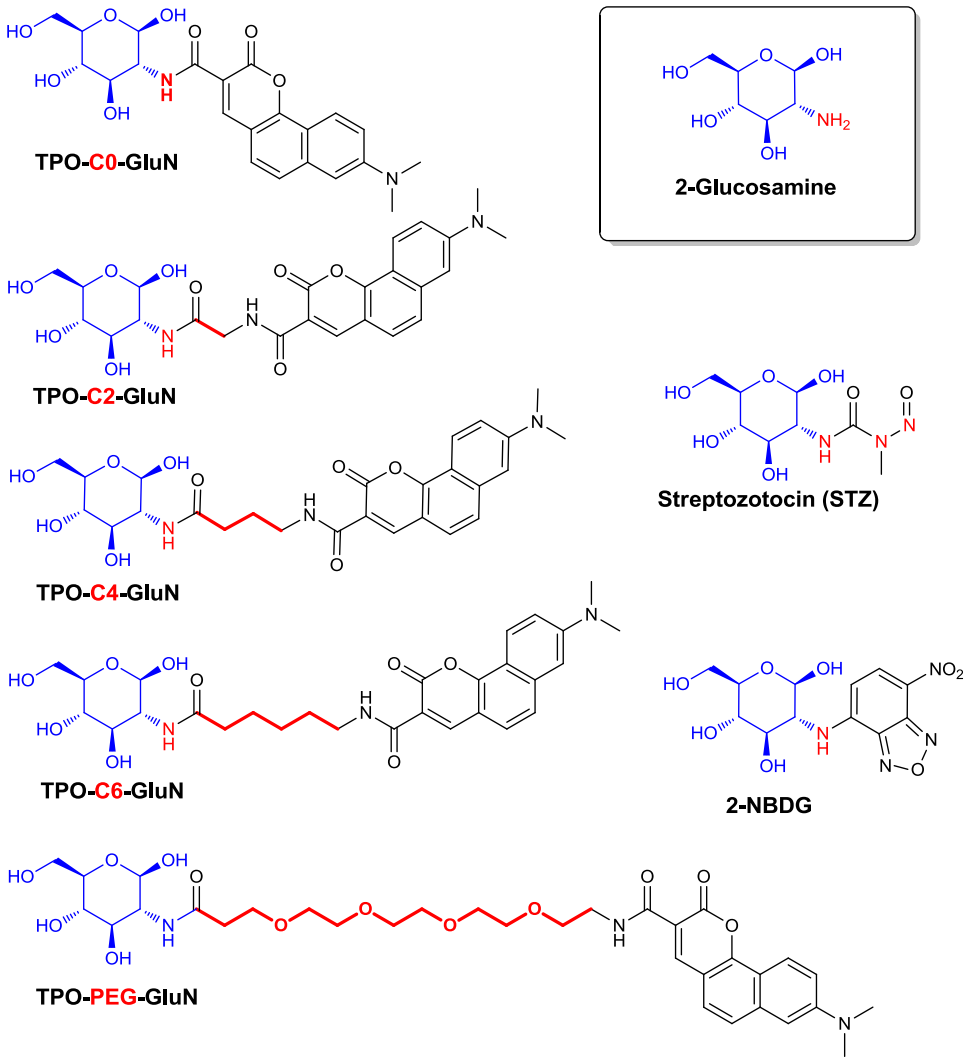

Figure 4.1 Glucosamine, Streptozotocin, 2-NBDG and TPO-GluN compounds.

4.4 Result and Discussion

4.4.1 Synthesis of two-photon Glucosamine analogues

To develop efficient beta cell specific probes, we designed and synthesized TP fluorophore conjugated to 2-amino-2-deoxy-D-Glucose (2-Glucosamine). Both Streptozotocin and 2-Glucosamine have higher affinity for GLUT2[24], which reveals the importance of nitrogen for the GLUT2 selectivity. Hence we have chosen to keep the 2-

amino group of glucosamine intact and planned to develop N-linked fluorophore. Previous reports have emphasized the importance of linkers for GLUT mediated uptake.[33,35,36] To have an unbiased study; we made five probes with different linker size, ranging from zero carbon to fifteen carbons. We chose the reported TP fluorophore; 8-(dimethylamino)-2-oxo-2H-benzo[h]chromene-3-carboxylic acid (DACCA) because of several benefits.[37] This core has (i) significant two-photon action cross section at longer wavelength (84 GM at 820 nm), (ii) good one photon quantum yield $\Phi = 0.29$, (iii) high photo stability and (iv) large stoke shift.[37] Because of the TP property and emission in Orange color (**Figure 4.1**) we named this probe as Two-Photon-Orange: **TPO**. In addition DACCA is neutral in charge, which may have minimum interference in GLUT mediated uptake.[38] We synthesized the N-Hydroxysuccinimide (NHS) ester (TPO-NHS) and used it as the key intermediate for the five analogues synthesis (**Scheme 4.1**). Next the **TPO-NHS** was coupled with four different amino-acid linkers to generate **TPO-C2**, **TPO-C4**, **TPO-C6** and **TPO-PEG** (**Scheme 4.2**). Finally, **TPO-acid** and other synthesized linkers were coupled with 2-glucosamine to give the corresponding products; **TPO-C0-GluN**, **TPO-C2-GluN**, **TPO-C4-GluN**, **TPO-C6-GluN** and **TPO-PEG-GluN**. These synthesized compounds were later evaluated for beta cell selectivity.

Scheme 4.1 Synthesis of **TPO-NHS**

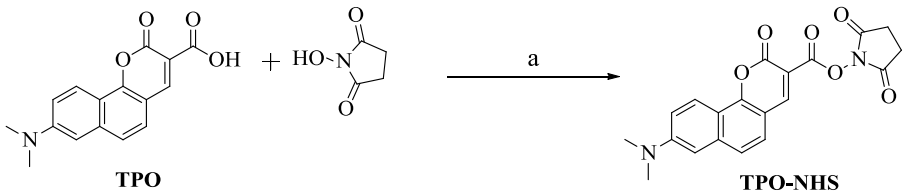

Reagents and conditions: (a) EDC, DCM, DIEA, 2 h at rt.

Scheme 4.2 Synthesis of **TPO-GluN** analogues.

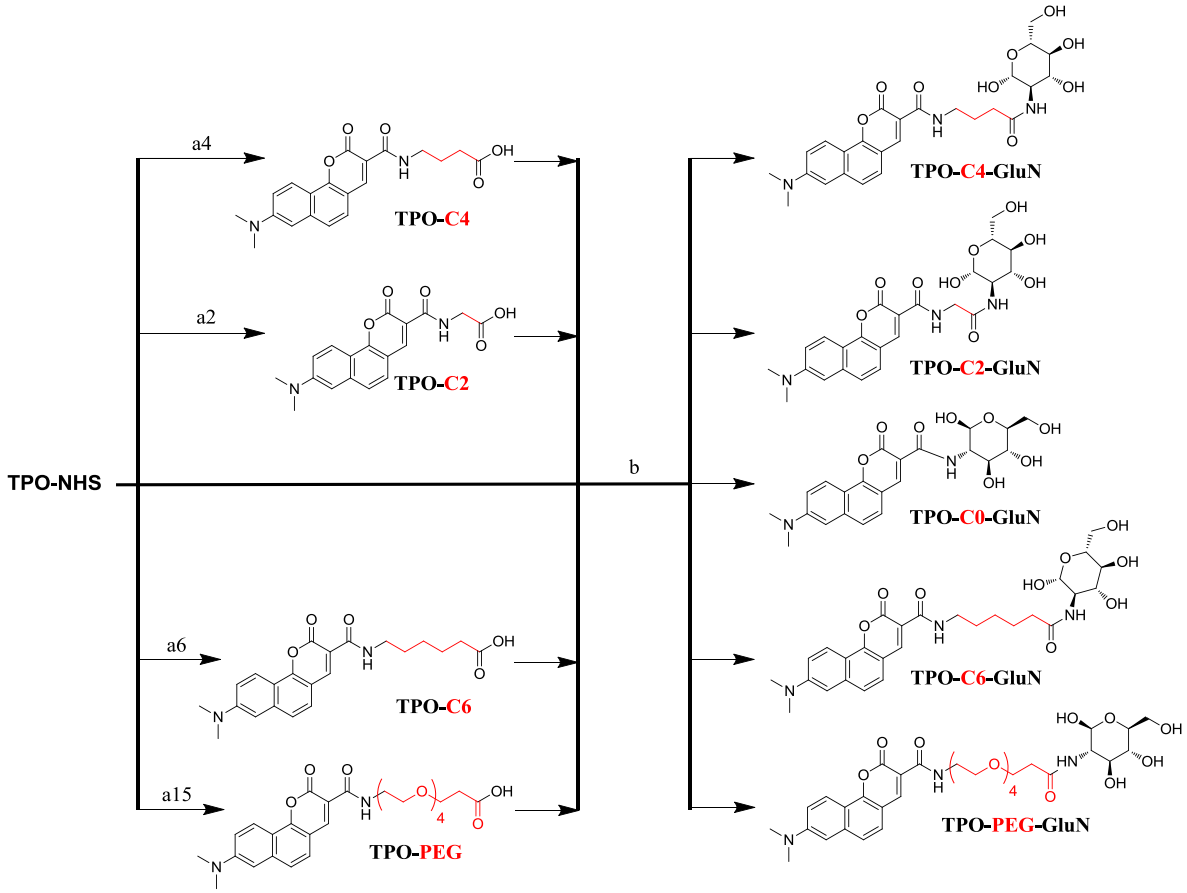

Reagents and conditions: (a), a* please see the table below, (b) D-Glucosamine, HATU, DIEA, DMF, 1 h at rt.

Table 4.1 Reagent and condition for **a***

a*	DCM, 1 h at rt, with	Product
-	-	TPO-C0
2	2-aminoacetic acid	TPO-C2
4	4-aminobutanoic acid	TPO-C4
6	6-aminohexanoic acid	TPO-C6
15	1-amino-3,6,9,12-tetraoxa-pentadecan-15-oic acid	TPO-PEG

*Represents the number in the column.

4.4.2 Photo-physical property study.

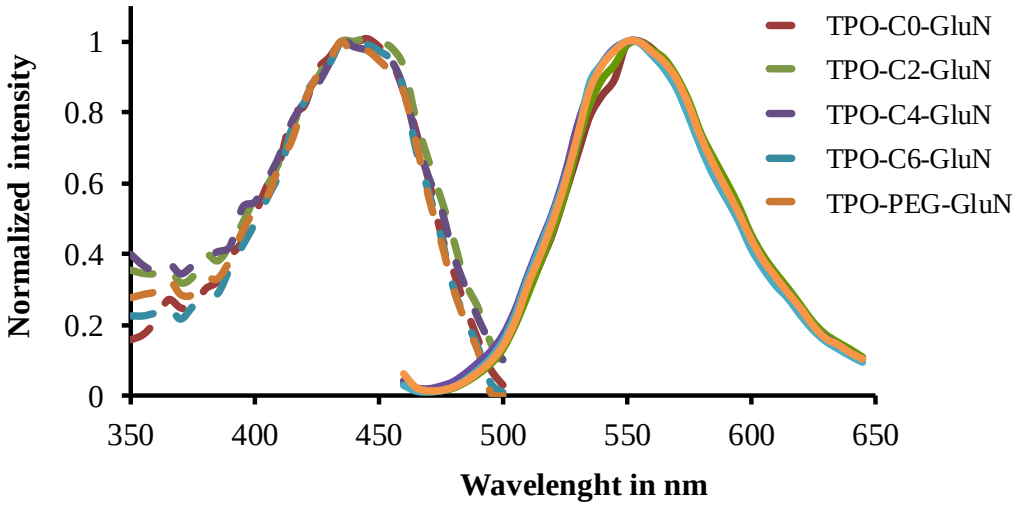

Figure 4.2 Absorption and emission spectra of **TPO-GluNs** measured in PBS buffer pH 7.4 at 10 μM dye concentration.

The spectral characterization of **TPO-GluN** analogues demonstrated that the incorporation of different linker size did not affect the maximum excitation and emission wavelengths or the fluorescence emission intensity.

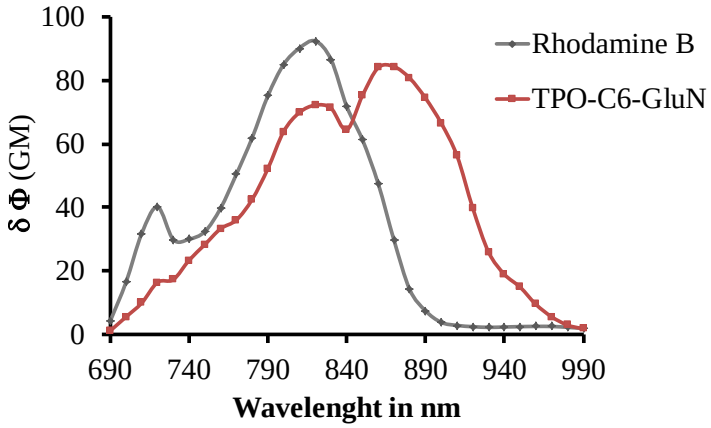

Figure 4.3 Two-photon cross-section of **TPO-C6-GluN**

Two-photon action cross section of **TPO-C6-GluN** was measured in Ethanol at 50 μM concentration with Rhodamine B as reference dye.

Table 4.2 Photo-physical data of TPO-GluN compounds

Compd	$^{a}\lambda_{max}$	$^{b}\lambda_{max}$	$^{c}\lambda_{max}$	^{d}QY	$^{e}\delta_{max}$*	δΦ
TPO-C0-GluN	435	555	870	0.27	300.19	81.05
TPO-C2-GluN	435	555	870	0.29	272.03	78.89
TPO-C4-GluN	435	555	870	0.31	313.28	97.12
TPO-C6-GluN	435	550	870	0.30	271.37	81.41
TPO-PEG-GluN	435	550	870	0.28	281.27	78.76

^{a},$^{b}\lambda_{max}$ of the one-photon absorption and emission spectra in nm. $^{c}\lambda_{max}$ of the two-photon excitation spectra in nm. ^{d}QY Fluorescence quantum yield. $^{e}\delta_{max}$ The peak two-photon cross section in 10^{-50} cm^4 s/photon (GM). The experimental uncertainty is of the order of 10-15 %. $^{a}\lambda_{max,}$ $^{b}\lambda_{max}$ and ^{d}QY were obtained in 1 mM PBS buffer at pH 7.4. Where as $^{e}\delta_{max}$* was measured in Ethanol.

4.4.3 Cellular uptake of TPO-GluN probes

Literature review revealed that, the commercially available insulin producing beta cell lines Ins1e[39], MIN6[39] and βTC6 have **GLUT1**[40-41] (***not GLUT2***) as their major glucose transporter. So we decided to work on the primary beta cells from mice. Mice pancreatic beta cells have GLUT2 as the major cell surface glucose transporter.[39] Islets of Langerhans from mice pancreas were isolated by collagenase P method as described earlier.[42] GLUT2 expressing beta cells are the major population (~70-80 %) of mice pancreatic islets and the rest are alpha (15-20 %) and Delta cells (5-10 %).[43] As the major population is GLUT2 expressing beta cells, we decided to use whole islet cells for the uptake experiment. Moreover, the presence of small population of non-GLUT2 expressing cells (~20-30 % alpha and delta cells) can act as an internal negative control and will reveal the selective uptake of the probe as well.

For the uptake study we used flow-cytometry to measure the uptake of two-photon glucosamine compounds (**TPO-GluN**) to the islet cells. The islet cells were incubated with 5 μM of **TPO-GluN** compounds for 2 h at 37 °C before the intensity

measurement with flow-cytometer. As shown in the **Figure 4.4**, the different **TPO-GluN** compounds have different uptake by the islet cells. We gated the flow cytometry dot-plot based on the population distribution. The control islet cells (unstained) were gated as dim (or dye –ve region) and the appearance of brighter cell population after staining was gated as bright (or dye +ve region) (**Figure 4.4 A**). We observed that, three glucosamine analogues **TPO-C2-GluN**, **TPO-C4-GluN** and **TPO-C6-GluN** gave population separation of ~75 % Bright cells and ~22 % as Dim cells (**Figure 4.4 A, B**). Whereas for **TPO-C0-GluN** and **TPO-PEG-GluN** the dim population was found out to be 14 % and 2 % respectively. These result showed that, **C2**, **C4** and **C6** linker compounds have better population separation over **C0** and **PEG** linker compounds. To further identify the best compound among the three **TPO-GluN** compounds (i.e. **C2**, **C4** and **C6**), we measured the fluorescence intensity of the Bright cells. We found the **TPO-C6-GluN** Bright cells has the highest intensity (**Figure 4.4 C**), representing the higher uptake in comparison to other dyes. This reveals that, by simply changing the linker size from **C0** to **C6**, on glucosamine analogue could result in a better GLUT2 uptake probe. However, the **TPO-PEG-GluN** did not give Dim and Bright population separation; this may be due to the nun-GLUT mediated entry of PEG probes to the cells. Finally because of both, (i) good population separation (75:22; Bright: Dim) and maximum uptake (highest fluorescent intensity) we choose **TPO-C6-GluN** as our best GLUT2 targeting compound. Next was to confirm whether the **TPO-C6-GluN** Bright cells are GLUT2 positive beta cells or not.

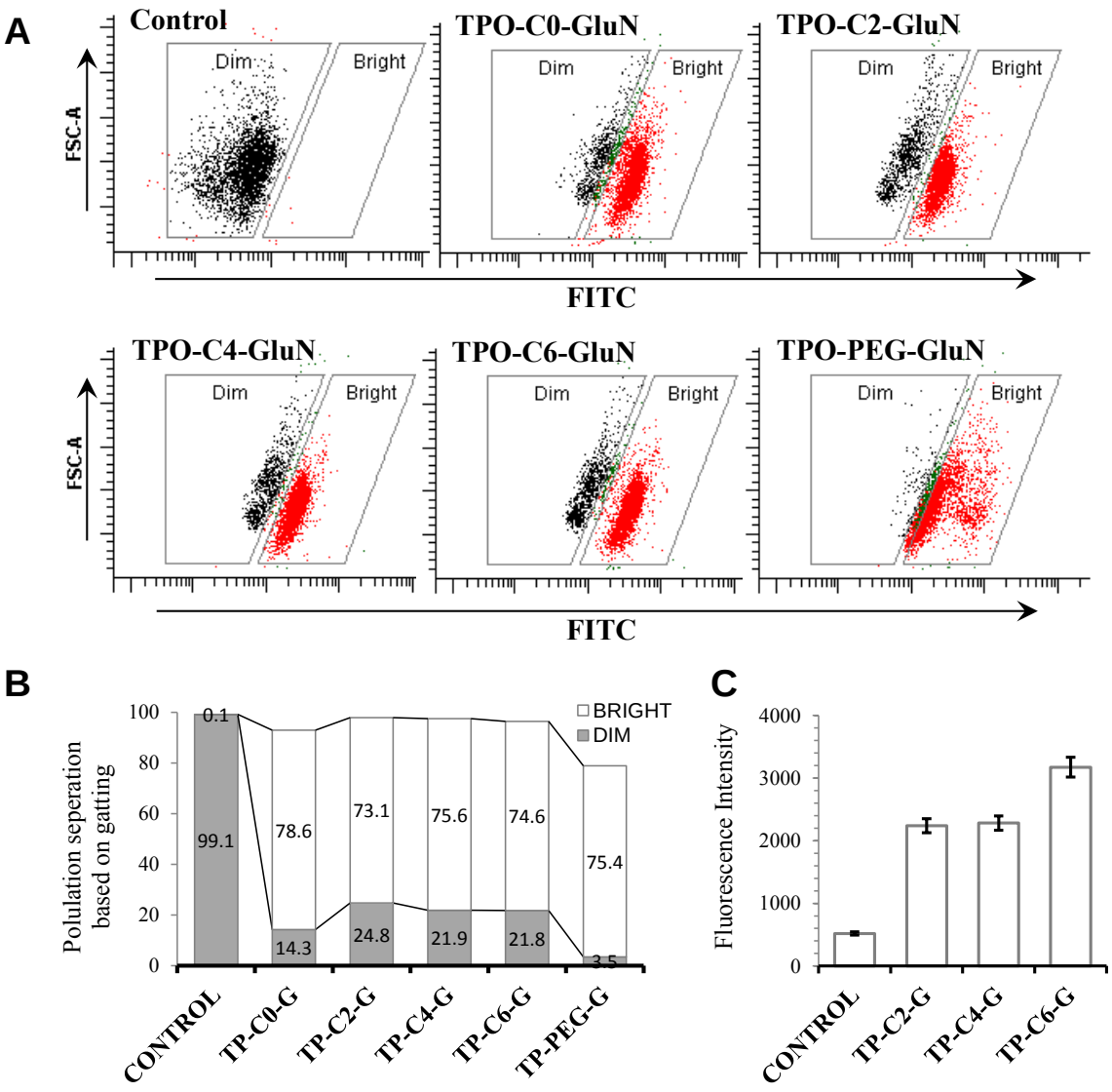

Figure 4.4 Islet cell staining with **TPO-GluN** compounds.

(A) Flow cytometry dot-plot showing the population distribution for islet cells stained with 5 μM **TPO-GluNs** compounds. Dim region coded as black color and Bright region coded as red color. (B) Show the bar diagram for the Dim and Bright cell population in percentage corresponding to each spectrum in A. (C) Bar diagram showing fluorescence intensity of Control, **TPO-C2-GluN**, **TPO-C4-GluN** and **TPO-C6-GluN** stained islet cells.

4.4.4 Characterization of TPO-GluN positive cells.

The flow cytometry study of five TPO-GluN compounds has revealed that, **TPO-C6-GluN** have highest uptake and good population separation with the islet cells. Despite

the fact that, **TPO-C6-GluN** stains 74.6 % of the islet cells brightly, this is in proportion with the beta cell population (~70-80 %) in islet cells.[43] Reconfirmation was necessary to identify that the **TPO-C6-GluN** stained cells were pancreatic beta cells. To do so, we isolated out both the **TPO-C6-GluN** Bright and Dim cells by Fluorescence-activated cell sorting and analyzed by insulin immunostaining (**Figure 4.5 A**). The anti-insulin antibody staining revealed that, the **TPO-C6-GluN** Bright cells are insulin positive beta cells and Dim cells are insulin negative other islet cells (**Figure 4.5 B, C**). With these experiments we concluded that, 2-Glucosamine containing compound with a six carbon chain linked neutral fluorophore can selectively stain mice pancreatic beta cells. We named the **TPO-C6-GluN** two-photon beta cells selective compound as **TP-β** (two-photon-beta) (**Figure 4.5 B**).

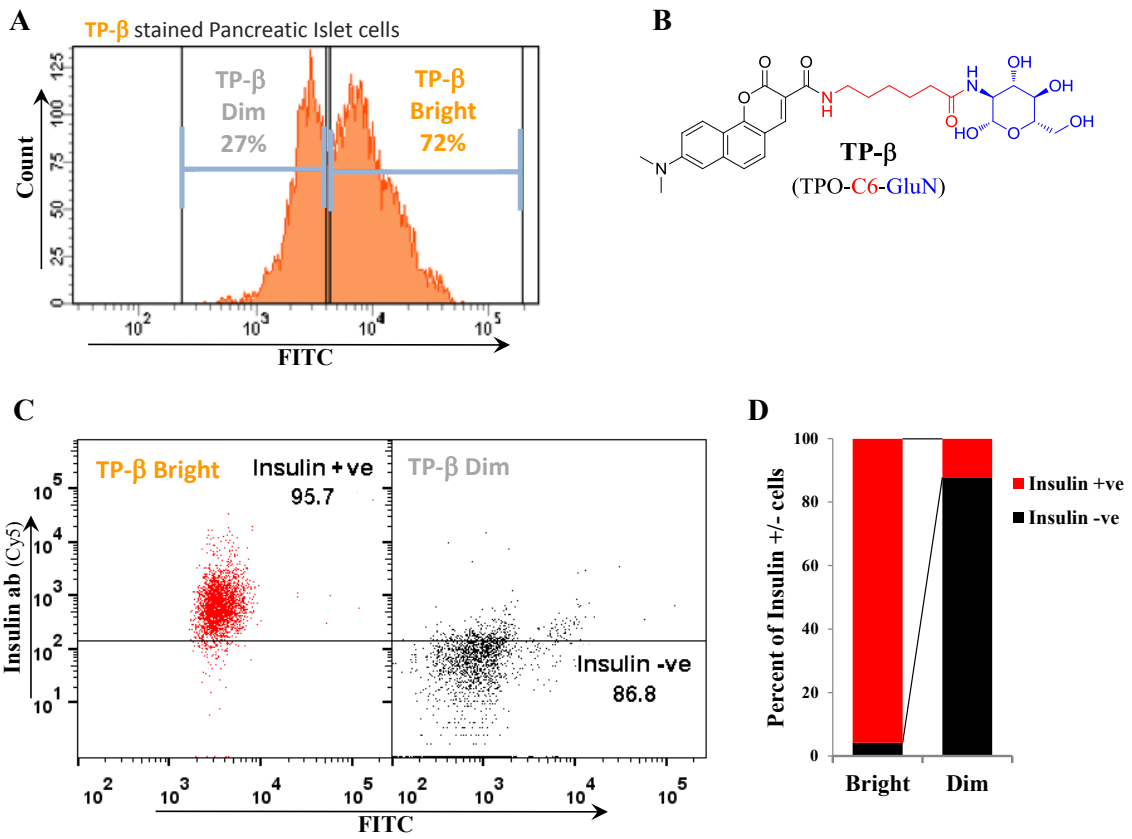

Figure 4.5 **TPO-C6-GluN** positive cells are beta cells.

(A) Histogram showing the population separation of islet cells after **TPO-C6-GluN** staining, gating show the bright and dim cell population. (B) Chemical structure of **TP-β** (**TPO-C6-GluN**.) (C) Dot-plot shows insulin immunostaining of FACS sorted islet cells based on **TPO-C6-GluN** dim/bright population. Left spectrum for dye bright and right spectrum for dye dim populations. (D) Bar diagram corresponding to spectrum on C shows the Dye Bright cells to be Insulin +ve beta cells and Dye Dim cells to be Insulin –ve cells. Red color code for insulin +ve cells and black color for insulin –ve cells.

4.4.5 Glucose competition with primary islet cells from mice.

Next we target to determine that, whether the **TP-β** uptake is GLUT mediated or not? We performed a competition experiment with increasing concentration of D-Glucose with mice pancreatic islet cells. As shown in **Figure 4.6** the uptake of **TP-β** is concentration dependently decreased with the increasing concentration of D-Glucose, this evident the glucose transporter mediated uptake of **TP-β**.

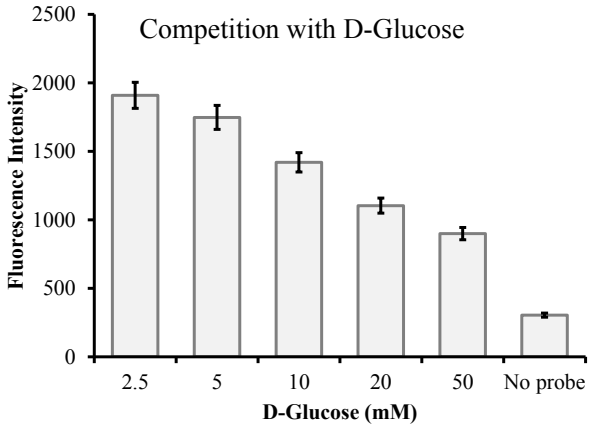

Figure 4.6 D-Glucose competition with **TP-β.**

Dissociated islet cells were incubated with DMEM media supplemented with different concentration of D-Glucose for 30 min at 37 °C before addition of dye. 5 μM **TP-β** final concentration was added to each tube and incubated for 2 h at 37 °C before analyzing with flow-cytometer BD LSRFortessa™.

4.4.6 Comparative cell uptake study with 2-NBDG

After validating the GLUT mediated uptake of **TP-β** to the beta cells, we aimed to compare it with the commercially available fluorescent glucosamine probe 2-NBDG (2-deoxyglucose-2-[N-(7-nitrobenz-2-oxa-1,3-diazol-4-yl)-amino]-2-deoxy-D-glucose). 2-NBDG is 2-amino-2deoxy-D-glucose directly attached to fluorescent core, has been reported earlier for the higher uptake in to the GLUT2 expressing COS-1 cells and primary beta cells from mice.[32] However, it also has been reported that, the various fluorescent glucose analogues with longer linker size have better GLUT mediated uptake compared to 2-NBDG. [33,35,44] When we examined the uptake of **2-NBDG** and **TP-β** to the islet cells with flow cytometry, we found that the later have considerably higher uptake than 2-NBDG. When the concentration of **2-NBDG** was twice the concentration of **TP-β**, still the fluorescence intensity of **2-NBDG** treated cell were 30 % to the **TP-β** treated cells (**Figure 4.7**).

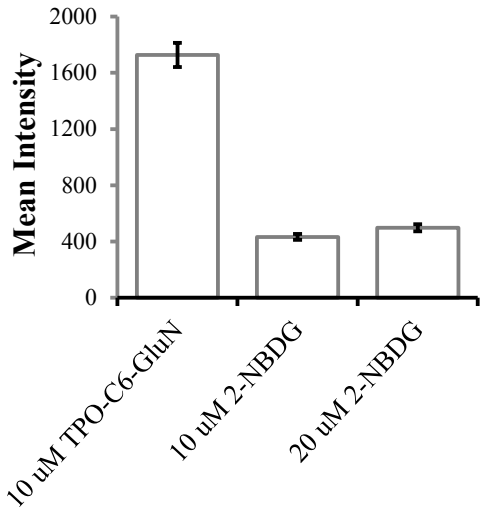

Figure 4.7 Comparison of **TP-β** with **2-NBDG**

Dissociated islet cells were incubated with 10 μM of **TP-β** or 10, 20 μM of **2-NBDG** in individual tubes with DMEM media supplemented with 5 mM D-Glucose for 2 h at 37 °C before analyzing with flow-cytometer BD LSRFortessa™.

4.4.7 *Ex vivo* two-photon imaging of pancreatic islet with TP-β.

We further evaluated the utility of **TP-β** for beta cell staining *ex vivo.* Freshly harvested mice pancreas was sectioned immediately at 200 and 300 μm thickness in live conditions. These sections were incubated at 37 °C with 1 μM to 50 μM of **TP-β** in DMEM media containing 2 mM D-Glucose. Among various time point evaluated we found that, 24 h incubation with 10 μM **TP-β** gives best islet selective staining. The bright field images of (~50-100 μm) thick pancreatic tissue section shows the clear contrast for islet in the pancreatic tissue (**Figure 4.8 A**). The fluorescence images show that pancreatic islets have much higher uptake of the **TP-β** than the surrounding acinar tissue. This clearly revealed the selective uptake of **TP-β** into the pancreatic islet of Langerhans. The TP 3D imaging of the tissue revealed the clear contrast between islet and the surrounding region in the entire depth of pancreatic tissue (**Figure 4.8 B**).

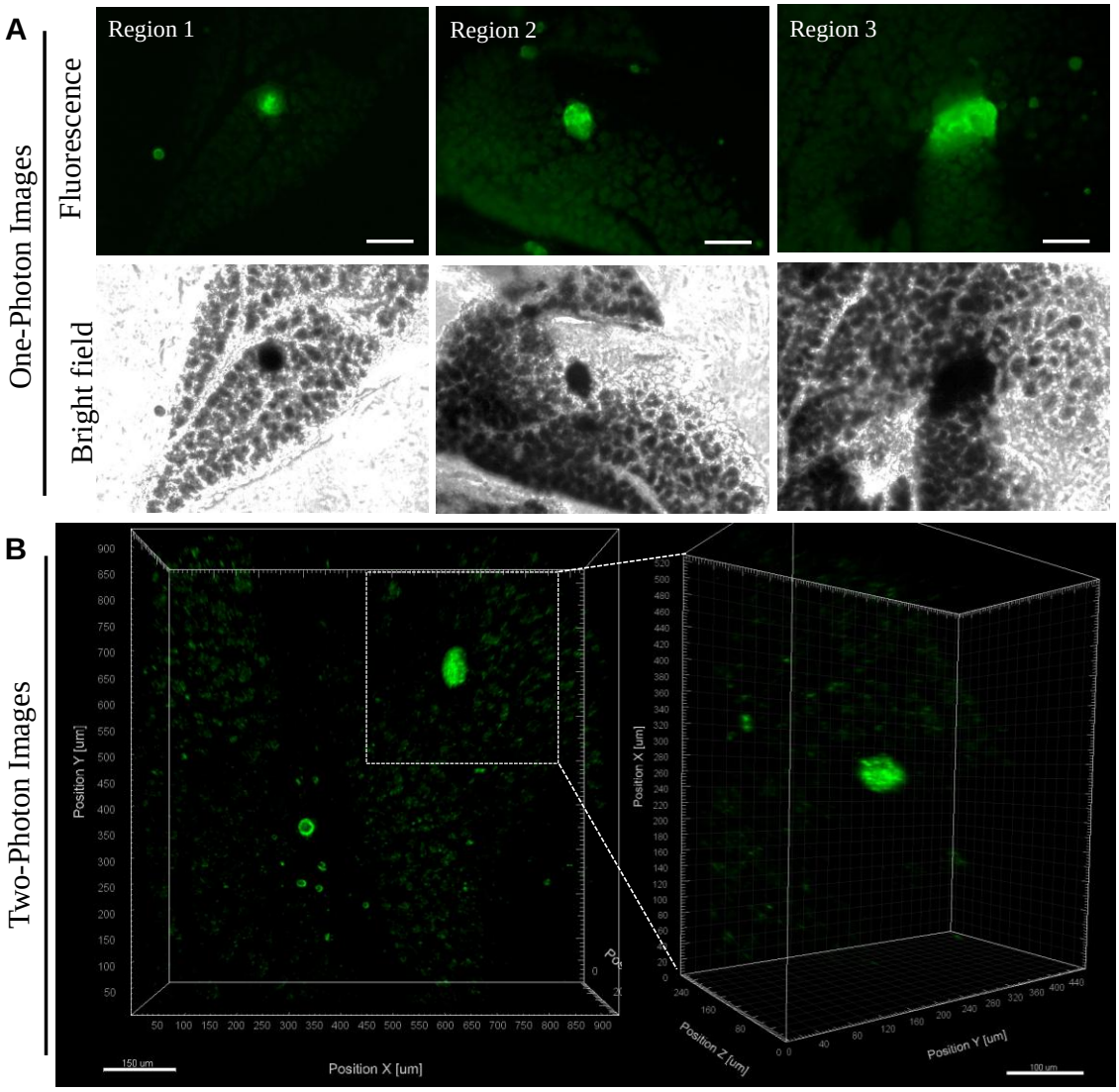

Figure 4.8 **TP-β** stained islets of Langerhans in pancreatic tissue.

(A) One-photon images of 3 representative regions of pancreatic tissue stained with 10 μM TP-β. One-photon Fluorescent Images with FITC filter set, with 10x objective of NIKON Ti Microscope. (**B)** 3D optical projection of pancreatic tissue stained with **TP-β** Insert show magnified view of the selected region from left image. Two-photon Images take with Leica SP5 10 x objective. For excitation 870 nm fs laser light is used and emission was collected form 450-600 nm. Live pancreatic tissue stained with 10 μM **TP-β** incubated for 24 h at 37 °C in DMEM containing 5 mM Glucose. Scale bar 150 μm.

4.5 Conclusion

To conclude, we have developed five new TP glucosamine based probes **TPO-GluNs** with different linker size. We found that, the six carbon chain length probe **TP-β** (**TPO-C6-GluN**) have maximum uptake in to the pancreatic beta cells and can be successfully utilized for the isolation of primary beta cells from mice. **TP-β** can be excited by 870 nm fs laser pulses for TP tissue imaging. The viability assay shows that **TP-β** has minimal toxicity even at 100 μM concentration up to two days. **TP-β** can efficiently stain pancreatic islets in live pancreatic tissue sections. This compound can be a useful probe in diabetic studies for TP imaging application of beta cells. With longer excitation wavelength it can be successfully utilized for 3D deep tissue TP imaging.

4.6 Experimental details.

4.6.1 Synthesis of TPO-GluN compounds.

4.6.1.1 Synthesis of TPO-NHS

TPO-acid was synthesized as per the literature report with overall 65 % yield.[37] TPO-acid (300 mg, 1 mmol) was dissolved in DCM (5 mL). Triethylamine (10 µl) was added to it and stirred for 10 mins. EDC (1-Ethyl-3-(3-dimethylaminopropyl)carbodiimide) (170 mg, 1.2 mmol) was added to the stirring solution and stirring was continued 1 h at rt. After this N-hydroxysuccinimide (140 mg, 1.2 mmol) was added and stirred for another 2 h at rt. The reaction was monitored by LCMS, the TPO-NHS was precipitated by diethylether addition to the reaction mixture. The precipitated orange solid was used without further purification.

4.6.1.2 Synthesis of TPO-linkers

TPO-NHS (380 mg, 1 mmol) was dissolved in 20 mL of DCM and distributed in into four different vials (each 5 mL). To each vial, one amino acid (0.5 mmol) was added and stirred for 1 h at rt. The four different amino acid used are 2-aminoacetic acid, 4-aminobutanoic acid, 6-aminohexanoic acid and 1-amino-3,6,9,12-tetraoxa-pentadecan-15-oic acid to result four corresponding TPO-linker (**TPO-C2**, **TPO-C4**, **TPO-C6** and **TPO-PEG**). The reaction was monitored by HPLC-MS. After completion of the reaction, DCM was added to the reaction mixture. The organic layer was collected (3 x 20 mL) and washed with water (2 x 10 mL). Organic layer dried over the anhydrous sodium sulphate, evaporated in rotary evaporator and purified by silica gel column

chromatography using DCM and Methanol as eluent. All TPO linker compounds were obtained as orange amorphous solid.

4.6.1.3 Synthesis of TPO-GluNs

In separate vials 0.2 mmol of each TPO-linker compound (including TPO-acid, **TPO-C2**, **TPO-C4**, **TPO-C6** and **TPO-PEG**) was taken, to which HATU (115 mg, 0.3 mmol) was added followed by 5 mL of DMF under N2 atmosphere and stirred for 2 mins at rt. 2-D-Deoxyglucosamine HCl (45 mg, 0.2 mmol) was treated with DIEA (14 μL, 0.10 mmol) and added to the each reaction vial. The reactions were stirred for another 2 h at rt. The solvent was then evaporated under reduced pressure and the resulting yellowish solid was purified by silica gel column chromatography using DCM and Methanol as eluent to obtain **TPO-GluN** compounds. Finally we obtained five compounds namely, **TPO-C0-GluN, TPO-C2-GluN, TPO-C4-GluN, TPO-C6-GluN, TPO-PEG-GluN.**

4.6.2 Characterization of TPO-GluN compounds.

4.6.2.1 Characterization of TPO-COOH

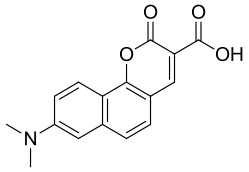

^{1}H NMR (DMSO-d_6, 300 MHz) δ (ppm): 8.39 (s, 1H), 7.84 (d, J = 9 Hz, 1H), 7.77 (dd, J = 1.5, 8.7 Hz, 1H), 7.58 (d, J = 8.7 Hz, 1H), 7.01 (dd, J = 2.1, 9 Hz, 1H), 6.73 (dd, J = 1.5 Hz, 1H), 2.60 (s, 3H), 2.50 (s, 3H), ^{13}C NMR (DMSO-d_6, 75 MHz) δ (ppm): 164.26, 157.55, 153.62, 150.95, 149.97, 138.21, 125.21, 123.42, 122.95, 116.11, 112.76, 110.38, 105.43, 43.06. . m/z ($C_{16}H_{13}NO_4$) calcd: 283.08; found 282.1.

4.6.2.2 Characterization of TPO-C0-2GluN

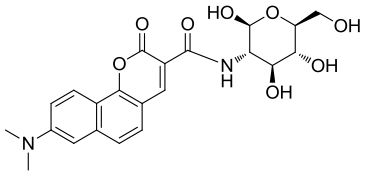

^{1}H NMR (DMSO-d_6, 300 MHz) δ (ppm): 8.89 (s, 1H), 8.79 (d, J = 8.4 Hz, 1H), 8.14 (d, J = 9 Hz, 1H), 7.66 (d, J = 8.7 Hz, 1H), 7.55 (d, J = 8.7 Hz, 1H), 7.31 (d, J = 9.3 Hz, 1H), 6.99 (s, 1H), 5.09 (d, J = 3 Hz, 1H), 3.92 (m, 4H), 3.65 (m, 6H), 3.11 (s, 6H). ^{13}C NMR (DMSO-d_6, 75 MHz) δ (ppm): 161.93, 161.51, 153.15, 151.24, 149.05, 138.43, 125.66, 123.72, 116.49, 113.98, 113.09, 111.42, 105.81, 90.97, 72.73, 71.67, 71.25, 61.43, 54.83, 53.69, and 42.04.

ESI-MS m/z (M +), calcd: 444.1, found 445.2 (M+1)

HRMS (ESI): calcd for (M+Na: $C_{22}H_{24}N_2NaO_8$) Exact Mass: 467.1425; found: 467.1433.

4.6.2.3 Characterization of TPO-C2-2GluN

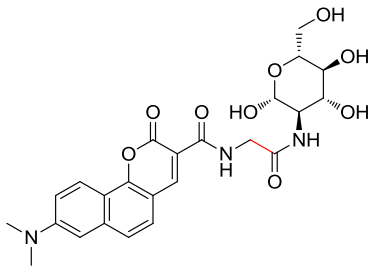

^{1}H NMR (DMSO-d_6, 300 MHz) δ (ppm): 8.79 (s, 1H), 8.68 (d, J = 8.4 Hz, 1H), 8.03 (d, J = 9 Hz, 1H), 7.56 (d, J = 8.7 Hz, 1H), 7.44 (d, J = 8.7 Hz, 1H), 7.20 (d, J = 9.3 Hz, 1H), 6.89 (s, 1H), 4.98 (d, J = 3 Hz, 1H), 3.81 (m, 4H), 3.55 (m, 6H), 3.11 (t, J = 9 Hz,

1H), 3.00 (s, 6H), 2.41 (d, J = 1.5 Hz, 2H). ^{13}C NMR (DMSO-d_6, 75 MHz) δ (ppm): 162.42, 161.90, 161.48, 153.12, 151.21, 149.02, 138.40, 125.63, 123.69, 116.46, 113.95, 113.03, 111.39, 105.78, 90.94, 72.70, 71.64, 71.22, 61.40, 54.80, 53.66, 42.01, 41.89..

ESI-MS m/z (M +), calcd: 501.1, found 502.1 (M+1)

HRMS (ESI): calcd for (M+Na: $C_{24}H_{27}N_3NaO_9$) Exact Mass:524.1640; found: 524.1636.

4.6.2.4 Characterization of TPO-C4-2GluN

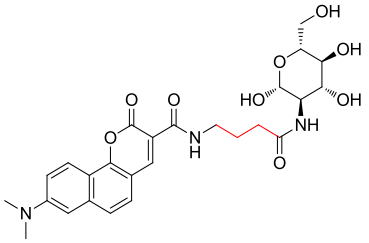

^{1}H NMR (DMSO-d_6, 300 MHz) δ (ppm): 8.81 (s, 1H), 8.72 (d, J = 8.7 Hz, 1H), 8.14 (d, J = 8.7 Hz, 1H), 7.66 (d, J = 8.7 Hz, 1H), 7.54 (d, J = 8.7 Hz, 1H), 7.31 (dd, J = 2.1, 9 Hz, 1H), 6.99 (d, J = 2.4 Hz, 1H), 4.95 (d, J = 3 Hz, 1H), 3.60 (m, 11H), 3.10 (s, 6H), 2.51 (m, 2H), 2.20 (m, 2H), 1.76 (m, 2H). ^{13}C NMR (DMSO-d_6, 75 MHz) δ (ppm): 171.96, 161.77, 160.95, 152.66, 150.85, 148.24, 137.99, 125.24, 123.33, 123.29, 116.16, 114.08, 112.75, 111.00, 105.44, 90.59, 72.06, 71.09, 70.43, 61.13, 54.34, 39.78, 32.77, 29.05, 25.58.

ESI-MS m/z (M +), calcd: 529.21, found 530.2 (M+1)

HRMS (ESI): calcd for (M+Na: $C_{26}H_{31}N_3NaO_9$) Exact Mass: 552.1958; found: 552.1961.

4.6.2.5 Characterization of TP-β (TPO-C6-2GluN)

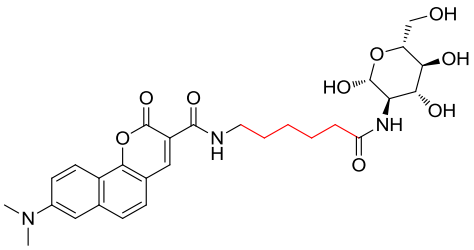

^{1}H NMR (DMSO-d_6, 300 MHz) δ (ppm): 8.8 (s, 1H), 8.12 (d, J = 9.3 Hz, 1H), 7.63 (d, J = 8.4 Hz, 1H), 7.56 (d, J = 8.1 Hz, 1H), 7.52 (d, J = 9 Hz, 1H), 7.29 (d, J = 9.3 Hz, 1H), 6.97 (d, J = 2.1 Hz, 1H), 4.94 (d, J = 3 Hz, 1H), 3.59 (m, 7H), 3.32 (m, 2H), 3.09 (s, 6H), 2.14 (t, J = 7.5 Hz, 2H), 1.53 (m, 4H), 1.33 (m, 6H). . ^{13}C NMR (DMSO-d_6, 75 MHz) δ (ppm): 172.28, 161.55, 161.05, 152.65, 150.80, 148.25, 137.97, 125.24, 123.26, 116.11, 114.00, 112.03, 111.03, 105.44, 105.58, 90.58, 72.05, 71.12, 70.38, 61.11, 54.25, 35.18, 31.53, 29.42, 26.17, 25.05, 22.09.

ESI-MS m/z (M +), calcd: 557.2, found 558.2 (M+1)

HRMS (ESI): calcd for (M+Na: $C_{28}H_{35}N_3NaO_9$) Exact Mass: 580.2266; found: 580.2262.

4.6.2.6 Characterization of TPO-PEG-2GluN

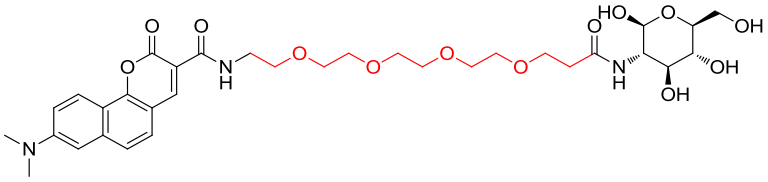

^{1}H NMR (DMSO-d_6, 300 MHz) δ (ppm): 9.14 (s, 1H), 8.79 (s, 1H), 8.23 (d, J = 9.3 Hz, 1H), 8.01 (s, 1H), 7.34 (dd, J = 7.5, 9 Hz, 2H), 7.13 (dd, J = 1.5, 9.3 Hz, 1H), 6.79 (s, 1H), 3.76 (t, J = 6.6 Hz, 2H), 3.69 (m, 17H), 3.46 (s, 3H), 3.11 (s, 6H), 2.95 (s, 2H), 2.88 (s, 2H), 2.63 (m, 3H), 1.37 (m, 2H). . ^{13}C NMR (DMSO-d_6, 75 MHz) δ (ppm): 174.26,

162.98, 161.95, 153.48, 150.83, 148.97, 138.36, 124.96, 124.30, 123.80, 115.85, 114.14, 113.93, 113.65, 111.52, 105.98, 70.66, 70.45, 69.75, 69.71, 66.71, 50.53, 40.44, 39.76, 36.72, 35.01, 31.98, 31.63, 29.74, 29.41, 22.74, 14.19.

ESI-MS m/z (M +), calcd: 691.2, found 692.3 (M+1)

HRMS (ESI): calcd for (M+Na: $C_{33}H_{45}N_3NaO_{13}$) Exact Mass: 714.2845; found: 714.2855.

4.6.2 Quantum yield measurements.

Quantum yield were calculated by measuring the integrated area of emission spectra for TPO-GluN compounds in comparison with the same measurement for TPO-acid ($\Phi = 0.29$) in aqueous media as reference compound.[37] Both the reference and TPO-GluN compounds were excited at 430 nm and emission spectra were collected from 460-660 nm. Quantum yields were calculated suing Equation 4.1, where F represents the area of fluorescent emission, n is reflective index of the solvent and Abs is absorbance at excitation wavelength selected for standards and samples. Emission was integrated between 460 to 650 nm.

Equation 4.1 Quantum yield measurement.

$$\Phi_{(sample)} = \Phi_{(ref)} \frac{F_{(sample)}}{F_{(ref)}} \frac{\eta_{(sample)}}{\eta_{(ref)}} \frac{Abs_{(ref)}}{Abs_{(sample)}} \qquad (1)$$

4.6.3 Two-photon absorption cross sections measurement.

The TP emission spectra of TPO-GluN compounds were deter-mined over a broad spectral region by the two-photon induced fluorescence method with Rhodamine B in methanol as a reference.[45], A PTI, Quanta Master™ spectro-fluorimeter and femtosecond Ti: Sapphire laser (Mira 900F, 220 fs pulse width, 76 MHz repetition rate,

tuning range 690 - 990 nm, Coherent (USA) were used. TP fluorescence measurements were performed in 10 mm fluorometric quartz cuvettes with 10 μM of represented TPO-GluN compounds in Methanol and 10 μM Rhodamine B as reference in same solvent.[45] The experimental fluorescence excitation and detection conditions were conducted with negligible reabsorption processes which can effect TPA measurements. The TP absorption cross section of the probes was calculated at each wavelength according to equation 4.2.[46]

Equation 4.2 Two-photon cross section measurement.

$$\delta_{sample} = \delta_{reference} \frac{\Phi_{(ref)} I_{(sample)} C_{(ref)} \eta_{(sample)}^{2} P_{(ref)}^{2}}{\Phi_{(sample)} I_{(ref)} C_{(sample)} \eta_{(ref)}^{2} P_{(sample)}^{2}} \qquad (2)$$

Where I is the integrated fluorescence intensity, C is the concentration, η is the refractive index, Φ is the quantum yield and P is the incident power on the sample, subscript 'ref' stands for reference samples, 'sample' stands for samples. The uncertainty in the measured cross sections was about ± 10 %.

4.6.4 Islet isolation, dissociation, culture and imaging

Primary pancreatic islets were isolated from the 10 to 16 week old C57BL/6 (WT) male or female mice. The animal handling and tissue harvesting is in accordance with the Institutional Animal Care and Use Committee of Singapore Bio-imaging Consortium (Agency of Science, Technology and Research, Singapore). Pancreatic islets were isolated by Collagenase P digestion and islet picking methods as described earlier.[42] Briefly, fresh pancreas was cut into small pieces and digested with 1 mg/mL collagenase P (Roche, Indianapolis, IN, USA) solution in Hank's Balanced Salt Solution (HBSS; Invitrogen) for 10 minutes at 37 °C on a shaker, followed by 4 times buffer washing to

remove the digested exocrine tissue. Manual picking of intact islets was carried out using Zeiss Stemi DV4 stereomicroscope. Primary pancreatic islet cells were dissociated by trypsinization and trituration method.[42] Approximately 50 - 100 islets were dissociated by incubating with 0.25 % Trypsin-EDTA (1X), phenol red (GIBCO) at 37 °C for 2 minutes followed by trituration with repeated pipetting. Finally, the dissociated islet cells were transferred to the 1 mM D-glucose DMEM with 10 % FBS and 1 % penicillin-streptomycin (GIBCO) for culture.

4.6.5 Flow cytometry

Primary islet cell cultures were generated from the islets of C57BL/6 (WT) male mice as described above. Cells were stained with 5 μM of **TP-β** for 2 h at 37 °C in DMEM media containing 1 mM D-Glucose and washed with Phosphate Buffer Saline (PBS) before acquisition on the BD LSR II analyzer. Cells were acquired using the appropriate filters for **TP-β** (Alexa 488; excitation laser light 488 nm and emission at 530/30 nm) and secondary antibody (Insulin – Cy5).

4.6.6 Immunostaining

Primary cells and islets were fixed in 4 % Paraformaldehyde and permeabilized with 0.1 % Triton-X 100. Fixed Cells were identified by primary antibodies against secretory markers at the respective dilutions: Beta cell - Insulin (DACO North America, Carpinteria, California, 93013 USA) 1:200. For secondary antibody staining, Alexa Fluor® 633 Goat Anti-Guinea Pig IgG (Invitrogen, Molecular Probes Inc, USA) were used.

4.6.7 OP and TP imaging

All confocal and TP imaging was done using Leica TCS SP5X MP (Leica Microsystems CMS GmbH, Mannheim, Germany) with 405 nm laser light for OP excitation and 870 nm femtosecond (fs) pulsed laser for TP excitation for TP-β. Images were taken using 10X dry, 40X water objectives. The TP excitation of **TP-β** was achieved by titanium-sapphire laser light set at wavelength 870 nm and an output power of 2710 mW. To obtain the probe signal, internal photomultiplier tube was set at 550 to 650 nm. Image analysis and intensity measurements were carried out by Leica Application Suite Advanced Fluorescence (LAS AF). 3D projection of Z-stack TP images were processed with IMARIS software (Bitplane AG, Switzerland.) and the intensity is depicted as false color.

4.6.8 Cytotoxicity assays

Cytotoxicity assays were carried out using the MTS reagent kit (Promega) for 1-48h, with 5, 10, 50 and 100 μM **TP-β** treated ins1e cells in accordance with the manufacturer's instructions.

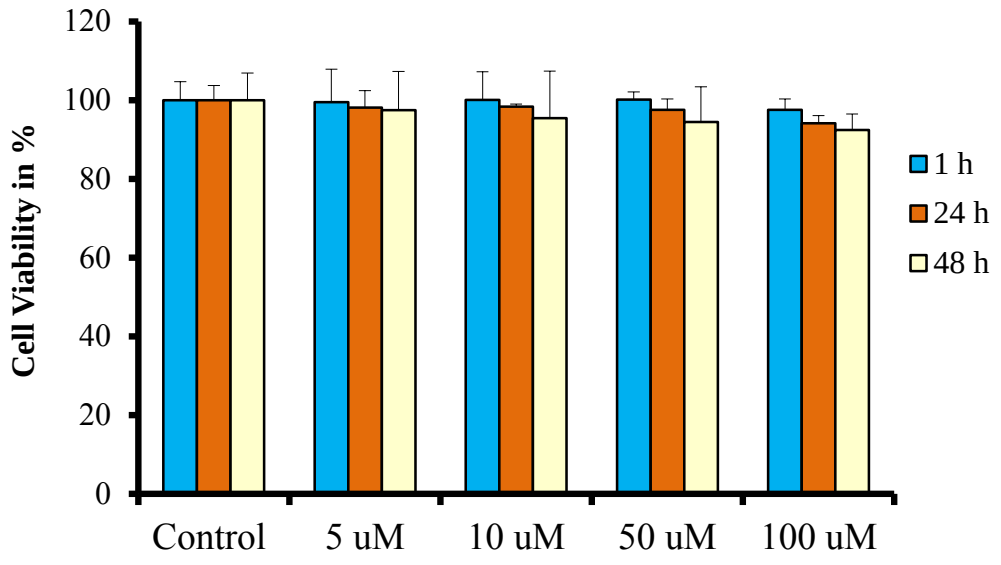

Figure 4.9 Cell viability study.

Cytotoxic effect of **TP-β** (TPO-C6-GluN) in ins1e cells. The cytotoxic effect of TP- β was tested by the MTS (3-(4,5-dimethylthiazol-2-yl)-5-(3-carboxymethoxyphenyl)-2-(4-sulfophenyl)-2H-tetrazolium, inner salt) assay using the Cell Titer 96 non-radioactive cell proliferation colorimetric assay kit (Promega) on ins1e cells. First, the ins1e cells (1 X 10^4cells in 100 μl of media) were seeded onto 96 well plate and then different concentrations (0 μM, 5 μM, 10 μM, 50 μM and 100 μM) of **TP-β** was added to the cells on the following day and incubated them at 37 °C for 1 h. After 1 h 20 μl of MTS solution was added to each well and incubated for another 4 hours before the absorbance was measured at 490 nm using Spectrometer. The same experiments were done for 24 h and 48 h. The control cells were 100 % alive without compound condition. At least 95 % of the **TP-β** treated cells were alive even after 48 hours of incubation at 100 μM concentration. This indicates that the **TP-β** is nontoxic to ins1e cells.

4.7 Reference

1. Leibiger, I. B.; Leibiger, B.; Berggren, P. O., Insulin signaling in the pancreatic beta-cell. *Annual review of nutrition* **2008,** *28*, 233-51.

2. Saudek, F.; Brogren, C. H.; Manohar, S., Imaging the Beta-cell mass: why and how. *Rev Diabet Stud. Spring* **2008,** *5* (1), 6-12.

3. van Belle, T. L.; Coppieters, K. T.; von Herrath, M. G., Type 1 diabetes: etiology, immunology and therapeutic strategies. *Physiological reviews* **2011,** *91* (1), 79-118.

4. Lin, Y.; Sun, Z., Current views on type 2 diabetes. *The Journal of endocrinology* **2010,** *204* (1), 1-11.

5. Koo, V.; Hamilton, P. W.; Williamson, K., Non-invasive *in vivo* imaging in small animal research. *Cellular oncology : the official journal of the International Society for Cellular Oncology* **2006,** *28* (4), 127-39.

6. Massoud, T. F.; Gambhir, S. S., Molecular imaging in living subjects: seeing fundamental biological processes in a new light. *Genes & development* **2003,** *17* (5), 545-80.

7. Speier, S.; Nyqvist, D.; Kohler, M.; Caicedo, A.; Leibiger, I. B.; Berggren, P. O., Noninvasive high-resolution *in vivo* imaging of cell biology in the anterior chamber of the mouse eye. *Nature protocols* **2008,** *3* (8), 1278-86.

8. Sweet, I. R.; Cook, D. L.; Lernmark, A.; Greenbaum, C. J.; Krohn, K. A., Non-invasive imaging of beta cell mass: a quantitative analysis. *Diabetes technology & therapeutics* **2004,** *6* (5), 652-9.

9. Pawley, J. B., Handbook of Biological Confocal Microscopy 3rd edn. *Springer, New York* **2006**.

10. Dunn, K. W.; Sutton, T. A., Functional studies in living animals using multiphoton microscopy. *ILAR journal / National Research Council, Institute of Laboratory Animal Resources* **2008,** *49* (1), 66-77.

11. Kobat, D.; Horton, N. G.; Xu, C., *In vivo* two-photon microscopy to 1.6-mm depth in mouse cortex. *Journal of biomedical optics* **2011,** *16* (10), 106014.

12. Speier, S.; Nyqvist, D.; Cabrera, O.; Yu, J.; Molano, R. D.; Pileggi, A.; Moede, T.; Kohler, M.; Wilbertz, J.; Leibiger, B.; Ricordi, C.; Leibiger, I. B.; Caicedo, A.; Berggren, P. O., Noninvasive *in vivo* imaging of pancreatic islet cell biology. *Nature medicine* **2008,** *14* (5), 574-8.

13. Russ, H. A.; Bar, Y.; Ravassard, P.; Efrat, S., *In vitro* proliferation of cells derived from adult human beta-cells revealed by cell-lineage tracing. *Diabetes* **2008,** *57* (6), 1575-83.

14. Kahraman, S.; Dirice, E.; Hapil, F. Z.; Ertosun, M. G.; Ozturk, S.; Griffith, T. S.; Sanlioglu, S.; Sanlioglu, A. D., Tracing of islet graft survival by way of *in vivo* fluorescence imaging. *Diabetes/metabolism research and reviews* **2011,** *27* (6), 575-83.

15. Herr, R. R.; Eble, T. E.; Bergy, M. E.; Jahnke, H. K., Isolation and characterization of streptozotocin. *Antibiotics annual* **1959,** *7*, 236-40.

16. Bhuyan, B. K.; Fraser, T. J.; Buskirk, H. H.; Neil, G. L., Antileukemic activity of streptozotocin (NSC-85998) and its analogs. *Cancer chemotherapy reports. Part 1* **1972,** *56* (6), 709-20.

17. Herr, R. R.; Jahnke, J. K.; Argoudelis, A. D., The structure of streptozotocin. *Journal of the American Chemical Society* **1967,** *89* (18), 4808-9.

18. Murray-Lyon, I. M.; Eddleston, A. L.; Williams, R.; Brown, M.; Hogbin, B. M.; Bennett, A.; Edwards, J. C.; Taylor, K. W., Treatment of multiple-hormone-producing malignant islet-cell tumour with streptozotocin. *Lancet* **1968,** *2* (7574), 895-8.

19. Thomas, N. W., The effect of streptozotocin on the fine structure of the beta cell of the cod pancreas. *Hormone and metabolic research = Hormon- und Stoffwechselforschung = Hormones et metabolisme* **1971,** *3* (1), 21-3.

20. Rerup, C. C., Drugs producing diabetes through damage of the insulin secreting cells. *Pharmacological reviews* **1970,** *22* (4), 485-518.

21. Takeda, J.; Kayano, T.; Fukomoto, H.; Bell, G. I., Organization of the human GLUT2 (pancreatic beta-cell and hepatocyte) glucose transporter gene. *Diabetes* **1993,** *42* (5), 773-7.

22. Wang, Z.; Gleichmann, H., GLUT2 in pancreatic islets: crucial target molecule in diabetes induced with multiple low doses of streptozotocin in mice. *Diabetes* **1998,** *47* (1), 50-6.

23. Hosokawa, M.; Dolci, W.; Thorens, B., Differential sensitivity of GLUT1- and GLUT2-expressing beta cells to streptozotocin. *Biochemical and biophysical research communications* **2001,** *289* (5), 1114-7.

24. Uldry, M.; Ibberson, M.; Hosokawa, M.; Thorens, B., GLUT2 is a high affinity glucosamine transporter. *FEBS letters* **2002,** *524* (1-3), 199-203.

25. FDA approved Drug Product, ZANOSAR (STREPTOZOTOCIN). **1982, May 7**.

26. Brentjens, R.; Saltz, L., Islet cell tumors of the pancreas: the medical oncologist's perspective. *The Surgical clinics of North America* **2001,** *81* (3), 527-42.

27. Sokoloff, L.; Reivich, M.; Kennedy, C.; Des Rosiers, M. H.; Patlak, C. S.; Pettigrew, K. D.; Sakurada, O.; Shinohara, M., The [14C]deoxyglucose method for the measurement of local cerebral glucose utilization: theory, procedure and normal values in the conscious and anesthetized albino rat. *Journal of neurochemistry* **1977,** *28* (5), 897-916.

28. Turkheimer, F.; Moresco, R. M.; Lucignani, G.; Sokoloff, L.; Fazio, F.; Schmidt, K., The use of spectral analysis to determine regional cerebral glucose utilization with positron emission tomography and [18F]fluorodeoxyglucose: theory, implementation and optimization procedures. *Journal of cerebral blood flow and metabolism : official journal of the International Society of Cerebral Blood Flow and Metabolism* **1994,** *14* (3), 406-22.

29. Dienel, G. A.; Cruz, N. F.; Adachi, K.; Sokoloff, L.; Holden, J. E., Determination of local brain glucose level with [14C]methylglucose: effects of glucose supply and demand. *The American journal of physiology* **1997,** *273* (5 Pt 1), E839-49.

30. Axelrod, J. D.; Pilch, P. F., Unique cytochalasin B binding characteristics of the hepatic glucose carrier. *Biochemistry* **1983,** *22* (9), 2222-7.

31. Yoshioka, K.; Takahashi, H.; Homma, T.; Saito, M.; Oh, K. B.; Nemoto, Y.; Matsuoka, H., A novel fluorescent derivative of glucose applicable to the assessment of glucose uptake activity of Escherichia coli. *Biochimica et biophysica acta* **1996,** *1289* (1), 5-9.

32. Yamada, K.; Nakata, M.; Horimoto, N.; Saito, M.; Matsuoka, H.; Inagaki, N., Measurement of glucose uptake and intracellular calcium concentration in single, living pancreatic beta-cells. *The Journal of biological chemistry* **2000,** *275* (29), 22278-83.

33. Lee, H. Y.; Lee, J. J.; Park, J.; Park, S. B., Development of fluorescent glucose bioprobes and their application on real-time and quantitative monitoring of glucose uptake in living cells. *Chemistry* **2011,** *17* (1), 143-50.

34. Tian, Y. S.; Lee, H. Y.; Lim, C. S.; Park, J.; Kim, H. M.; Shin, Y. N.; Kim, E. S.; Jeon, H. J.; Park, S. B.; Cho, B. R., A two-photon tracer for glucose uptake. *Angewandte Chemie* **2009,** *48* (43), 8027-31.

35. Park, J.; Um, J. I.; Jo, A.; Lee, J.; Jung, D. W.; Williams, D. R.; Park, S. B., Impact of molecular charge on GLUT-specific cellular uptake of glucose bioprobes and *in vivo* application of the glucose bioprobe, GB2-Cy3. *Chem. Commun.* **2014,** *50* (66), 9251-4.

36. Zhang, M.; Zhang, Z.; Blessington, D.; Li, H.; Busch, T. M.; Madrak, V.; Miles, J.; Chance, B.; Glickson, J. D.; Zheng, G., Pyropheophorbide 2-deoxyglucosamide: a new photosensitizer targeting glucose transporters. *Bioconjugate chemistry* **2003,** *14* (4), 709-14.

37. Kim, H. M.; Yang, P. R.; Seo, M. S.; Yi, J. S.; Hong, J. H.; Jeon, S. J.; Ko, Y. G.; Lee, K. J.; Cho, B. R., Magnesium ion selective two-photon fluorescent probe based on a benzo[h]chromene derivative for *in vivo* imaging. *The Journal of organic chemistry* **2007,** *72* (6), 2088-96.

38. (a) Sahagun, G.; Moore, S. A.; Hart, M. N., Permeability of neutral vs. anionic dextrans in cultured brain microvascular endothelium. *The American journal of physiology* **1990,** *259* (1 Pt 2), H162-6; (b) Nayak, T. K.; Dennis, M. K.; Ramesh, C.; Burai, R.; Atcher, R. W.; Sklar, L. A.; Norenberg, J. P.; Hathaway, H. J.; Arterburn, J. B.; Prossnitz, E. R., Influence of charge on cell permeability and tumor imaging of GPR30-targeted 111in-labeled nonsteroidal imaging agents. *ACS chemical biology* **2010,** *5* (7), 681-90.

39. Kaminski, M. T.; Lenzen, S.; Baltrusch, S., Real-time analysis of intracellular glucose and calcium in pancreatic beta cells by fluorescence microscopy. *Biochimica et biophysica acta* **2012,** *1823* (10), 1697-707.

40. Tal, M.; Thorens, B.; Surana, M.; Fleischer, N.; Lodish, H. F.; Hanahan, D.; Efrat, S., Glucose transporter isotypes switch in T-antigen-transformed pancreatic beta cells growing in culture and in mice. *Molecular and cellular biology* **1992,** *12* (1), 422-32.

41. Arya, A.; Looi, C. Y.; Cheah, S. C.; Mustafa, M. R.; Mohd, M. A., Anti-diabetic effects of Centratherum anthelminticum seeds methanolic fraction on pancreatic cells, beta-TC6 and its alleviating role in type 2 diabetic rats. *Journal of ethnopharmacology* **2012,** *144* (1), 22-32.

42. Lernmark, A., The preparation of and studies on, free cell suspensions from mouse pancreatic islets. *Diabetologia* **1974,** *10* (5), 431-8.

43. Steiner, D. J.; Kim, A.; Miller, K.; Hara, M., Pancreatic islet plasticity: interspecies comparison of islet architecture and composition. *Islets* **2010,** *2* (3), 135-45.

44. Vendrell, M.; Samanta, A.; Yun, S. W.; Chang, Y. T., Synthesis and characterization of a cell-permeable near-infrared fluorescent deoxyglucose analogue for cancer cell imaging. *Organic & biomolecular chemistry* **2011,** *9* (13), 4760-2.

45. Makarov, N. S.; Drobizhev, M.; Rebane, A., Two-photon absorption standards in the 550-1600 nm excitation wavelength range. *Optics express* **2008,** *16* (6), 4029-47.

46. Lee, S. K.; Yang, W. J.; Choi, J. J.; Kim, C. H.; Jeon, S. J.; Cho, B. R., 2,6-Bis[4-(p-dihexylaminostyryl)styryl]anthracene derivatives with large two-photon cross sections. *Organic letters* **2005,** *7* (2), 323-6.

Chapter: 5

Discovery of Inorganic Polyphosphate Probes and its Application for Tissue Imaging

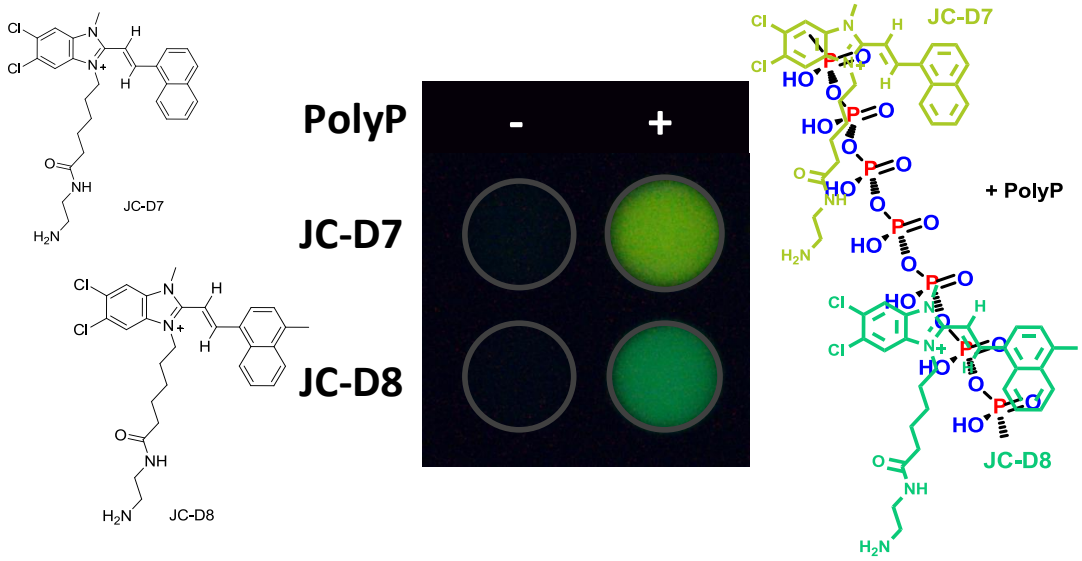

Chapter 5

5.1 Introduction

Inorganic polyphosphate (polyP) is a linear polymer made up of many orthophosphates linked together by phosphor-anhydride bonds identical to the ones found in ATP. PolyP is a biological macromolecule, which has been found in various studied organisms ranging from bacteria to humans[1,2]. The length of polyP can vary depending on the organism. In mammalian organisms polyP is found in sizes ranging from 10 to 100 phosphate groups[3,4]. Although, it has been known for many decades that polyP is present in the mammalian organisms, a significant increase in the studies specifically addressing the function of polyP only occurred in the past few years. A number of reports from different groups indicate that polyP is ubiquitous in the mammalian cells where it plays multiple and diverse physiological roles. It has been demonstrated that polyP plays a major role as a regulator of blood coagulation and pro-inflammatory agent[5-7], acts as gliotransmitter in mammalian brain[8], modulates TRPM8 ion channel activity[9], regulates cell proliferation[10]. Furthermore, it was proposed that polyP is involved in mitochondrial bioenergetics processes[4] and in activation and formation of the mitochondrial permeability transition pore[11,12]. Combined, these data support the notion that, similar to microorganisms, mammalian polyP is a versatile biopolymer, which is critically important for physiological and pathological functions in cell.

5.2 Objective

One of the key challenges faced by the field of polyP studies is the very limited number of methods for direct detection and investigation of polyP in mammalian cells and tissues. One of the central experimental approaches in polyP studies involves the use of DAPI probe and fluorescent microcopy[5,13-17]. Although the DAPI probe has high affinity towards polyP it is also known to interfere with other poly anions, notably RNA[18]. The low abundance of polyP, as is the case in mammalian cells could make data interpretation difficult. Thus, currently usage of this approach is limited by the lack of polyP specific fluorescent probe. Earlier, we have demonstrated that *in vitro* screening with fluorescence dye libraries can lead to the discovery of various selective imaging probes, such as: DNA[19], RNA[20], Heparin[21], GTP[22], glutathione[23] and more[24]. In this present work, we report the discovery of novel highly selective polyP sensors from a benzimidazolinium dye library and its application for analytical polyP assay of purified polymer as well as polyP staining in live cells and tissue samples.

5.3 Results and Discussion

The main motivation of this current work is the discovery of selective fluorescence probe for polyphosphate and its application in live cell and tissue samples.

5.3.1 Discovery of the polyP specific fluorescent probe

Among the various fluorescence dye libraries available in house, we applied benzimidazolinium dye library (named **JC; Figure 5.1 A**) for the primary screening. This positively charged dye library was reported earlier for discovery of selective probes for negatively charged analytes Heparin[21] and GTP[22]. As polyP is a polymer of negatively

charged phosphate groups (**Figure 5.1 A**), we hypothesized the presence of polyP selective probes in **JC** library (which contains 96 diverse fluorescence molecules). To evaluate our hypothesis we performed a primary screening of these compounds with four different concentration of polyP (0.5, 2.5, 5 and 10 μg/mL) in 20 mM HEPES buffer (pH 7.4). Out of the five JC compounds that exhibited turn-on effect upon incubation with polyP, **JC-D7** and **JC-D8** (**Figure 5.1 B**) were nominated for the better selectivity profile. Two final compounds JC-D7 and JC-D8 were synthesized based on the solid phase chemistry (**Scheme 5.1**). The chemical characterization was done by HRMS and NMR.

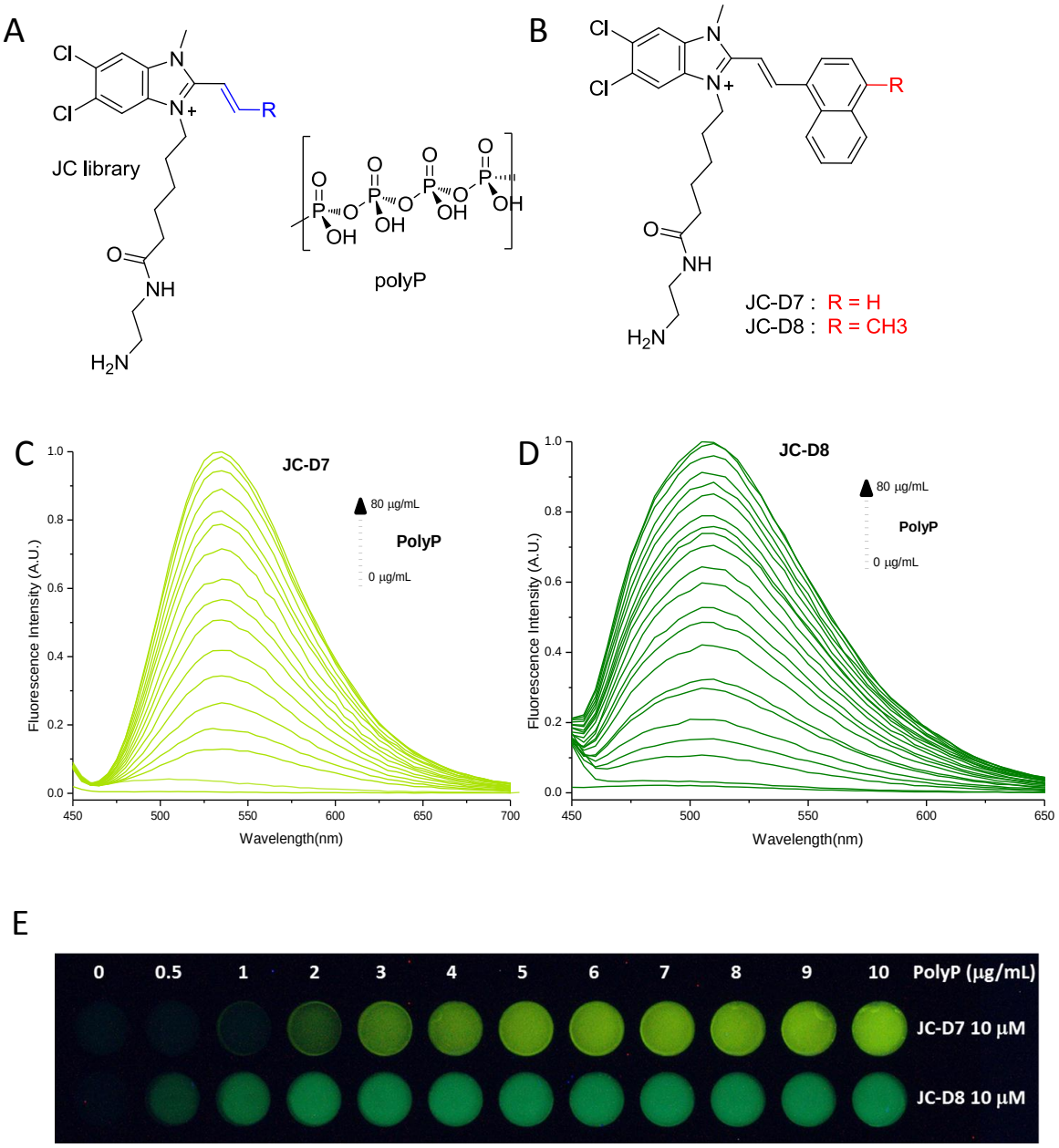

Figure 5.1 Structure and fluorescent properties of JC-D7/D8 compounds.

A. Structure of benzimidazolium dye library (JC library), R represents 96 different aromatic building blocks, (Reference-22) and repeating units of phosphate representing polyphosphate (polyP). **B.** Structure of JC-D7 and JC-D8. **C.** Fluorescence emission spectra (excitation: 390 nm, cutoff: 420 nm) of JC-D7 (10 μM) and **D.** JC-D8 (10 μM) with 0-80 μg/mL polyP (average chain length 60) in 20 mM HEPES (pH 7.4). **E.** JC-D7 and JC-D8 (10 μM) with indicated concentration of polyP in 20 mM HEPES buffer (pH = 7.4) in 96-well plate under 365 nm UV lamp.

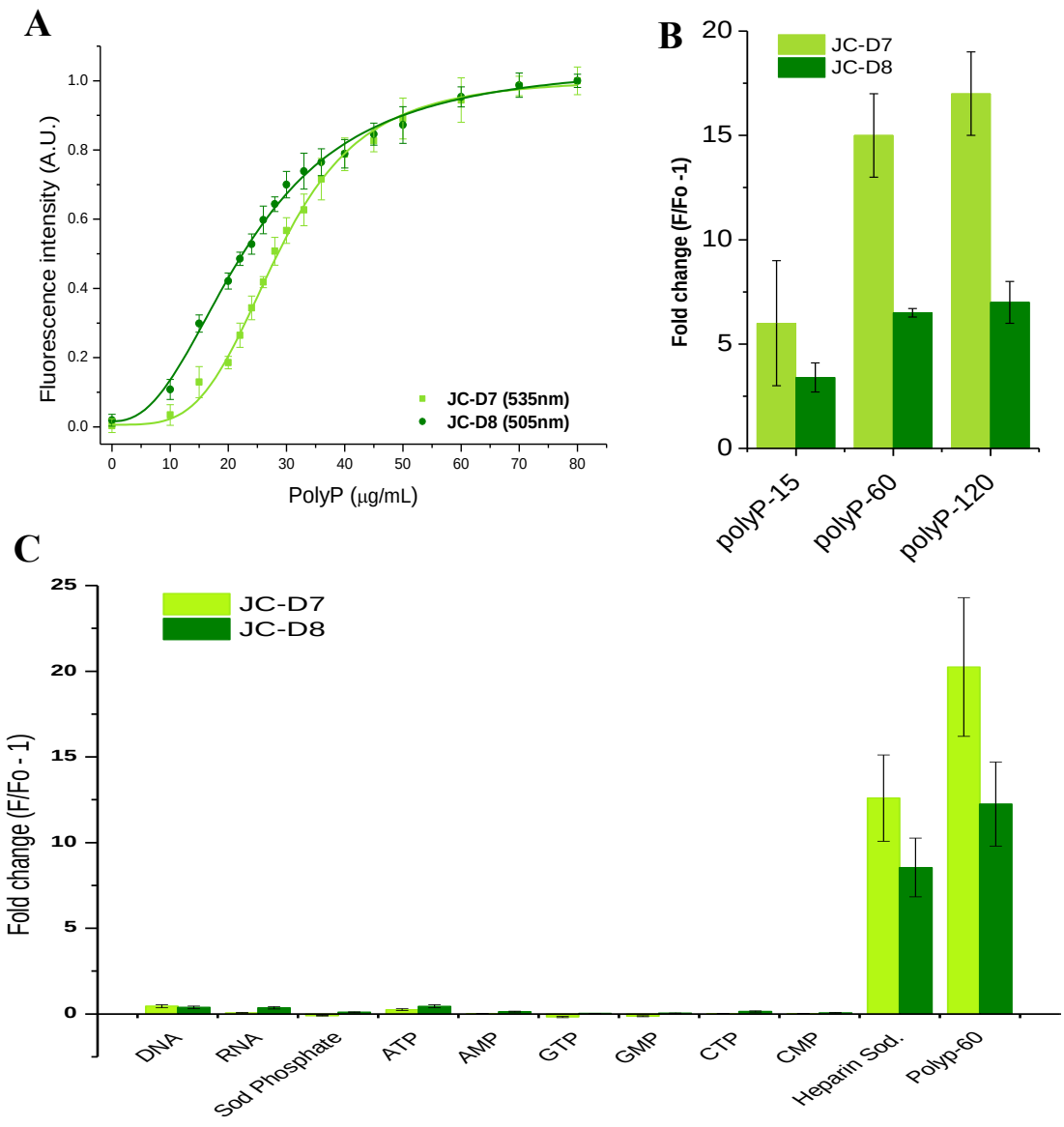

Figure 5.2 PolyP response and selectivity of JC-D7/D8 compounds.

A. Fluorescence binding curve of JC-D7 (535 nm) and JC-D8 (505 nm) as a function of 0-80 μM polyP concentration in HEPES buffer pH 7.4. **B.** Dependence of the fluorescence intensity on the polyP chain length. Each sample contained 10 μg/mL of polyP of the average length of 15, 60 and 120 units of orthophosphate. **C.** Fluorescence response of JC-D7 (at 535 nm) and JC-D8 (at 505 nm) toward a series of analytes. The fluorescence intensities of the each of the dye in the presence of each analyte (F) were compared with fluorescence intensities of dye (Fo) in 20 mM HEPES buffer (pH 7.4). Bars represent the ratio of (F/Fo – 1). The concentration of macromolecule analytes

(DNA, RNA) 100 μg/mL, that of small-molecule analytes (Sodium Phosphate, ATP, AMP, GTP, GMP, CTP and CMP) 1 mM, Sodium Heparin and polyP is 20 μg/mL.

In the presence of polyP both JC-D7 and JC-D8 exhibited remarkable 54.28 and 46.25 fold fluorescence increase respectively (**Figure 5.1 C** and **D**). Dissociation constants measured from the titration curves (**Figure 5.2 A**) demonstrated that JC-D8 (k_d = 23.4 μg/mL ± 0.4) has moderately higher affinity towards polyP than JC-D7 (k_d = 28.4 μg/mL ± 0.4). The minimum detection limit of polyP based on visual detection; for JC-D7 is 2 μg/mL, whereas for JC-D8 it is 0.5 μg/mL (**Figure 5.1 D**).

As can be seen in **Figure 5.2 C**, JC-D7 and JC-D8 did not show any significant increase in fluorescence in the presence of a large number of biological phosphates: sodium orthophosphate, nucleotides (ATP, AMP, GTP, GMP, CTP and CMP) and polymers like DNA and RNA. Most importantly JC-D7 and JC-D8 did not increase the fluorescence in the presence of RNA, the polymer known to be ubiquitously present in the living organisms and leads to the fluorescence increase of DAPI[18]. Interestingly, like DAPI probes JC-D7 and JC-D8 also showed turn on response with heparin but fortunately this biological polymer is not commonly found inside the cells. We should also note that increase in fluorescence intensity of JC-D7 and JC-D8 with polyP is significantly higher in HEPES buffer (20 mM at pH 7.4) comparing to salt containing buffers (e.g. KCl, NaCl or $CaCl_2$). See **Figure 5.8** for an example of dramatic fluorescence drop in 150 mM KCl buffer. This reduced fluorescence intensity is likely due to the fact that higher ionic strength of solution may reduce the interaction of JC-D7 and JC-D8 with polyP. Furthermore, we have found that these probes demonstrated

stronger fluorescence response with longer chain polyP compared to the shorter polymers (average length of polyP-15 units of orthophosphates) (**Figure 5.2 B**). Overall, our experiments identify two probes with good potential for investigation of polyP distribution and metabolism in living cells.

5.3.2 Validation of polyP staining in live cells

An essential feature of a fluorescent indicator that makes it suitable for live cells imaging is the probes cellular permeability. In order to investigate the rate of the probe uptake by the cell, 5 μL of 1 mM solution of JC-D7 or JC-D8 (dissolved in DMSO) was applied to 0.5 ml of the imaging media. **Figure 5.3 A** shows primary neurons and astrocytes imaged before and after the addition of dyes with excitation at 405 nm and emission detection in the range 505 -590 nm. These cells start to take up the indicator rapidly, reaching a steady state (plateau) fluorescence within 8-10min (n = 30, **Figure 5.3 Aa** and **inset**). However, considering the difference in density of the cells in various preparations (primary culture, acute slice, etc.), we recommend loading with JC-7/D8 for about 30 min to achieve optimal staining.

JC-D7/D8 indicators were found not only to have good permeability in single cell of low confluence preparation (such as primary neuronal/astrocytic culture), but also in tissue samples of whole fly brains (**Figure 5.3 B**) or rodent acute brain slices (**Figure 5.3 C**). It is important to note that even in high density tissue preparations, such as brain slices, at higher magnification detection of the JC-D7/D8 signal could be observed (**Figure 5.3 D**).

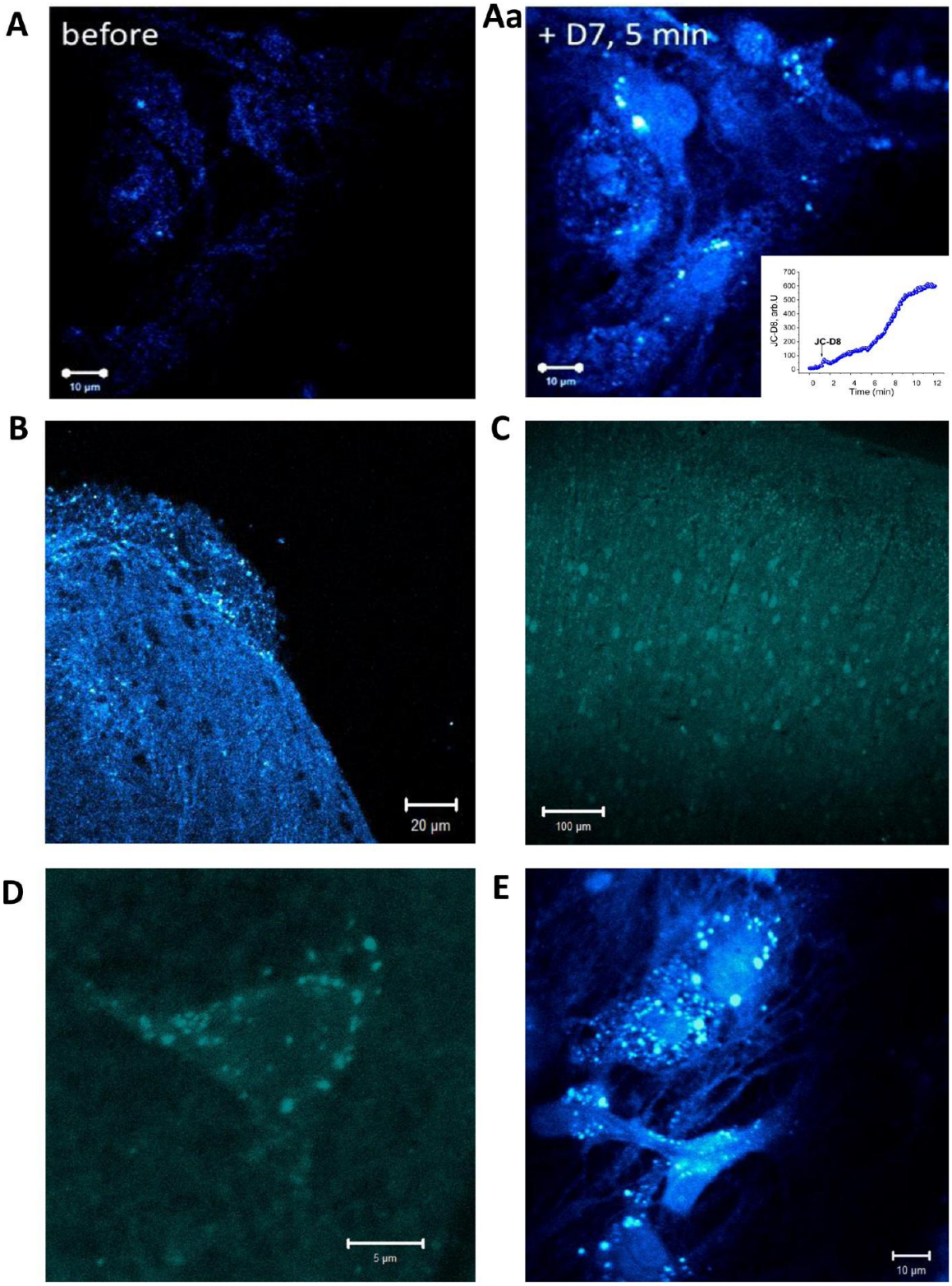

Figure 5.3 PolyP distribution in live tissues, stained with JC-D7/D8.

Mixed murine astrocytic-neuronal primary culture before (**A**) and after (**Aa**) loading with JC-D7; **Aa, inset** Kinetics of JC-D7/D8 loading into cultured rat astrocytes; **B**, whole *Drosophila melanogaster* brain; **C**- acute brain slice from rat, **D** scanned image of higher magnification (smaller scan area, note the scale bar) of the same slice preparation shown in panel C; **E**-compartmentalization of polyP into rat astrocyte from primary co-culture.

Loading single cells with JC-D7/D8 allowed us to visualize localization of polyP in different compartments. Although exact localization of the polyP needs further conformation we suggest that these locations might include mitochondria, membrane vesicles or polyP granules (**Figure 5.3 E**). We believe that combination of this dye with other indicators will help to characterize the distribution of polyP within the cell.

Despite the high affinity of the JC-D7/D8 probes to polyP *in vitro*, it is still questionable if changes in the fluorescence intensity of the indicator correspond to the changes in the concentration of endogenous polyP in the live cell. In order to test whether this indicator is sensitive to changes of the levels of endogenous polyphosphate, we transfected cells (SH-SY5Y) with polyP producing enzyme mgPPK (mitochondrially targeted, GFP tagged inorganic polyphosphate kinase from *Saccharomyces cerevisiae*) construct. The outcome of transfection of the mgPPK construct manifested in increased levels of mitochondrial polyP. We found that both indicators JC-D7 and JC-D8 are able to visualize changes in the level of endogenous polyP content (**Figure 5.4 A**, n = 44).

On the other hand, when GFP-tagged, polyP hydrolyzing enzyme, exopolyphosphatasePPX1 from yeast is expressed in the mitochondria of cultured cells (MTX-GFP-PPX construct)[11], we observed lower fluorescence intensity of both indicators JC-D7 and JC-D8 in the mitochondria of these cells (**Figure 5.4 B**, n = 19).

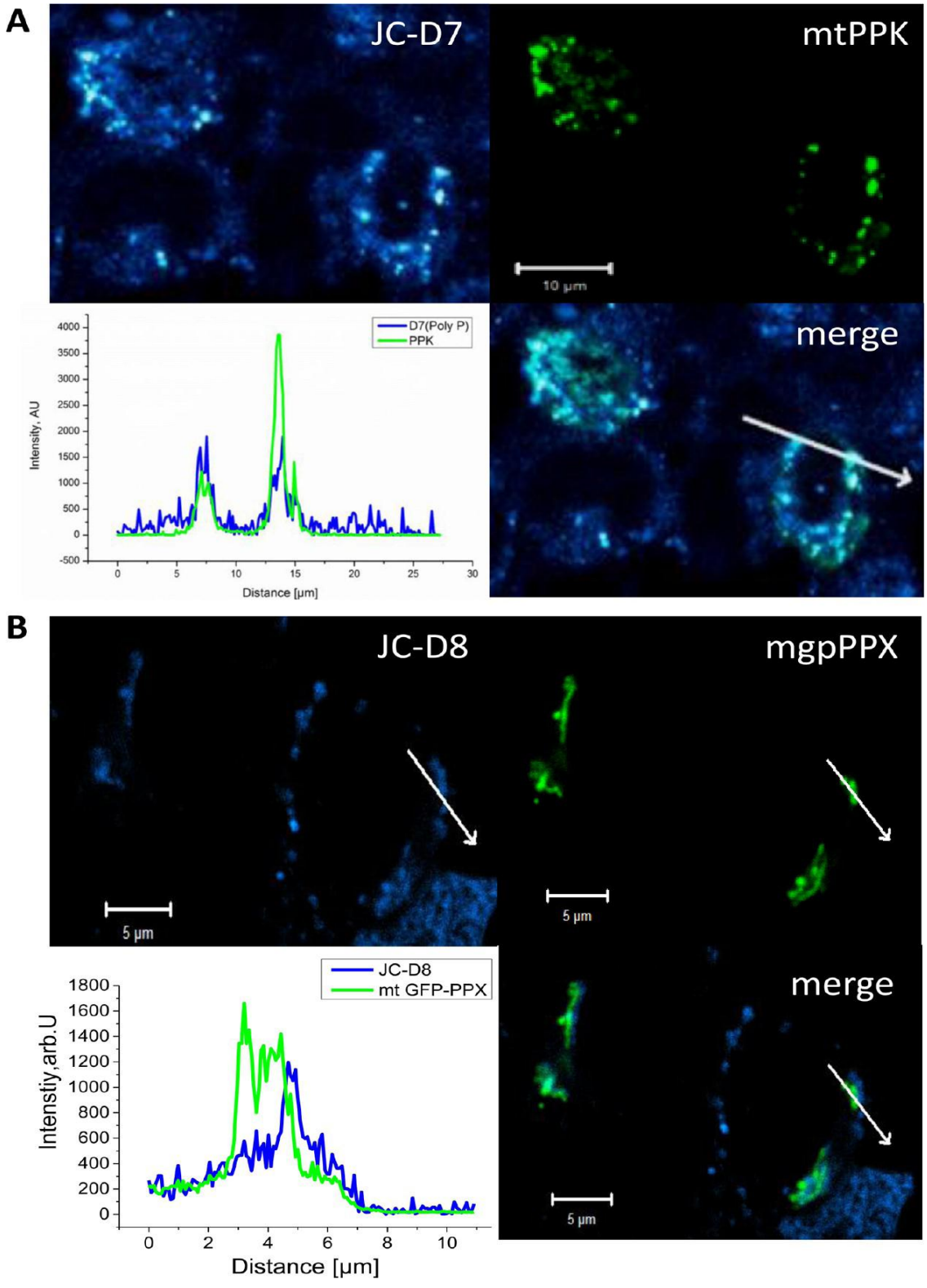

Figure 5.4 Specificity of the JC-D7/D8 probe in rat primary culture.

A, Overexpression of mitochondrially targeted, GFP-labelled polyphosphate kinase (mgPPK) results in increased level of JC-D7 fluorescence. **A, inset**- co-localization profile depicted by arrow shows that areas with increased levels of mtPPK expression correspond to areas with increased levels of endogenous polyphosphate. Correspondingly, **B,** mitochondrially targeted GFP-labelled exopolyphosphatase (mgPPX) overexpression leads to increase activity of the enzyme and therefore to a decreased levels of polyphosphate in GFP-positive mitochondria. (**B, inset**) GFP and JC-D8 signal do not significantly overlap.

Taken together, this data indicate that by using the novel fluorescent probe JC-D7/D8 we have been able to measure changes in endogenous poly P levels in live cells.

Another important characteristic of the fluorescent indicator is not only the ability to bind the object of interest, but also able to measure changes in the concentrations of polyP in the live cell. We previously demonstrated that mitochondrial uncoupler FCCP dramatically decreased the level of mitochondrial polyphosphate[4]. In the present experiments, when primary neurons and astrocytes were loaded with JC-D7 or JC-D8 indicator, application of 1 μM of FCCP induced slow and progressive drop in the intensity of JC-D7/D8 fluorescence (**Figure 5.5 A**, **Aa**, n = 17). It should be noted that based on our control experiments levels of auto-fluorescence were low and can't explain changes caused by FCCP addition. In addition to the mitochondria, high amounts of polyP have been found in lysosomes[8,25]. Specifically, secretory lysosomes have been proposed recently as a source of releasable ATP/(PolyP) in astrocytes. It has been shown that glycyl-phenylalanine 2-naphthylamide (GPN), a substrate for lysosomal cathepsin C, can coordinately collapse the lysosomes integrity and repress the ATP release stimulated by metabolic stress or glutamate receptor activation[26]. Here, when we applied GPN to JC-D7/D8 labeled cells, we observed a dramatic increase in fluorescence (**Figure 5.5 B**, n = 17) suggesting the release of vesicular polyP into the cytosol. Similar increase in fluorescence has been observed upon application of the calcium ionophore ionomycin,

which is known to induce release of polyP from secretory vesicles (1 μM, n = 12) (**Figure 5.5 C**). Thus, we demonstrate that JC-D7 and JC-D8 can be used for registering kinetic changes of the intracellular concentration of polyP.

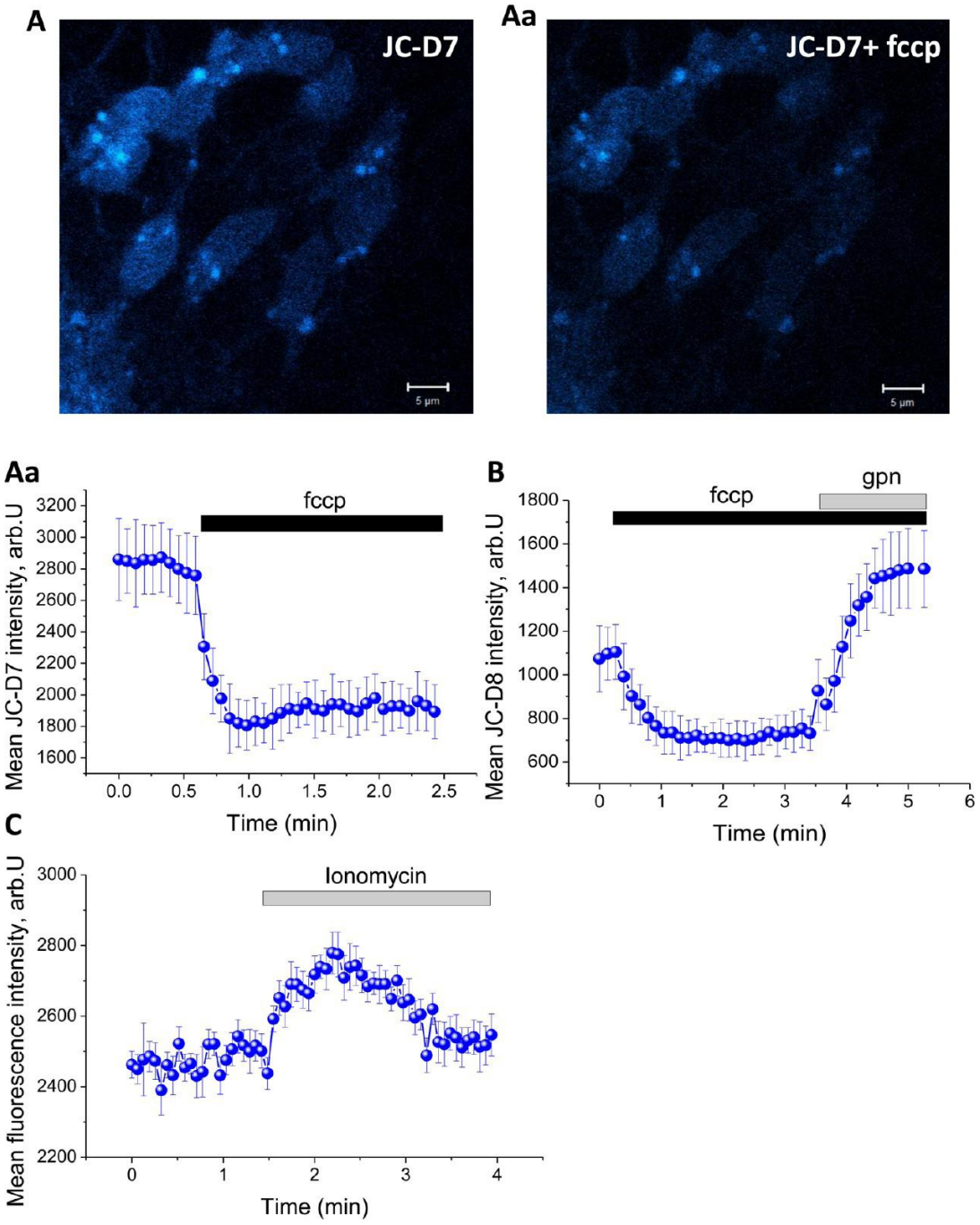

Figure 5.5 Kinetic PolyP measurement in SH-SY5Y cells, by JC-D7/D8.

Detection of changes in polyP levels in response to mitochondrial membrane depolarization by addition of FCCP (**A, Aa**), lysosomal release upon application of glycylphenylalanine 2-naphthylamide (GPN), **B**) or to ionomycin (**C**) – a calcium ionophore, that promotes equilibration of calcium gradients between intracellular compartments.

5.3.3 Estimation of polyP levels in live cell models of Parkinson's disease

One of the most significant advantages of the JC-D7/D8 probes is that their use not only can help to identify cellular localization but also allows estimation of levels of intracellular endogenous polyP in living cells. Recently it was demonstrated that in the brain, the level of the intracellular polyP could be dependent on the energy status of the mitochondria[4] or on the level of polyP in cellular vesicles[8]. Taking into account that most of familial forms of Parkinson's disease (PD) are known to have mitochondrial dysfunction and changes in signal transmission[27,28] we hypothesized that this pathology might result in abnormal levels of polyP. Here we tested this idea using JC-D7/D8 indicators. Specifically, we investigated the difference of the level of polyP in LRRK2 or PINK1 (PD related genes) knock-out animals or PD patient's fibroblasts. We found that cells with PINK1 or LRRK2 deficiency demonstrate significantly higher levels of polyP (1.9-fold increase in LRRK2 KO cells, $n = 99$; $p<0.005$; 2.9-fold increase in PINK1 deficient cells, $n = 89$; $p<0.005$; **Figure 5.6 A-B**). These experiments demonstrate how utilization of the probe allowed us to uncover the existence of the mechanism which involves polyP and likely links its metabolism with development of PD. We should note that although a lot of information is known about PD the actual mechanism of neurodegeneration remains unclear. Thus, identification of a novel macromolecule which is potentially involved in this process might uncover new horizons in study of this devastating disorder.

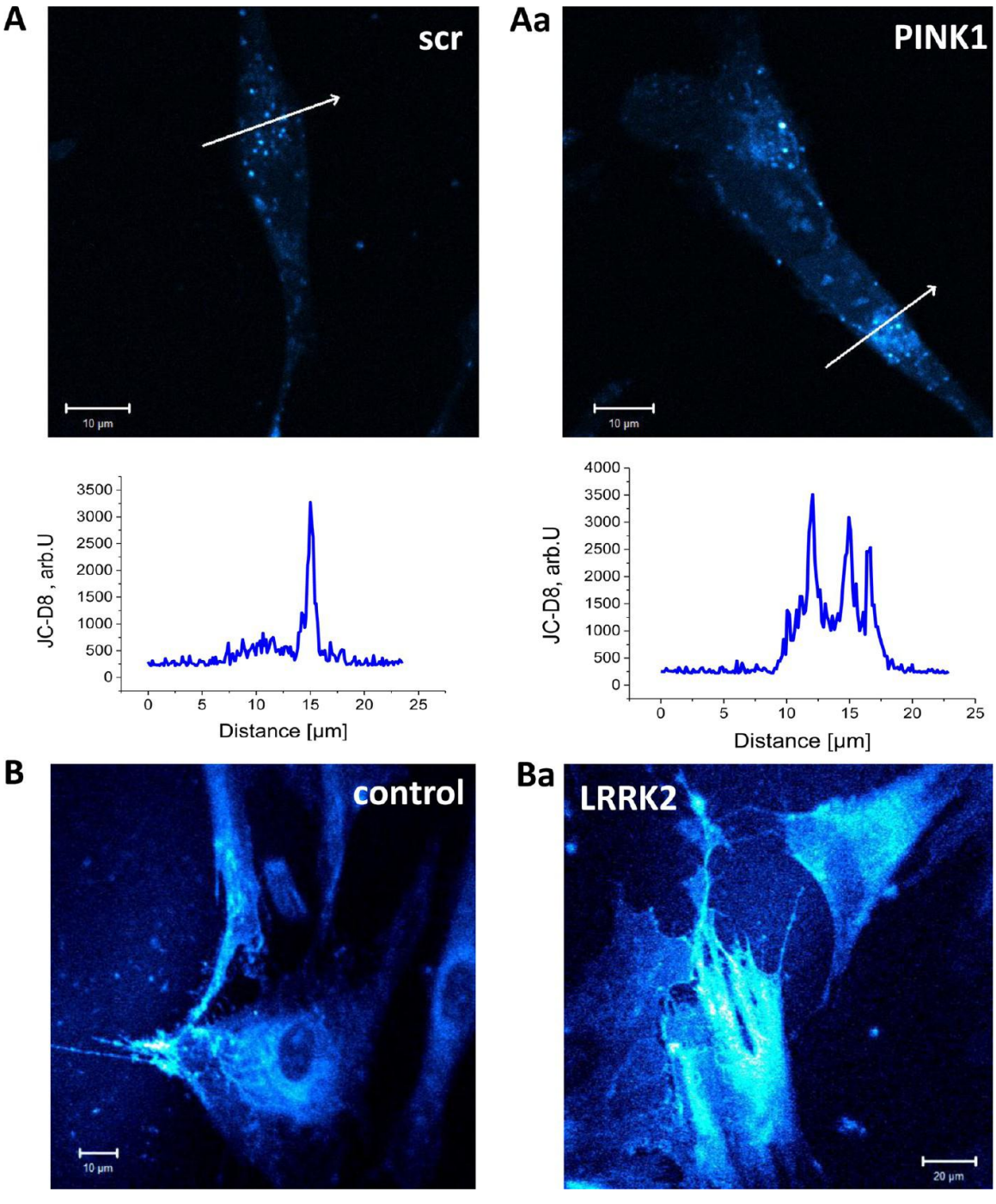

Figure 5.6 Differential distribution of PolyP in LRRK2 or PINK1 knock-out cell lines, as detected by JC-D7/D8.

SH-SY5Y cells with PINK1 (**A**) or fibroblasts with LRRK2 (**B**) deficiency demonstrate significantly higher levels and differential distribution (**inset A** versus **Aa**) of endogenous polyP.

5.3.4 Comparative imaging of DAPI-polyP and JC-D8.

In order to compare the DAPI and JC-D8 we load primary co-culture neurons and astrocytes with these indicators. **Figure 5.7** shows that indicators distributed not equally in the cells that could be due to different compartmentalization of polyP in these cells as well as difference in the specificity of indicators. We also checked if JC-D8 may have a possible toxic effect on the cells that can raise difficulties during long experiments. We have found that 2 hours incubation of the primary co-culture neurons and astrocytes with DAPI (1 μM) or JC-D8 (5 μM) induce significant increase in number of dead cells treated with DAPI (from 2.9±0.2 % in control to 40.9±2.8 %, n = 5 experiments; $p<0.0001$), but not JC-D8 cells (only 4.1±0.9 % dead cells.

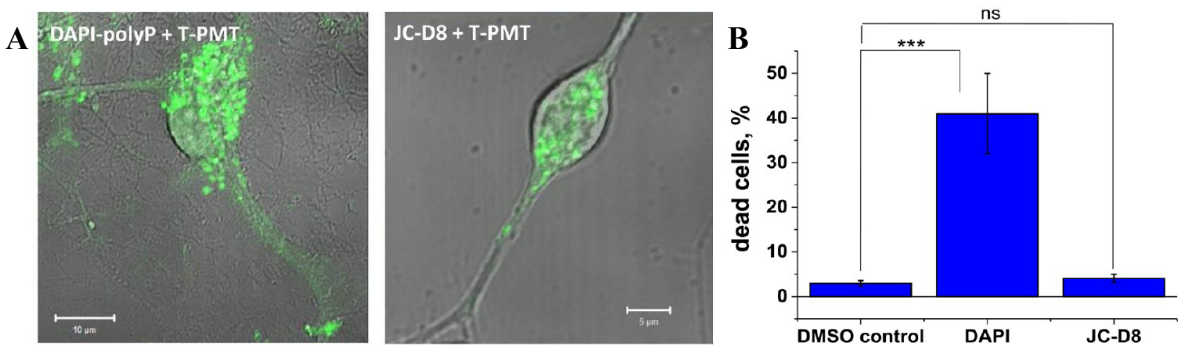

Figure 5.7 JC-D8 exhibit lower cell toxicity comparing to DAPI.

(**A**) Difference in the staining between DAPI-polyP and JC-D8 primary neurons and astrocytes. The images of polyP indicators are combined with bright field image. (**B**) Toxicity of DAPI and JC-D8 in primary cultures neurons and astrocytes. Cells were exposed to indicators for two hours and number of live and dead cells assessed by Hoechst 33342 and PI. *** $p<0.0001$

In the present study we describe the identification of two new fluorescent probes which have an excellent selectivity towards polyP and are suitable for polyP staining of living cells and tissues. Importantly these probes can be used for monitoring of the polyP

distribution and metabolism in real time experiments. It should be noted that the DAPI probe is a good alternative for polyP labeling in living cells. Furthermore *in vitro* assays show that DAPI has higher affinity towards polyP comparing to JC-D7 and JC-D8 probes[15]. However, one of the disadvantages of DAPI is the fact thatthe fluorescent signal from DAPI-polyP can be easily distinguished from DAPI-DNA signal, DAPI-RNA signal can potentially be misinterpreted as DAPI-polyP signal[18]. Taking into account that RNA is widely distributed inside the cells this makes data interpretation of DAPI staining somewhat ambiguous. This is particularly critical when DAPI is used for polyP identification in mammalian cells which in many conditions have very low amounts of polyP. This requires the need to use DAPI staining in combination with the expression of polyP hydrolyzing enzymes as a negative control[11]. We propose the newly identified probes will allow for significantly more reliable assays of polyP in living cells.

One interesting question is the nature of interaction of the dyes with polyP and the reason for the dye specificity. We propose that this selectivity originates from the fact that polyP is the polymer with the highest density of the negative charge out of all known biological polymers. This idea is supported by the fact that the probes contain a polyamine group as a part of their chemical structure. Recent experiments indicate that polyamines including spermine and spermidine are strong chelators of polyP[29]. It is possible that presence of similar amine groups in JC-D7 and JC-D8 is responsible for their electrostatic interactions with polyP, while specific spectral properties are determined by the presence of the fluorescent group.

While we propose that JC-D7/D8 probes to have a number of practical advantages comparing to currently existing methods we should point out that we identified two

important limitations which should be taken into account. Firstly, we have found that when used with *in vitro* samples the fluorescence was non-detectable in the presence of salt solutions. Presumably this is due to the fact that the increase in the ionic strength results in the decrease in probe-polyP interactions. This should be taken into account when the probe is used for quantification of the purified polyP samples, which should be done in low salt solutions. Furthermore, although staining of living cells is polyP specific, due to the effects of the ionic strength it is likely that dissociation constants for the probe inside the cells are higher than what can be estimated based on the measurements which used synthetic polymers. Secondly, we have found that stained live cells can be analyzed easily using confocal but not wide field fluorescent microcopy, which produced a diffused staining pattern presumably due to the ubiquitous presence of polyP in various compartments.

5.4 Conclusion

In conclusion, kinetic changes of the level of poly P as well as specific polyP distribution cannot be measured with any biochemical methods. While use of DAPI probe makes those assays possible employing fluorescence imaging approach, its use also raises concerns due to potential interference of the indicator due to variable levels of RNA and DNA in mitochondria and other cellular compartments under different conditions. The presented probes allow us to achieve higher specificity for polyP labeling which largely excludes possible contributions of DNA and RNA. Using the novel indicators we have been able to detect increased level of poly P in brain slices obtained from an animal model of Parkinson's disease. This finding demonstrates the potential for

practical use of the probes in live samples. However, care should be taken and specific protocols developed for each particular set of experimental conditions.

5.5 Experimental details

5.5.1 Primary screening.

Fluorescence intensities were measured using a SpectraMax M2 plate reader in a 96-well plate. JC compounds were dissolved to a final concentration of 10 μM (20 mM HEPES buffer, pH 7.4, containing 1 % (v/v) DMSO) and incubated with different analytes at different serial concentration in 20 mM HEPES buffer (pH 7.4). The excitation wavelength was set at 390 nm and the emission spectra were recorded from 450 to 700 nm. The fluorescence fold increase ratios were determined by referring the maximum fluorescence intensity of JC compounds in the presence and absence of analytes.

The quantum yield (Φ) of JC-D7 before and after the addition polyphosphate is 0.007 and 0.38, respectively. Whereas, the quantum yield of JC-D8 in the absence and presence of polyphosphate is 0.008 and 0.37, respectively (supporting information for quantum yield measurement detail and equation). Because of the comparatively low quantum yield of JC-D7 than JC-D8, the earlier has slightly higher fold increase.

5.5.2 Selectivity study

Benzimidazolium compounds were transferred to Greiner 96 well black polypropylene plates (final concentration as 10 μM) and tested against DNA and RNA 100 μg/mL, other analytes: Sodium Phosphate, ATP, AMP, GTP, GMP, CTP and CMP 1

mM and Heparin Sodium and polyP is 20 μg/mL in 20 mM HEPES buffer (pH = 7.4) with 1 % DMSO. Fluorescent spectra were recorded on a SpectraMax M2 fluorescent plate reader with excitation at 390 nm (cutoff: 420 nm), emission 450 to 700 nm.

5.5.3 Preparation of acute brain slices

All mouse experiments were carried out in compliance with institutional ethical and welfare standards and under Home Office regulation. Slices were prepared using standard procedures as previously described[30]. Briefly, transverse acute brain slices (100-200 μm) were prepared from 20-24-week-old WT, PINK1 KO and LRRK2 KO C57BL/6 mice. The animals were euthanized by cervical dislocation, brains were collected and tissue was immediately sliced at 4 °C using a vibratome (Leica VT1200S). The tissue slices were cut and maintained in physiological saline at room temperature (24 °C) for ~1h before imaging.

5.5.4 Live cell imaging

SHY-SY5 cells, human skin fibroblasts, whole Drosophila brains, mixed primary brain cultures or acute brain slices were loaded for 30 min at room temperature with 5 μM JC-D7 or JC-D8 in a HEPES-buffered salt solution (HBSS) composed (mM): 156 NaCl, 3 KCl, 2 $MgSO_4$, 1.25 KH_2PO_4, 2 $CaCl_2$, 10 glucose and 10 HEPES, pH adjusted to 7.35 with NaOH.

Confocal images were obtained using a Zeiss 710 CLSM microscope equipped with a META detection system and a 40x oil immersion objective. JC-D7/D8 fluorescence was determined with excitation at 405 nm and emission above 450 nm. Illumination intensity was kept to a minimum (at 0.1-0.2 % of laser output) to avoid phototoxicity and the

pinhole set to give an optical slice of ~2 μm. For images in experiments comparing levels of fluorescence in different cells the imaging setting were kept at the same level. For better visual representation the different false-color was chosen.

The DAPI-polyP fluorescence was detected with excitation 405 nm and emission between 480-520 nm. The images were analyzed using Zeiss software.

5.5.5 Toxicity Experiments

For toxicity assays cells were exposed to 20 μM propidium iodide (PI) and 4.5 μM Hoechst 33342 (Molecular Probes, Eugene, OR) for 30 min prior to imaging. The PI is excluded from viable cells and exhibits a red fluorescence following a loss of membrane integrity, while the Hoechst 33342 labels all nuclei blue. This allows expression of the number of dead (red stained) cells as a fraction of the total number of nuclei counted. Each experiment was repeated four or more times using separate cultures.

5.5.6 Statistical analysis

Statistical analysis was performed with the aid of Origin 9 (Microcal Software Inc.,) software. Means expressed ± the standard error of the mean (s.e.m.).

5.5.7 Synthetic scheme of JC-D7 and JC-D8

Scheme 5.1 Synthesis of JC-D7 and JC-D8.

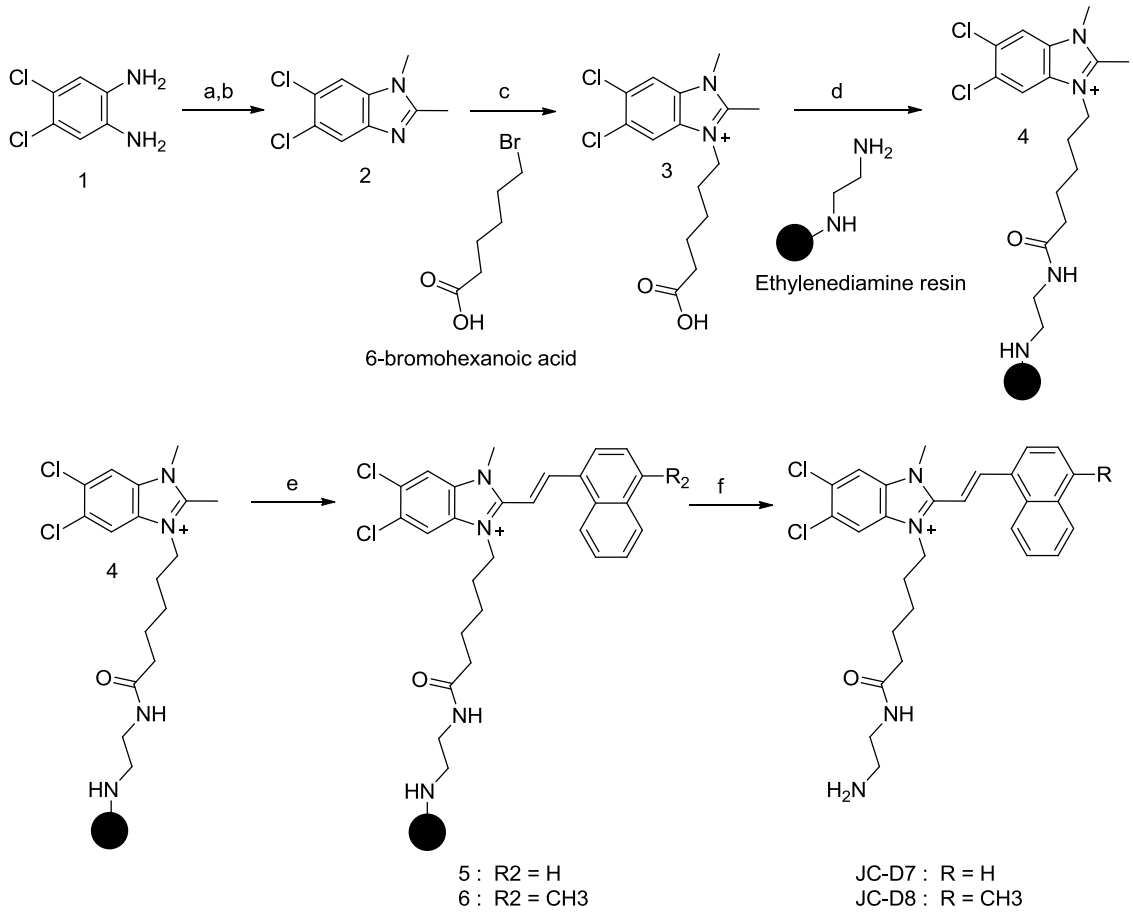

Reagents and conditions: (a) triethylorthoacetate, catalytic amount of p-toluenesulfonic acid (H+), toluene, reflux; (b) KOH, MeI, acetone; (C) NaI, Acetonitryl, 80 °C; (d) HATU, DIPEA, 30 % DMF/DCM; (e) 1-naphthaldehyde (for 5), 4-methyl-1-naphthaldehyde (for 6), pyrrolidine, NMP; (f) 5 % TFA/DCM.

Synthetic procedure up to the key intermediate **4** has been explained earlier by (Wang et al;, JACS, 2006; ref-1d). Resin **4** (10 mg, 1 eq) was added to two individual containers containing, (4-methyl-1-naphthaldehyde; 10eq) and **(**1-naphthaldehyde; 10 eq) separately. To both 1-methyl-2-pyrrolidinone (300 uL) solution and pyrrolidine (2 uL)

was added and the reactions were stirred under N_2 atmosphere for 24 h at rt. The resin was filtered and washed with DMF (5 times), alternatively dichloromethane and methanol (5 times), dichloromethane (5 times) and dried in vacuum.

Resins 5 and 6 (10 mg) were suspended in 5% trifluoroacetic acid/dichloromethane cleavage cocktail solution (0.5 mL) and shook for 15 min. The resins was filtered off and washed with dichloromethane (1 mL) and methanol (1 mL). The solution was collected and evaporated until dry to obtain the Benzimidazolium dyes **JC-D7**and**JC-D8**.

5.5.8 Characterization of JC-D7 and JC-D8

JC-D7: ^{1}H NMR (CD_3OD, 300 MHz) δ (ppm) 8.34 (d, 1H, J = 12 Hz), 8.30 (d, 1H, J = 9.3 Hz), 8.19 (s, 1H), 8.14 (m, 1H), 8.09 (s, 1H), 7.92 (dd, 2H, J = 4.5, 7.8 Hz), 7.64 (td, 1H, J = 4.9, 1.2 Hz), 7.57 (td, 1H, J = 4.9, 1.2 Hz), 7.21 (t, J = 4.5 Hz, 1H), 6.98 (d, J = 12 Hz, 1H), 6.93 (d, J = 7.2 Hz, 1H), 4.12 (s, 1H), 4.09 (s, 1H), 3.51 (s, 3H), 3.35 (t, J = 6 Hz, 2H), 3.16 (m, 4H), 2.96 (t, J = 6 Hz, 2H), 2.07 (t, J = 7.2 Hz, 2H), 1.91 (m, 6H). ^{13}C NMR (CD_3OD, 75 MHz) δ (ppm) 176.97, 151.82, 147.71, 135.29, 132.89, 132.75, 132.71, 132.53, 132.18, 131.92, 130.21, 129.01, 128.34, 127.42, 126.83, 124.62, 116.23, 112.14, 47.79, 46.62, 40.82, 38.14, 36.41, 33.51, 29.30, 27.02, 25.92, 25.03. HRMS (ESI): m/z calcd ($C_{28}H_{31}Cl_2N_4O$): 509.1869; found: 509.1847.

JC-D8: ^{1}H NMR (CD_3OD, 300 MHz) δ (ppm) 8.42 (d, J = 5.4 Hz, 1H), 8.41 (d, J = 12 Hz, 1H), 8.18 (s, 1H), 8.13 (m, 1H), 7.64 (m, 3H), 7.08 (d, J = 7.5 Hz, 1H), 6.93 (d, J = 12 Hz, 1H), 6.82 (d, J = 7.2 Hz, 1H), 4.11 (broad, 2H), 3.52 (s, 3H), 3.35 (t, 6Hz, 2H), 3.16 (m, 4H), 2.96 (t, J = 5.7 Hz, 2H), 2.59 (s, 3H), 2.07 (t, J = 7.5 Hz, 2H), 1.92 (m,

4H). ^{13}C NMR (CD_3OD, 75 MHz) δ (ppm) 177.167, 152.22, 148.11, 140.16, 134.46, 133.08, 132.87, 132.43, 132.11, 131.29, 128.83, 128.42, 127.76, 127.46, 126.53, 125.40, 116.40, 111.62, 47.95, 46.82, 41.02, 38.34, 36.62, 33.71, 29.51, 27.22, 26.16, 25.23, 19.93.HRMS (ESI): m/z calcd ($C_{29}H_{33}Cl_2N_4O$): 523.2026; found: 523.2042.

5.5.9 Quantum-Yield Measurements.

Quantum yields were calculated by measuring the integrated emission area of the florescent spectra and referring them to the area measured for Fluorescein in 0.1 N NaOH ($\Phi = 0.95$) with excitation at 450 nm[30,31]. Quantum yield of the JC compounds were then calculated using the equation below, where *F* represents the area of fluorescent emission, η is the reflective index of the solvent and the *Abs* is the absorbance and excitation wavelength selected for standards and samples. Emission was integrated from 450 nm to 650 nm.

Equation 5.1 Quantum yield measurement

$$\Phi_{(sample)} = \Phi_{(ref)} \frac{F_{(sample)}}{F_{(ref)}} \frac{\eta_{(sample)}}{\eta_{(ref)}} \frac{Abs_{(ref)}}{Abs_{(sample)}} \qquad (1)$$

5.5.10 Primary screening.

Benzimidazolium compounds were transferred to Greiner 96 well black polypropylene plates (final concentration as 10 μM) and tested with 0.5 μM, 1 μM, 5 μM and 10 μg/mL polyP (60). Control intensity was measured in10 mM HEPES buffer (pH = 7.4). Fluorescent spectra were recorded on a SpectraMax M2 fluorescent plate reader with excitation at 390 nm (cutoff: 420 nm), emission 450 to 700 nm.

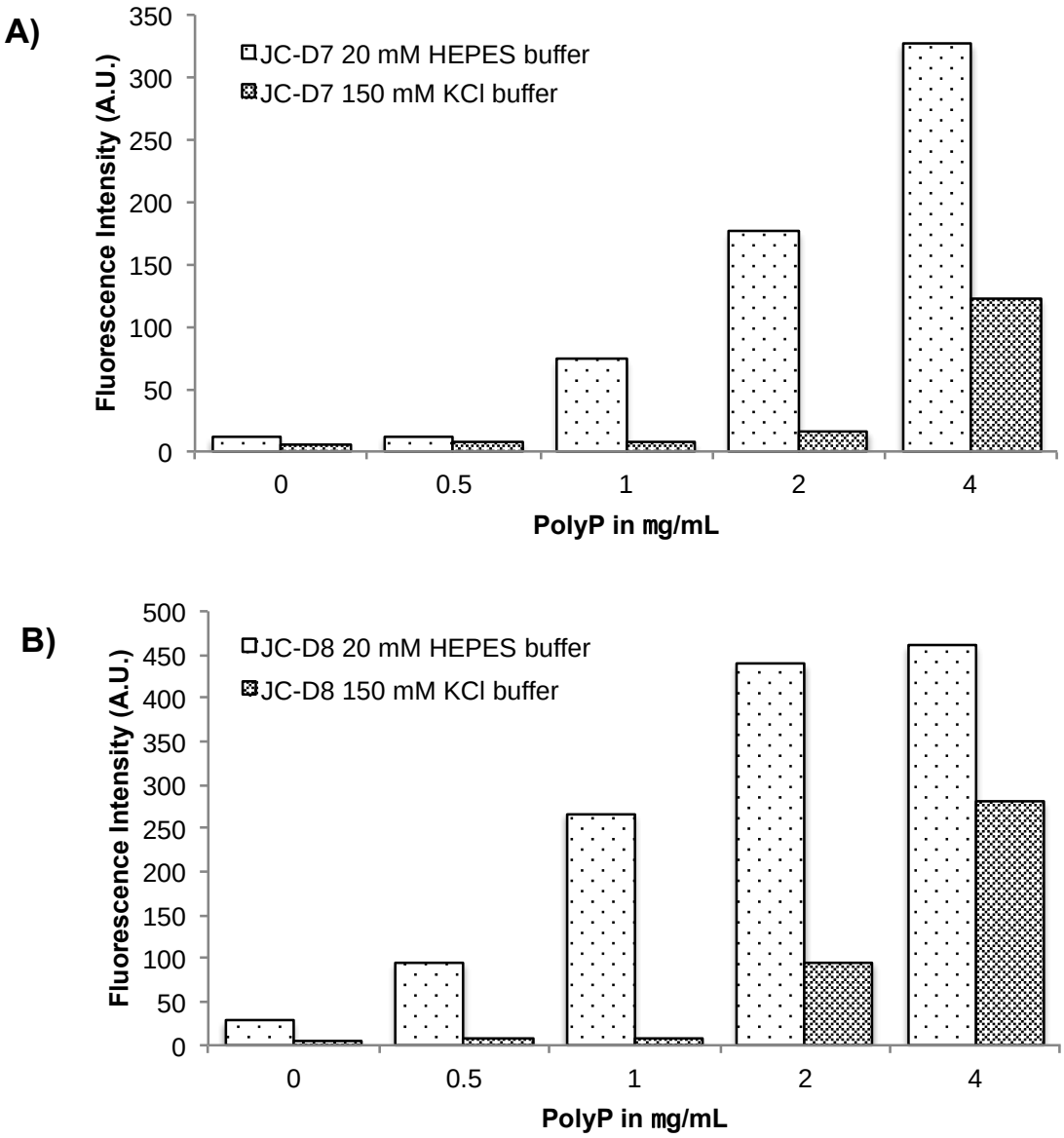

Figure 5.8 Fluorescence response of JC-D7/D8 in different buffers.

JC-D7 and JC-D8 fluorescence for PolyP was tested in 20 mM HEPES (4-(2-hydroxyethyl)-1-piperazineethanesulfonic acid) buffer at pH 7.4 and 150 mM KCl (Potassium chloride) buffer at pH 7.4. We found that the probes, JC-D7 and JC-D8 show reduced fluorescence intensity in 150 mM KCl buffer solutions, in comparison with HEPES buffer.

5.6. Reference

1. Kornberg, A.; Rao, N. N.; ult-Riche, D. Inorganic polyphosphate: a molecule of many functions. *Annu. Rev. Biochem.* **1999,** *68*, 89-125.

2. Kulaev, I.; Vagabov, V.; Kulakovskaya, T. New aspects of inorganic polyphosphate metabolism and function. *Journal of Bioscience and Bioengineering* **1999,** *88* (2), 111-129.

3. Kumble, K. D.; Kornberg, A. Inorganic polyphosphate in mammalian cells and tissues. *J. Biol. Chem.* **1995,** *270* (11), 5818-5822.

4. Pavlov, E.; Aschar-Sobbi, R.; Campanella, M.; Turner, R. J.; Gomez-Garcia, M. R.; Abramov, A. Y. Inorganic polyphosphate and energy metabolism in mammalian cells. *J. Biol. Chem.* **2010**.

5. Moreno-Sanchez, D.; Hernandez-Ruiz, L.; Ruiz, F. A.; Docampo, R. Polyphosphate is a novel pro-inflammatory regulator of mast cells and is located in acidocalcisomes. *J. Biol. Chem.* **2012,** *287* (34), 28435-28444.

6. Smith, S. A.; Mutch, N. J.; Baskar, D.; Rohloff, P.; Docampo, R.; Morrissey, J. H. Polyphosphate modulates blood coagulation and fibrinolysis. *Proc. Natl. Acad. Sci. U. S. A* **2006,** *103* (4), 903-908.

7. Muller, F.; Mutch, N. J.; Schenk, W. A.; Smith, S. A.; Esterl, L.; Spronk, H. M.; Schmidbauer, S.; Gahl, W. A.; Morrissey, J. H.; Renne, T. Platelet polyphosphates are proinflammatory and procoagulant mediators *in vivo*. *Cell* **2009,** *139* (6), 1143-1156.

8. Holmstrom, K. M.; Marina, N.; Baev, A. Y.; Wood, N. W.; Gourine, A. V.; Abramov, A. Y. Signalling properties of inorganic polyphosphate in the mammalian brain. *Nat. Commun.* **2013,** *4*, 1362.

9. Zakharian, E.; Thyagarajan, B.; French, R. J.; Pavlov, E.; Rohacs, T. Inorganic polyphosphate modulates TRPM8 channels. *PLoS. One.* **2009,** *4* (4), e5404.

10. Wang, L.; Fraley, C. D.; Faridi, J.; Kornberg, A.; Roth, R. A. Inorganic polyphosphate stimulates mammalian TOR, a kinase involved in the proliferation of mammary cancer cells. *Proc. Natl. Acad. Sci. U. S. A* **2003,** *100* (20), 11249-11254.

11. Abramov, A. Y.; Fraley, C.; Diao, C. T.; Winkfein, R.; Colicos, M. A.; Duchen, M. R.; French, R. J.; Pavlov, E. Targeted polyphosphatase expression alters mitochondrial metabolism and inhibits calcium-dependent cell death. *Proc. Natl. Acad. Sci. U. S. A* **2007,** *104* (46), 18091-18096.

12. Pavlov, E.; Zakharian, E.; Bladen, C.; Diao, C. T.; Grimbly, C.; Reusch, R. N.; French, R. J. A large, voltage-dependent channel, isolated from mitochondria by water-free chloroform extraction. *Biophys. J.* **2005,** *88* (4), 2614-2625.

13. Kulakova, A. N.; Hobbs, D.; Smithen, M.; Pavlov, E.; Gilbert, J. A.; Quinn, J. P.; McGrath, J. W. Direct quantification of inorganic polyphosphate in microbial cells using 4'-6-diamidino-2-phenylindole (DAPI). *Environ. Sci. Technol.* **2011,** *45* (18), 7799-7803.

14. Omelon, S.; Georgiou, J.; Henneman, Z. J.; Wise, L. M.; Sukhu, B.; Hunt, T.; Wynnyckyj, C.; Holmyard, D.; Bielecki, R.; Grynpas, M. D. Control of vertebrate skeletal mineralization by polyphosphates. *PLoS. One.* **2009,** *4* (5), e5634.

15. Aschar-Sobbi, R.; Abramov, A. Y.; Diao, C.; Kargacin, M. E.; Kargacin, G. J.; French, R. J.; Pavlov, E. High Sensitivity, Quantitative Measurements of Polyphosphate Using a New DAPI-Based Approach. *J. Fluoresc.* **2008**.

16. Diaz, J. M.; Ingall, E. D. Fluorometric quantification of natural inorganic polyphosphate. *Environ. Sci. Technol.* **2010,** *44* (12), 4665-4671.

17. Gomes, F. M.; Ramos, I. B.; Wendt, C.; Girard-Dias, W.; De, S. W.; Machado, E. A.; Miranda, K. New insights into the in situ microscopic visualization and quantification of inorganic polyphosphate stores by 4',6-diamidino-2-phenylindole (DAPI)-staining. *Eur. J. Histochem.* **2013,** *57* (4), e34.

18. Martin, P.; Van Mooy, B. A. Fluorometric quantification of polyphosphate in environmental plankton samples: extraction protocols, matrix effects and nucleic acid interference. *Appl. Environ. Microbiol.* **2013,** *79* (1), 273-281.

19. Feng, S.; Kim, Y. K.; Yang, S.; Chang, Y. T. Discovery of a green DNA probe for live-cell imaging. *Chem. Commun. (Camb.)* **2010,** *46* (3), 436-438.

20. Cervantes, S.; Prudhomme, J.; Carter, D.; Gopi, K. G.; Li, Q.; Chang, Y. T.; Le Roch, K. G. High-content live cell imaging with RNA probes: advancements in high-throughput antimalarial drug discovery. *BMC. Cell Biol.* **2009,** *10*, 45.

21. Wang, S.; Chang, Y. T. Discovery of heparin chemosensors through diversity oriented fluorescence library approach. *Chem. Commun. (Camb.)* **2008,** (10), 1173-1175.

22. Wang, S.; Chang, Y. T. Combinatorial synthesis of benzimidazolium dyes and its diversity directed application toward GTP-selective fluorescent chemosensors. *J. Am. Chem. Soc.* **2006,** *128* (32), 10380-10381.

23. Ahn, Y. H.; Lee, J. S.; Chang, Y. T. Combinatorial rosamine library and application to *in vivo* glutathione probe. *J. Am. Chem. Soc.* **2007,** *129* (15), 4510-4511.

24. Vendrell, M.; Zhai, D.; Er, J. C.; Chang, Y. T. Combinatorial strategies in fluorescent probe development. *Chem. Rev.* **2012,** *112* (8), 4391-4420.

25. Pisoni, R. L.; Lindley, E. R. Incorporation of [32P]orthophosphate into long chains of inorganic polyphosphate within lysosomes of human fibroblasts. *J. Biol. Chem.* **1992,** *267* (6), 3626-3631.

26. Zhang, Z.; Chen, G.; Zhou, W.; Song, A.; Xu, T.; Luo, Q.; Wang, W.; Gu, X. S.; Duan, S. Regulated ATP release from astrocytes through lysosome exocytosis. *Nat. Cell Biol.* **2007,** *9* (8), 945-953.

27. Burchell, V. S.; Gandhi, S.; Deas, E.; Wood, N. W.; Abramov, A. Y.; Plun-Favreau, H. Targeting mitochondrial dysfunction in neurodegenerative disease: Part II. *Expert. Opin. Ther. Targets.* **2010,** *14* (5), 497-511.

28. Burchell, V. S.; Gandhi, S.; Deas, E.; Wood, N. W.; Abramov, A. Y.; Plun-Favreau, H. Targeting mitochondrial dysfunction in neurodegenerative disease: Part I. *Expert. Opin. Ther. Targets.* **2010,** *14* (4), 369-385.

29. Smith, S. A.; Choi, S. H.; Collins, J. N.; Travers, R. J.; Cooley, B. C.; Morrissey, J. H. Inhibition of polyphosphate as a novel strategy for preventing thrombosis and inflammation. *Blood* **2012,** *120* (26), 5103-5110.

30. Angelova, P.; Muller, W. Oxidative modulation of the transient potassium current IA by intracellular arachidonic acid in rat CA1 pyramidal neurons. *Eur. J. Neurosci.* **2006,** *23* (9), 2375-2384.

Chapter: 6

6.1 Conclusions

Diversity oriented fluorescent library (DOFL) approach was developed with the intention to rapidly generate large pool of fluorescent compounds. DOFL in combination with High through-put screening has become a robust and very powerful technique for sensor and probe development. A conventional target oriented approach provides the detailed mechanistic interaction between the sensor and the target. However the main limitation of this approach is slower rate for probe development and less scope for novel probe expansion. In contrast DOFL in combination with HTS has opened the way for discovery of large number of novel sensor/imaging probes for diverse targets like, small molecule detection, proteins, cells or tissue imaging probes.

To expand our potential bio-imaging tool box for tissue imaging probe development, we selected ACEDAN for diversity oriented TP fluorescent library synthesis. We developed two ACEDAN based library named **TPG** and TPC using series of anime building blocks. Solid phase chemistry provides highly pure compounds without further purification (80 compounds in each library). These compounds were further diversified to acetyl (TPGAC, TPCAC) and chloroacetyl (TPGCA, TPCCA) by using simple solid phase activate ester chemistry. All developed compounds were characterized for their one photon and two photon photo-physical properties. Next, we setup a high throughput fluorescent image based screening for these compounds with pancreatic cell lines β-cell, α-cell and acinar cell, a novel imaging probe **TP-α** (two-photon alpha) was

discovered, suitable for selective staining of mice pancreatic alpha cells. This was the first TP fluorescent probe which selectively stains pancreatic alpha cells of mice pancreatic islets over other islet cells. We further demonstrate the distribution of pancreatic alpha cell on the surface of intact islet by TP 3D imaging. *In vitro* selectivity of **TP-α** towards glucagon over insulin and other several analytes explains the selectivity of the probe for glucagon producing α-cells.

After the development of two-photon α-cell selective probe we aimed for the development for pancreatic β-cell selective two-photon probe. Pancreatic beta cells are well studied and known to have higher GLUT2 expression on the cell surface. GLUT2 is a high affinity Glucosamine transporter. So we developed five new TP glucosamine based probes TPO-GluNs with different linker size. We found that, the six carbon chain length probe **TP-β** (**TPO-C6-GluN**) have maximum uptake in to the pancreatic beta cells and can be successfully utilized for the isolation of primary beta cells from mice. **TP-β** show negligible cytotoxicity. **TP-β** can be excited by 870 nm fs laser pulses for TP tissue imaging. **TP-β** can selectively stain beta cells *ex vivo* in mice model. These results demonstrates that, **TP-β** can be a useful probe in diabetic studies for TP imaging application of beta cells. With longer excitation wavelength it can be successfully utilized for 3D deep tissue TP imaging.

Inorganic polyphosphate (polyP) is a linear polymer made up of many orthophosphates linked together by phosphoanhydride bonds identical to the ones found in ATP. PolyP is a biological macromolecule, which has been found in various organisms ranging from bacteria to humans. The kinetic changes of the level of poly P as well as

specific polyP distribution cannot be measured with any biochemical methods. While use of DAPI probe makes those assays possible employing fluorescence imaging approach, its use also raises concerns due to potential interference of the indicator due to variable levels of RNA and DNA in mitochondria and other cellular compartments under different conditions. We discover two probes JC-D7 and JC-D8 as PolyP selective probe over DNA, RNA and other phosphate containing analytes. These presented probes allow us to achieve higher specificity for polyP labeling which largely excludes possible contributions of DNA and RNA. Using the novel indicators we have been able to detect increased level of polyP in brain slices obtained from an animal model of Parkinson's disease. This finding demonstrates the potential for practical use of the probes in live samples. However, care should be taken and specific protocols developed for each particular set of experimental conditions.

6.2 Future prospective

6.2.1 Development of multimodal tracker for β-cell imaging.

Type 1 Diabetes Mellitus one of the most common metabolic disorder in human, is caused by the auto-immune destruction of pancreatic beta cells, leading to insulin deficiency in blood and impaired glucose homeostasis. In Chapter 4, we found that **TP-β** compound can be efficiently utilized for beta cells imaging and isolation. However, the fluorescent imaging can only be suitable for *ex vivo* islet or tissue imaging. Because of the deep and scattered localization of pancreatic islets in the pancreatic tissue, the non-invasive imaging modality could be a better alternative. However the non-invasive

techniques like MRI, PET and CT have the limitation of lower spatial resolution. Moreover each modality has very different sensitivity, which demands higher enrichment of contrast agent on the target cells. Because of these challenges the non-invasive beta cell imaging has remained as a challenge. Our primary results show the success of **TP-β** for enrichment and selectivity to the β-cell. Our next aim will be to explore the PET derivative of **TP-β** for whole animal imaging.